SYNTHESIS, CHARACTERIZATION AND CATALYTIC APPLICATIONS OF TIN- CONTAINING MOLECULAR SIEVES

A THESIS
SUBMITTED TO THE
UNIVERSITY OF PUNE
FOR THE DEGREE OF
DOCTOR OF PHILOSOPHY
(IN CHEMISTRY)

BY
PRASHANT S. NIPHADKAR

RESEARCH GUIDE
DR. PRAPHULLA N. JOSHI

CATALYSIS AND INORGANIC DIVISION
NATIONAL CHEMICAL LABORATORY
PUNE-411008, INDIA
SEPTEMBER 2011

CERTIFICATE

Certified that the work incorporated in the thesis entitled **" SYNTHESIS, CHARACTERIZATION AND CATALYTIC APPLICATIONS OF TIN-CONTAINING MOLECULAR SIEVES**" submitted by **Mr. Prashant S. Niphadkar,** for the degree of **Doctor of Philosophy,** was carried out by the candidate under my supervision/guidance in the Catalysis Pilot Plant, Catalysis Division, National Chemical Laboratory, Pune, India. Material obtained from other sources has been duly acknowledged in the thesis.

DR. PRAPHULLA N. JOSHI
(Supervisor/Research Guide)

DELARATION

I declare that the thesis entitled **"SYNTHESIS, CHARACTERIZATION AND CATALYTIC APPLICATIONS OF TIN- CONTAINING MOLECULAR SIEVES",** submitted for the Degree of Philosophy to the University of Pune, has been carried out by me at the National Chemical Laboratory, Pune under the supervision of my research guide **Dr. Praphulla N. Joshi.** The work is original and has not been submitted in part or full by me for any other degree or diploma to this or any other university.

(PRASHANT S. NIPHADKAR)

ACKNOWLEDGEMENT

It is my great pleasure to express my heartfelt gratitude to my research supervisor, Dr. P. N. Joshi, Principle scientist, National Chemical Laboratory, Pune, for his constant support, sincere guidance, numerous discussion and constructive suggestions through out the course of this investigation. His wide knowledge, logical way of thinking, understanding, encouraging and personal guidance has provided a good basis for the present thesis. I will be remaining ever grateful to him for teaching me scientific and non-scientific lessons. I appreciate all his contributions of time and ideas and providing me CPP facility to make my Ph.D.

It gives me a great pleasure to express my deep sense of gratitude to Dr. V. V. Bokade, Dr.(Mrs.) S.S. Deshpande and Dr. K. R. Patil for their expert and guidance and suggestions in carrying out the research work.

I would like to thank to Dr. Rajiv Kumar (former head) and Dr. A. P. Singh, Chairperson of Catalysis Division, for their permission for Ph.D. work and co-operation given to me in completing my research work.

I owe my special thanks to Dr. D. Srinivas, Dr. C. V. V. Satyanarayana, Dr.(Ms.) S. Umbarkar, Dr. S. P. Mirajkar, Dr.(Ms.) S. V. Awate, Dr. K. Selvaraj, Dr. C. S. Gopinath, Dr.(Ms.) Nandini Devi, Dr. T. Raja, Dr. Kinage, Dr. C. V. Rode, Dr. P. Dhepe, Dr .R. A. Shaikh, Mr. Tejas Gaydhankar, Ms. V. Samuel, Mr. R. K. Jha, Mr. P.K. Purushothaman for their help and support. I would like to acknowledge the help received from Mr. Madhu and Mr. Milind.

I am also special thanks to my friends Dr. Mahesh Kasture, Dr. D. S. Bhange, Dr. Mahesh Kadgaokar, Mr. H. Gurav, Mr. Kokate, Mr. R. Sahu many others from whom I have received in valuable help and support.

It gives me great pleasure to thank CPP group, Mr. A. Maulavi, Mr. H.T. Jagtap, Mr.S. R. Kadam, Mr. P.M. Dhutraj and all project assistant for their constant help and encouragement.

Words are not enough to express my love and gratitude to my family members. It gives me great pleasure to thanks my parents, my brothers Nitin & Ganesh and their family member for always providing unconditional support and helping me over the years. Thanks to my dear wife Shilpa for her tremendous patient, unfailing support and encouragement she have shown in her own way during my long period of studies.

I take this opportunity to thank Dr. S. Pal, Director, NCL, Pune, for allowing me to carryout research and providing all infrastructural facilities at NCL for the Ph.D. work.

Prashant S. Niphadkar

CONTENTS

CHAPTER 6

List of Figures

List of Tables

ABSTRACT

SYNTHESIS, CHARACTERIZATION AND CATALYTIC APPLICATIONS OF TIN- CONTAINING MOLECULAR SIEVES

An isomorphous substitution of Al^{3+} or Si^{4+} by various metal ions like Ti^{4+}, Zr^{4+}, Sn^{4+}, V^{4+} etc in the zeolitic and non-zeolitic molecular sieves has resulted into the formation of different Al-free metallosilicates possessing considerable Lewis acidity. Medium pore Sn-MFI, large pore Sn-BEA microporous stannosilicate molecular sieves and Sn-substituted mesoporous molecular sieves have shown excellent catalytic performance in several hydrocarbon transformation reactions of commercial and academic interest. Despite the significance of stannosilicate molecular sieves, the synthesis and characterization of microporous and micro/mesoporous stannosilicate composite consisting of MCM-41 and MFI as meso- and micro- structural components have not been systematically explored. This thesis describes the studies on the synthesis, characterization and catalytic applications of tin-containing microporous molecular sieves and micro-/mesoporous composite molecular sieves having meso- and micro- structural components. The synthesis of tin silicate –1 (Sn-MFI) molecular sieve by Dry Gel Conversion (DGC) method was carried out and the results obtained by varying the synthesis parameters such as crystallization time, temperature, water content at the bottom of autoclave, molar ratios of $(TPA)_2O/ SiO_2$ and SiO_2/SnO_2 in dry gel are discussed on the basis of crystallization kinetics and physico-chemical properties of Sn-MFI. An optimization of reaction parameters in heterogeneously catalysed vapour phase N-methylation of aniline over Sn-MFI molecular sieves was carried out and the catalytic performance of Sn-MFI was compared with that of Al-MFI,Ti-MFI and Si-MFI. The synthesis of silica-based Sn-MFI, Al-MFI and Al-Sn-MFI molecular sieves containing both Lewis and Brønsted acid site were carried out by hydrothermal crystallization method. The influence of synergy between Lewis and Brønsted acid sites on acid catalyzed aniline N-methylation reaction was investigated to maximize the aniline conversion as well as N-methyl aniline (NMA) selectivity. In this thesis, the work related to oxyanion induced hydrothermal synthesis of microporous stannosilicate molecular sieve with BEA topology (Sn- BEA) using fluoride route and without using seed is carried out. The influence of molar ratios of TEA^+/ SiO_2 and SiO_2/SnO_2 in initial gel composition

on the crystallization period, % crystallinity and physico-chemical properties of Sn-BEA were also investigated. This thesis also describes a study of synthesis of Micro-/meso-porous stannosilicate composites (Sn-MFI/MCM-41) by a simple two-step crystallization process. The influences of various process parameters such as, aging time, re-crystallization temperature, gel composition variables such as molar ratios of $TPAOH/SiO_2$, $CTMABr/SiO_2$ and SiO_2/SnO_2 on the type of the phase formation were investigated. The tin-containing samples were characterized by Powder XRD, AAS, IR, DRUV-Vis and SEM etc.

The data obtained by optimization of synthesis parameters and its influence on product quality, characterization and catalytic performance of various tin-containing molecular sieves represented a convenient vehicle for the method of preparation and evaluation of tailor-made material for a particular application.

The objective of the present thesis is to study the synthesis, characterization and catalytic properties of Sn containing molecular sieve. The thesis is divided in seven (7) chapters and a brief summary is given below.

Chapter 1 provides a general introduction related to synthesis routes, characterization techniques and catalytic applications of microporous, mesoporous and micro-/mesoporous composite molecular sieves with and/or without Sn. A review of the literature to date in these areas is included. The objectives and scope of the research work are outlined briefly at the end of this chapter.

Chapter 2 describes the synthesis of tin silicate –1 (Sn-MFI) molecular sieve by Dry Gel Conversion (DGC) method. The results obtained by varying the synthesis parameters such as crystallization time, temperature, water content at the bottom of autoclave, molar ratios of $(TPA)_2O/ SiO_2$ and SiO_2/SnO_2 in dry gel are discussed on the basis of crystallization kinetics and physico-chemical properties of Sn-MFI. An *in-situ* high temperature X-ray diffraction studies were carried out to elucidate the thermal expansion properties of silica based MFI type molecular sieves with and without tin. The nature, strength and density of surface acid sites in Sn-MFI molecular sieve with different Sn-content were characterized by N1s XPS of chemisorbed pyridine and details are included in this chapter.

Chapter 3 gives an account of heterogeneously catalysed vapour phase N-methylation of aniline over Sn containing microporous molecular sieve synthesized

during this investigation. This includes 1) comparison of catalytic performance of Sn-MFI with Al-MFI,Ti-MFI and Si-MFI and 2) optimization of reaction parameter.

Chapter 4 deals with the synthesis and characterization of Al-Sn-MFI with different degree of isomorphous substitution of Al^{3+} in Sn-MFI framework. The samples containing both Lewis and Brønsted acid sites were studied for the investigating the synergy effect between Bronsted and Lewis acidity in alkylation's of aniline with methanol aiming at maximizing the aniline conversion and N-methylaniline selectivity .

Chapter 5 presents the seedless synthesis of microporous stannosilicate molecular sieve with BEA topology (Sn- BEA) using fluoride route. It also describes the influence of molar ratios of TEA^{+}/ SiO_2 and SiO_2/SnO_2 in initial gel composition on the crystallization period, % crystallinity and physico-chemical properties of Sn-BEA. Various characterization was carried out by Powder XRD, AAS, IR, DRUV-Vis and SEM. The performance of Sn-BEA in BV oxidation reaction is also included in this chapter.

Chapter 6 describes the preparation and characterization of Sn-containing mesoporous molecular sieve. It describes :

- Synthesis and characterization of Micro-/meso-porous stannosilicate composites (Sn-MFI/MCM-41) obtained via two-step crystallization process
- Optimization and establishing synthesis parameter-phase relationship for Sn-MFI/MCM-41 composites.
- Brief study of hydroxyalkylation of p-Cresol over Sn-MCM-41 and Sn-MFI/MCM-41

Chapter 7 summarizes the conclusions reached in this thesis and gives suggestions for further research.

CHAPTER 1

INTRODUCTION

1.1. GENERAL BACKGROUND

The term "molecular sieve" was coined by J.W. Mcbain in 1932 to define porous solid materials [1], which have the ability to separate components from a mixture on the basis of the molecular size and shape. The discovery of molecular sieves can be traced back to 1756 when the word zeolite was first used. The term *molecular sieve* became a lot more popular among scientific community from 1956, when new and better molecular sieves had been synthesized and sensible applications were developed. The past couple of decades have witnessed the discovery of new molecular sieves and development of known molecular sieves by alternative, lower cost, synthesis routes, and the fine tuning of their textural properties for potential applications. According to the International Union of Pure and Applied Chemistry (IUPAC) rules, pores are classified as micropores when their diameter d is in the range of 0.2–2 nm, mesopores when 2 nm < d < 50 nm, or macropores when d > 50 nm [2].

Many kinds of porous materials such as, (pillared) clays, anodic alumina, carbon nanotubes and related porous carbons have been extensively described in the literature [3]. However, by virtue of the main features such as regular structure, large pore size and high surface area, the microporous material (zeolite) and mesoporous material (M41S) have attracted considerable attention in rapidly growing field of modern science and technology especially as a prospective heterogeneous catalyst/catalyst support, adsorbent and template for the synthesis of nanostructures.

1.2. MICROPOROUS MOLECULAR SIEVE: Zeolite

Zeolite is the most technological important molecular sieve. Zeolite is crystalline microporous silica based framework structures. Several of zeolite topologies are extensively used as heterogeneous catalysts in industry particularly in oil refining, petrochemical sector and production of fine and specialty chemicals [4-6]. The technological applications of zeolitic molecular sieve are as varied as chemical make up (as change of chemical composition of molecular sieve). Heterogeneous catalysis, adsorption and ion exchange make extensive use of zeolite molecular sieve. Therefore, the study on the synthesis, characterization and catalytic

applications of different topology of zeolites and related materials is a useful subject in heterogeneous catalysis.

Traditionally, zeolite is defined as crystalline materials in which Si and Al are tetrahedral coordinated by oxygen atoms in a three-dimensional network. The crystallographic unit cell of the zeolites may be represented as:

$$M_{x/n}\,[(AlO_2)_x\,(SiO_2)_y]\,zH_2O$$

Where, M is a charge compensating cation with valency '*n*'. The presence of trivalent Al atoms in the lattice develops a unit negative charge per Al atom in the framework, compensated either by cation such as proton (H^+) thus producing acidity in zeolites.

Following main characteristics of the zeolites are responsible for the utility of these materials as workhorses in chemical industry:

- High surface area, ion exchange and adsorption capacity.
- Tunable adsorption properties from hydrophobic to hydrophilic.
- Active sites, for example acid and basic sites, can be generated in the framework and their strength and concentration can be tailored for a particular application.
- The sizes of their channels and cavities match with the dimensions of most of the molecules involved in various chemical processes, and the strong electronic fields existing in those micropores together with an electronic confinement of the guest molecules.
- The complex channel structure in the zeolites allows different kinds of shape selectivity, i.e. product, reactant, and transition state.

In view of the growing industrial importance and inherent scientific interest in structural complexity and diverse chemistry of these materials, considerable efforts have been directed into synthesis of zeolites. There has been subsequent rise in the number of known synthetic zeolites and also the discovery of zeolite-like or zeolite related materials referred as "zeotypes" [7-8].

1.2.1. Classification of Zeolite

Several attempts have been made to classify the families of zeolites on the basis of their crystal structure [4-6,9], chemical composition[4,5,10], effective pore diameter[4,5,11], and natural occurrence[4,5].

Zeolites have been classified on the basis of silica-alumina ratios into three type, viz low, intermediate and high silica /alumina zeolites. Typical examples of low silica zeolite are A, X etc which possess Si/Al ratios between 1 and 1.5. Example of the intermediate silica alumina zeolite (Si/Al=2 to 5) are L, mordenite, omega, FAU, while example of high silica zeolite (Si/Al= more than 10) are ZSM-5, ZSM-11, EU-1, dealuminated Y, mordenite etc. Silica molecular sieves (Silicalite-1 and Silicalite-2) contain Si/Al from several thousand to infinity. Zeolites have also been classified according to their effective pore diameter. The effective pore diameter of the zeolite depends upon the number of tetrahedral present in the ring aperture. On the basis of pore openings, zeolites are commonly classified into small pore (6 or 8-member ring, e.g. Linde A, ZK-5, chabazite), medium pore (10-member ring, e.g. ZSM-5, ZSM-11, ZSM-33 etc), large pore (12-member ring, Linde X, Y, L, BEA etc) and ultra large pore (14-or more member ring, e.g. UDT-1).

1.2.2. Nomenclature

Although, there is no systematic nomenclature for molecular sieve materials, the structure commission of International Zeolite Association (IZA) and IUPAC have assigned a three capital alphabets as structural codes to synthetic and natural zeolites[50-52] These three capital letters have been used to identify structure types (Table 1.1). The codes for zeolite identification have generally been derived from the names of the type of species, and do not include numbers and characters other than roman letters. Structure type codes are independent of chemical composition, distribution of various possible T atoms, (e.g. Si^{4+}, Al^{3+}, Ti^{4+}, etc.), cell dimensions or crystal symmetry. Till today, structural code to around 900 material has been assigned. Some of them are tabulated in Table 1.1

Table 1.1: Some structural codes of zeolite

Structural code	Zeolite	Structural code	zeolite
ANA	Analcime	LTA	Linde Type A
BEA	Beta	LTL	Linde Type L
EUO	EU-1	MEL	ZSM-11
FAU	X & Y	MFI	ZSM-5
FER	Ferrierite	MOR	Mordenite

1.2.3. Synthesis of Zeolite

Zeolites and their analogues are commonly prepared by the hydrothermal method. Hydrothermal method involved heating highly basic hydrogel formed by mixing source of silica, an alumina and alkali or alkaline earth metal hydroxide at 60-200^{o}C. Well known examples of such zeolites are A, X, Y, L, Mordenite [12-16]. Early work on zeolite synthesis utilized only inorganic reaction component but in 1961 the range of reactants was expanded to include quaternary ammonium cation [17-18]. This in turn led to the discovery of high silica zeolite such Beta [19] and ZSM series [20-29]. Organic quaternary ammonium cations and amines act as structure directing agents (SDA), void filler and/or gel modifier or mineralizer. These amines/organic cations are trapped inside the pores of molecular sieves during nucleation and crystal growth. Although, the exact mechanism for the templating effect is not fully understood, it is visualized that zeolites grow around the template and stabilize certain pore structures and subunits. Interestingly, a particular organic molecule can lead to the different molecular sieves framework and different organic molecules utilized in the gel lead to the formation of a particular structure. For instance, tetramethylammonium cation can form as many as 17 structures.

The basic steps which normally involved during a zeolite/molecular sieve synthesis are [30]:

I. Hydrolysis of metal source to form an initial phase.
II. Dissolution/mineralization of the gel phase.
III. Nucleation of zeolite structure. This could be from the gel or solution phase.
IV. Continued crystallization and crystal growth of structure from either the

gel or from the solution.

V. Dissolution of any initial but metastable phases.

VI. Continued crystallization and crystal growth of new, more stable crystalline phases while initial metastable crystals are dissolving.

VII. Dissolution of further metastable phases.

VIII. Nucleation of equilibrium phases.

IX. Crystallization and final growth of the final crystalline condensed phases.

Hence it is clear that hydrothermal synthesis of zeolite/ molecular sieve consists of the series of complex physico chemical process. A large number of variables affect the formation of a specific zeolite phase, such as batch composition, reactant sources, Si/Al ratio, alkalinity, water content, inorganic cations, organic templates, solvents, temperature, aging, stirring, and seeding.

1.2.3.1. ***Other method for Synthesis of Zeolite***

Other methods for synthesis of zeolite with desire quality, many new routes have been developed on basis of conventional hydrothermal method.

1.2.3.1.1. Solvothermal synthetic route

In solvothermal synthetic route, synthesis of zeolite is carried out using non-aqueous system. In general, slow reaction rate is commonly observed for the non-aqueous solvent-mediated synthesis because the available solvating ability falls rather short of that of water. The first patent on the non-aqueous synthesis (solvothermal synthesis) of zeolites was obtained by BASF in 1982 for the synthesis of ZSM-5 (MFI) from NaOH, silica, and Al(OH), in ethereal solvents or in ether—water mixtures [31].Till now, synthesis of silicalite-l (MFI), ZSM-39 (MTN), and ZSM-48 **[**32] all-silica form of sodalite (SOD) [33] are reported by this method.

1.2.3.1.2. Ionothemal synthetic route

In 2004, Morris and co-works reported the first use of ionic liquids (IL) and eutectic mixtures as solvent in the synthesis of aluminophosphate zeolite analogs, and named this method as ionothermal synthesis [33] to distinguish it from hydrothermal or solvothermal zeolite synthesis conducted in a predominantly molecular solvent, such as water or other non-aqueous solvents. Ionothermal synthetic route is almost used for synthesis of different open-framework of aluminophosphate [34-35.]

1.2.3.1.3. Fluoride synthetic route

Fluoride ion, in this method, is used as mineralizer instead of OH^- in hydrothermal synthesis. Flanigen and Patton reported for the first time use of fluoride ion as mineralizer in the synthesis of Silicalite-1[36]. Remarkable feature of this route is (1) The zeolitic structures, which could not be achieved using the hydroxide route, can be realized using this system [37]. (2) Formation of large single crystals and this may be due to slower nucleation. (3) Beneficial effects of F^- have also been observed for the incorporation of heteroatom (e.g., B, Al, Ga, Fe, Ti, Sn) other than silicon in the frameworks of high-silica zeolites [37,38] and (4) A high degree of the framework perfection was observed for high-silica zeolites prepared in fluoride media due low density $Si\text{-}O^-$ and OH-Si defect site[39].

The important issue is the incorporation of fluoride ion into the product. The unambiguous location of fluoride by diffraction or MAS NMR methods have shown that the F- ion appears always to be occluded in small cages within the zeolite framework, usually close to a 4-T-ring window [40]. Fluoride ions could therefore be considered as a structure-director and has been shown from NMR studies to interact strongly with framework silicon atoms.

Most common and preferred fluoride sources are NH_4F, NH_4HF_2 and HF. Fluoride may also be combined with the source of framework material elements such as $(NH_4)_2SiF_6$ or $AlF_3.H_2O$ and Si and Al tetrahedral can released on hydrolysis. The utility of fluoride as mineralizer spread its application from high to low pH systems and further to non-aluminosilicate syntheses [37-40]. By applying this method, MFI, FER, MTT, MTN, BEA etc zeolite and new material like IQT series are successfully prepared.

1.2.3.1.4. Dry gel Conversion

The vapor-phase transport (VPT) method was introduced as an alternate method to synthesize Al-ZSM-5 [41]. According to this method, an aluminosilicate hydrogel is prepared and dried into amorphous dry gel. The resultant dry gel is then converted into micropoprous crystals in presences of mixed vapours of steam and organic structure-directing agent. When only water is supplied from gas phase, the method is termed as steam-assisted dry gel conversion method. A common term ‘dry

gel conversion (DGC)' is used irrespective of the gas phase composition [42]. As a result of great scientific and industrial merits, a great deal of attention has been devoted in establishing the recipe for preparation of different microporous [41-50] and mesoporous [51] materials via DGC method. This methods is not a mere technique alternative to the conventional synthesis route but has great merit in developing 1) possible continuous production process, 2) reduction of the consumptions of expensive templates, 3) rapid crystallization and 4) no need for waste water treatment.

1.2.3.1.5 Microwave-assisted hydrothermal route

Microwave (MW) is an electromagnetic radiation (0.3—300 GHz). Microwave dielectric heating has been widely used in many chemical reactions, such as organic and inorganic synthesis, selective sorptions, oxidation-reductions, and polymerization among many other processes. Microwave-assisted synthesis is generally much faster, cleaner and more energy efficient than the conventional methods. Mobil Oil Corp first reported procedure for the microwave synthesis of zeolites. After that, synthesis of nearly all type of zeolite structure reported in last decades.

Beside above discussed synthesis route, there are still some more routes for synthesis of porous material is reported which are not commonly in use.

1.2.4. Nature of the active sites

In the catalytic application of zeolite, the reactivity of zeolite and selectivity of product in organic transformation reaction are governed by acidity profile and accessibility active centers in zeolite. There are two types of sites associated with the zeolite namely, 1) Acid site and 2) Basic site:

1.2.4.1. *Acidity*

There are two type of acid site associated with zeolite e.g. Bronsted and Lewis acid site [4,6.7]. These acid sites are created by the imbalance in the charge between silicon and aluminium ion in the framework zeolites. Each aluminium atoms of framework induces a potentially active acid site. Bronsted acid site in catalyst arises

when cation viz Na, K and Cs are replaced by protons (H^+). Lewis sites are found in trigonally coordinated aluminium atoms because they accept a pair of electron [4,6,7].

Bronsted acidity is generally associated with zeolite when trivalent metal (e.g. Al, B and Ga) substituted in zeolitic framework (e.g. isomophous substitution of trivalent metal ion). In case of isomophous substituted tetravalent metal ions such Ti, Sn in Al free silicate like MFI and MEL, the framework charge is zero, and do not have Bonsted acid sites. The weak acid catalytic activity associated with these catalysts is mainly due to Lewis acid site. This Lewis acidity arises due to electron negativity of isomphous substituted tetravalent metal in zeolitic framework [52]. Detail of isomphous substitution and its effect on overall property of zeolitic material is going to discuss in section 1.2.5.

1.2.4.2. *Basicity*

Like acid sites, basic site may be of Bronsted or Lewis type. Bronsted basic sites is related to basic –OH group and Lewis sites are related to lone pairs of electrons present in framework. The applications of basic zeolites in catalysis and adsorption have been reported in literature [52].

1.2.5. Isomorphous substitution

Replacement of an element in a crystal lattice of zeolite analogs with other element is called isomorphous substitution and it is one of the fast developing areas in synthesis of new molecular sieve materials. Isomorphous substitution of T (tetrahedral) element in a zeolitic molecular sieve leads to the modification of physico-chemical and catalytic properties of zeolitic material. For a steady insertion of into tetrahedral site of zeolite lattice, a heteroelement must obey certain theoretical rules [6,7,53] such as 1) first rule of Pauling requiring a specific range for the ratio of ionic radii between M^{n+} and O^{2-}, 2) a heteroelement should be flexible to accept the stable tetrahedral coordination and 3) an oxidation state of heteroelement should be compatible with overall(stable) framework charge.

The first replacement in the zeolite frameworks was reported by Goldsmith (1952) in the synthesis of a germanium containing thomsonite wherein Ge^{+4} replaced Si^{+4} in lattice [54]. Later, Barrer et al [55] succeeded in obtaining of Ga and Ge bearing zeolite. In past half century, it has been established that substitution of tri-,

tetra, and pentavalent metal ions such as B^{3+}, Fe^{3+}, Ga^{3+}, Cr^{3+}, In^{3+}, Ti^{4+}, Ge^{4+}, Sn^{4+}, Zr^{4+}, V^{5+}, Sb^{5+} and P^{5+} in different type zeolite framework modifies the Bronsted acidity and shape selectivity. However, Flenigen et al [56] and Gabelica et al [53] reported that there are around 19 different transition and main metal group ions with valance ranging from I-V, as given below, which are incorporated in at least one framework type.

Valency I : Li

Valency II : Co, Fe, Mg, Zn, Mn, Be, Ni, Sn

Valancy III : B, Al, GA, Fe, Cr

Valancy IV : Si, Ge, Ti

Valancy V : As, V

Substitution of trivalent metal leads to a negative charged framework and have the potential for Bronsted acidity and cation exchange properties. Incorporation of tetravalent metal create neutral structure, hence does not show Bronsted acidity and ion exchange properties. Due to electro negativity of tetravalent metal, this material, however, shows affinity toward electron e. g. Lewis acidity. Lewis acidity created by such means has been exhibited very exciting result in organic transformation reaction [58-60]. Synthesis, characterization and catalytic application of Ti containing different type of zeolitic frame work have been reported since 1980 [61]. However, exhibition of chemoselective reaction by some Sn containing molecular sieve [59] and possibility higher acidity of Sn containing material due to more electronegativity of Sn than Ti has been triggered up the interest of searcher on Sn containing molecular sieve. But, there is still very little report on synthesis of Sn containing microporous molecular sieve.

1.2.5.1. *Isomorphous substitution of Sn in zeolitic material (Sn containing Microporous molecular sieve)*

Sn (Tin) is a chemical element with atomic number 50 with possible oxidation state i.e. +2 and slightly more stable +4. Tin has two crystalline forms. Above 13.2^{o}C, the stable form is called β-tin/white tin/metallic tin. When temperature below 13.2^{o}C, another stable form will form and is called as α-tin/grey tin/nonmetallic tin. In α-tin, each atom has four tetrahedral bonds resulting in three dimensional covalent

bonding throughout crystal. Structure of α-tin has an analogous structure to diamond form of carbon. The white β-tin has each atom in a some what distorted octahedral environment (four nearest neighbors at 3.016 Å and two further neighbores at 3.175 Å)[62,63].

Tin forms dioxide when it is heated in the presence of air. It is most important raw material for commercial application of Tin in Tin chemistry. Research on tin/tin dioxide attracts a lot of interest because it has been widely used gas sensor[64-69], electrode[70-71], transistor[72], solar cell[73-82], homogenous[82] and heterogeneous[83-85] catalyst.

Since 1995, with the ever-growing demands for modification zeolite materials with desired structures and functions, isomphourous substitution of Sn^{+4} in zeolitic framework (Sn containing Microporous molecular sieve) has aroused considerable attention. It was supposed that introduction Sn in the zeolitic structure possible exhibits useful/better application such as adsorbent [86], ionic conductor [87, 88] and catalyst for several hydrocarbon transformation process [52, 58] because of ability to valence change (redox $Sn^{2+} \leftrightarrow Sn^{4+}$)[52, 89-90] and possibility higher Lewis acidity due to more electronegativity of Sn [52].

The first report on the hydrothermal synthesis of tin containing molecular sieve was appeared in 1976 authored by Dwyer et al [91]. After a gap of 10 years, Skeels et al. claimed [92, 93] the post synthesis of tin containing molecular sieve in US patent (1987) and European patent (1989). Later, several authors reported the posiblity of isomorphous substitution of tin in place of aluminium in a number of zeolites such as fujasite, mordenite, ZSM-5, zeolite L and omega either by post modification or hydrothermal synthesis [94,95]. Later, Exxon [96] reported the synthesis of stannosilicate of novel structure in presence of alkali metals and Al or Ga, where Sn^{4+} ions are reported octahedrally coordinated.

In year 1994-1996, Mal et al [97-103] reported hydrothermal synthesis of Sn containing MFI, MEL, MTW and BEA zeolitic topology in alkaline medium. A. Corma et al and his group [58, 104,105] reported the synthesis of defect free Sn-

BEA by fluoride route in 1999-2002. In 2009[106], Grieken et al described synthesis of Sn-MFI from SiO_2-SnO_2 xerogels.

Even though, Synthesis Sn-cotaining microporous molecular sieve is reported, the challenges associated with synthesizing these Sn containing microporous molecular sieve continue to be the essence of the current research. In addition to this, developing new cost-effective and environmental friendly routes to prepare known materials is also attracting the attention of the researchers in the relevant areas. Understanding the mechanism of formation, investigating the influence of various synthesis variables on physicochemical properties and the nature of the interactions taking place at the surface that control adsorptive and/or catalytic behavior are the key issues.

1.2.6. MFI (ZSM-5) Type Zeolite

MFI (ZSM-5) is medium pore high silica zeolite. It was first discovered by Mobil Oil. It is a crystalline microporous solid containing cavities and channels of molecular dimension 0.5 to 0.6 nm. Due to relatively higher silica and lower aluminium content, it exhibits higher thermal and hydrothermal stability. Their building blocks are formed from pentasil units linked through edges to form chains and these chains are connected to form corrugated sheets. These sheets link to form a three-dimensional framework. Unlike others, these zeolites have pores of uniform dimension and have no large super cages. ZSM-5 consists of two intersecting channels formed by rings of 10 oxygen atoms [107,108]. These two channels have slightly different pore dimensions. One runs parallel to the a-axis of the unit cell, which is sinusoidal and nearly of circular dimension (0.54 x0.56 nm). The other runs parallel to the b-axis and has a straight but elliptical opening with dimensions 0.51 x 0.55nm. These channels intersect to form a three dimensional 10 ring channel system. The crystal structures of ZSM-5 was reported on IZC web site[109], and is depicted in Fig. 1.1. On account of this unique two-dimensional pore structure, ZSM-5 exhibits unique shape-selective catalytic properties. In addition to shape and size selective catalysis, the generation of acidic sites within the zeolite pores gives rise to a highly efficient solid acid catalysis. The isomorphous replacement of silicon with aluminium in a ZSM-5 framework T site gives rise to a charge imbalance. Silicalite -1, an

aluminium free molecular sieve has an isotypic framework structure. Substitution of other elements for Si or Al does not change the framework structure.

An isomorpous substitution of Sn in MFI framework was found to be a potential application as such as adsorbent [86], ionic conductor [87-88] and catalyst for liquid phase hydroxylation of phenol [100] as well as ethyl benzene [101] and vapor phase aniline alkylation [110].

STRUCTURE OF ZSM-5 (MFI)

Chemical Composition	$Na_n[Al_nSi_{96-n}O_{192}] \sim 16\ H_2O$
Symmetry	Orthorhombic
Unit cell constants	a = 20.1, b = 19.9 and c = 13.4 Å
Space Group	Pnma
Pore Structure	10 membered ring structure ; 5.1 x 5.5 Å [100]
	5.6 x 5.3 Å [010]

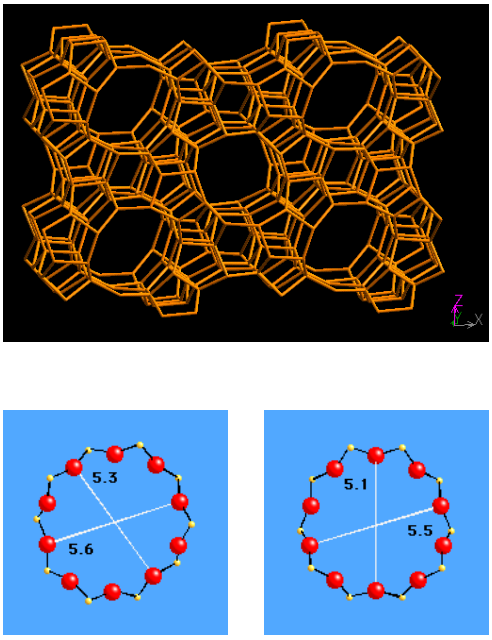

Fig. 1.1. Structure of ZSM-5 a) The MFI framework topology b) 10-ring viewed along [010] (Straight channel) and c) 10-ring viewed along [100] Sinusoidal. [Ref.109]

1.2.7. BEA Type Zeolite

Zeolite beta (BEA) is a high-silica, large-pore crystalline aluminosilicate material. Zeolite beta has two mutually perpendicular straight channels each with cross section of 0.76 X0.64 nm along the a-axis and b-axis direction and a helical channel of 0.55 X 0.55 nm along the C-axis. The crystal structures of beta were reported on IZC web site [109], and are depicted in Fig. 1.2.

The structure of zeolite beta consists of an intergrowth of two distinct structures termed Polymorphs A and B. The polymorphs grow as two-dimensional sheets and the sheets randomly alternate between the two. Both polymorphs have a three dimensional network of 12-ring pores. The intergrowth of the polymorphs does not significantly affect the pores in two of the dimensions, but in the direction of the faulting, the pore becomes tortuous, but not blocked. Very recently polymorph C has been proposed by Corma et al [110].

A catalytic material obtained by an isomorpous substitution of Sn in BEA framework (Sn-BEA) has exhibited an excellent activity in Baeyer Villiger (BV) reaction [58] with practically 100% yield of products of commercial important. Furthermore, Sn-BEA was also reported to be promising catalyst for other various commercially important reactions such as Meerwein–Ponndorf–Verley (MPV) reactions [112], phenol hydroxylation [103] and intramolecular carbonyl-ene reactions [113].

STRUCTURE OF BEA

Chemical Composition	Na^{+}_{7}| **[**$Al_7Si_{57}O_{128}$**]**
Unit cell constants	a = 12.661 b = 12.661 c = 26.046 A
Space Group	$P4_122$
Pore Structure	12 membered ring structure ; 6.6 x 6.7 Å [100] 5.6 x 5.6 Å [001]

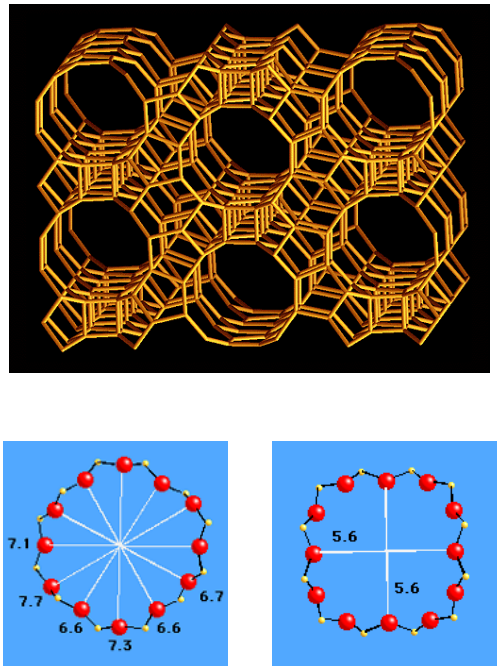

Fig.1.2. Structure of BEA a) The BEA framework topology b) 12-ring viewed along [100] and c) 12-ring viewed along [001]. [Ref. 109]

1.3. MESOPOROUS MOLECULAR SIEVE

The main restriction of microporous zeolitic/molecular sieve is the size constraints up to 2 nm and consequently the reactant molecules trapped and transformed inside them were also small. The catalytic transformation of molecules with diameter larger than 2 nm, especially important for the preparation of fine chemicals, requires molecular sieve with larger pore diameters. Thus the usefulness of the microporous molecular sieves in processing high weight reactants of increasing importance was limited by their smaller pore size. Hence, there has been an ever-

growing interest in expanding the pore sizes of the microporous molecular sieves from the micropore region to mesopores region.

Attempts to improve the diffusion of reactants to the catalytic sites have so far focused on increasing the zeolite pore sizes [114], on decreasing zeolite crystal size [115], or on providing an additional mesopore system within the microporous crystals [116,117]. However, the discovery of the M41S family of siliceous mesoporous molecular sieves [118, 119] brought about the beginning of a new age in the porous materials chemistry by opening new ways for expanding the available size of microporous in material. These materials possess especially large and uniform well defined pore [119-124], whose diameter can be varied in the range of approximately 1.5-10 nm. Parallel to the development of M41S materials, many other ordered mesophases such as HMS [125-126], FSM-16[127], PCH[128], SBA[129], MSU[130], KIT [131] etc. have also been reported. By virtue of the main features such as regular structure, large pore size and high surface area, the M41S materials have attracted considerable attention in rapidly growing field of modern science and technology especially as a prospective heterogeneous catalyst/catalyst support, adsorbent and template for the synthesis of nanostructures. The most popular members of M41S family are MCM-41 (hexagonal), MCM-48 (cubic) and MCM-50(lamellar). MCM-41 has a one-dimensional, hexagonally ordered pore structure, MCM-48 has a three dimensional, cubic-ordered interlocking, bicontinuous pore structure and MCM-50 has lamellar structure [118, 119,132]. Models of these structures are shown in Fig.1.3. It is noteworthy to mention here that, although, the formation of siliceous mesoporous molecular sieves was first reported in 1992, a process for the formation of ‘ low-bulk density silica ’ had been patented by Chiola et al. in 1971[133], wherein tetraethyl orthosilicate (TEOS) was hydrolyzed in the presence of cationic surfactant. Although this patent does not describe the porosity of the resulting materials, in 1997, Di Renzo et al.[134] showed that the reaction products are similar to MCM-41.These materials are fundamentally different from zeolite by the fact that, their pore wall is amorphous. Similar to zeolite synthesis where organic molecule play an essential role as structure directing a agent (SDA),

the most outstanding feature of preparation of the M41S materials is the significant role of the templating agents (surfactant) during the synthesis.

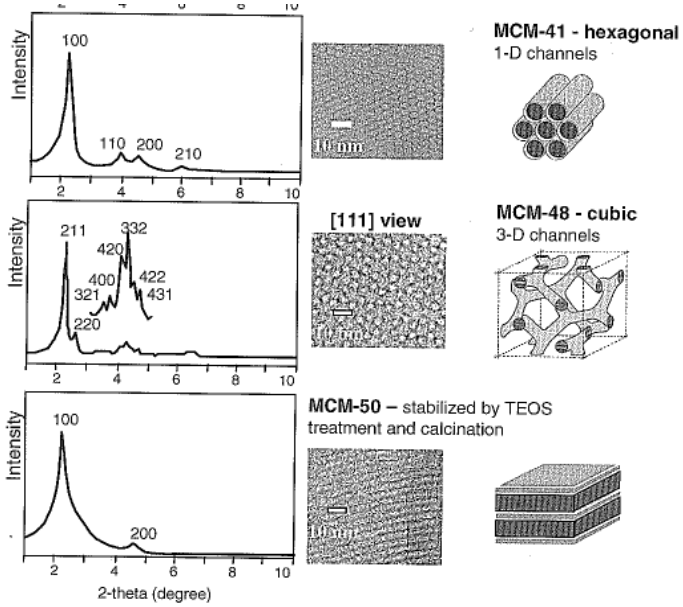

Fig. 1.3 M41S family of order mesiporous materials-X-ray powder diffraction patterns, reprentattive TEM images and proposed structure.

Even though M41S materials can be used for number applications such as catalyst/catalyst support, adsorbent, sensor and an excellent inorganic template for the synthesis of nanostructures[135-142], pure siliceous mesoporous molecular sieves posses a neutral framework and hence limit their catalytic application. Therefore, attempts were made to modify the nature of framework by isomorphous substitution of desired heteroatom during hydrothermal synthesis. Another route followed to modify the property of silica based mesoporous molecular sieves is to incorporate the heteroatom by grafting [143,144]or impregnation[145,146].

1.3.1. Isomorphous substitution in mesoporous molecular sieve

When hydrothermal method is used to substitute silicon by trivalent cations like Al^{3+}, B^{3+}, Ga^{3+} and Fe^{3+} etc [147-152] in the walls of the mesoporous silica, the framework possesses negative charges that can be compensated by protons providing acid sites. The number of acid sites and strength depend on the amount and nature of the incorporated metal. Such materials are used in acid catalyzed reactions and have potential applications in various petroleum refining processes [153-154]. When tetravalent cations like Ti^{4+}, Sn^{4+}, V^{4+} etc [155-158] are incorporated, the

corresponding mesoporous materials are used in oxidation reactions of bulky molecules using either H_2O_2 or TBHP as oxidant [154-156,159-161]. The synthesis and characterization of mesoporous silica modified by metals like Cr [162-164], Mn [165] or Mo has been found to be catalytically active in the hydroxylation of phenol, 1-naphthol and oxidation of aniline with aqueous H_2O_2.

On account of Lewis acidic properties of Sn substituted M41S and other mesoporous material, synthesized either by hydrothermal or by post synthesis modification method, they have shown their excellent performance in several hydrocarbon transformation reactions such as hydroxylation of phenol and 1-napthol, epoxidation of norborne, MPV reaction, Mukaiyama-type aldol condensation, BV , transesterifications , synthesis of poly(L-lactic acid), acylation of aromatics and heteroaromatics , selective oxidative dehydrogenation of cyclohexane, benzylation of aromatics and conversion of biomass products into fine chemicals[166-176]

1.4. MICRO/ MESOPOROUS COMPOSITE

Zeolite, microporous molecular sieve, is an important component in acid catalysed reaction and is recognized as essential in process of petroleum. An ordered and rigid microporous structure of zeotype material shows molecular sieving effect which leads to shape selective catalyst for several important reactions. However, in numerous cases, the sole presences of microspores also impose significant limitation on the range of reactions. This is clearly the case for reactions involving reactants or products that are so larger that they are effectively excluded from the zeolite micropores. In addition to this, the diffusion of molecule through micropores is slow which is limiting the application of zeotype microporous material [177-178].

To overcome constraint of micopore nature of zeolitic material, substantial effort has been focused on increasing the pore size of micoporous material (zeolite). Synthesis of mesoporous M41S material is one achievement in the synthesis of porous material. The high surface area, tunable pore size and variable wall composition of mesoporous silicates (M41S) can overcome the size constraints of zeolitic material because they can be incorporate relatively large size species inside pore. However, mesoporous silicates (M41S) are not crystalline material, the wall of M41S are amorphous. An amorphous character of M41S leads weak or medium acidity of

material which may greatly limit their extensive uses [154, 179-181]. In addition to this, poor hydrothermal property in polar system limits its industrial application [182].

Thus, to upgrade performance of microporous and mesoporous molecular sieve, great interest has been triggered to synthesis new kind of composite material, which combines the advantages of these two kind of molecular sieves. Results of this, few articles concerning this study have been published [183-187] in the year 1996-2000. Kloetstra et al.[183-185] first reported zeolite faujasite overgrown with a thin layer of mesoporous MCM-41, by successive synthesis of FAU and MCM-41 or by adding FAU crystals to MCM-41 synthesis gel. Karlsson et. al.[186] and Huang et al[187] also prepared composite material by simultaneous synthesis of MFI/MCM-41phase using a two –template approach at optimized template and synthesis temperature. Later, Guo et al [188] reported synthesis of Beta/MCM-41 composite material by two step crystallization method. In 2001-2011, synthesis, characterization and catalytic application of nearly all combination i.e. MCM-41/Beta, MCM-41/ZSM-5, MCM-41/Y, MCM-48/Beta, MCM-48/ZSM-5,SBA-15/ZSM-5, Mesoprous ZSM-5 etc have been reported [189].

1.4.1 Synthesis of composite material

The improved hydrothermal properties and enhanced acidity, the synthesis of stable material containing both micro- and mesoporosity has been focus of research during 2000-2010. For synthesis of composite material, different routes have been tried which are schematically highlighted in Fig 1.4.

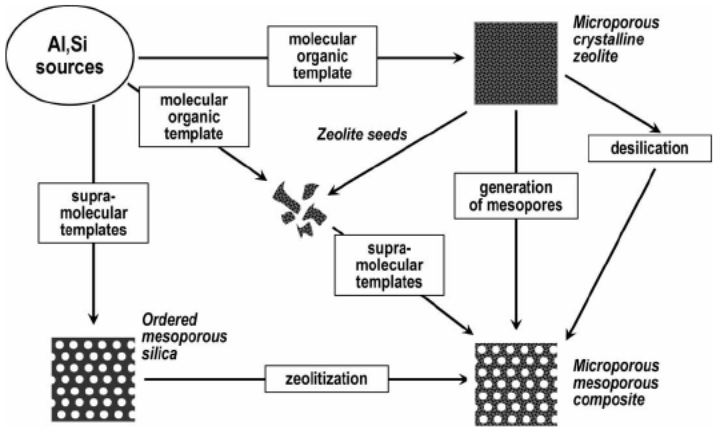

Fig 1.4. Schematic representation of different strategies for applied composite synthesis [190].

1.4.1.1. *Recrystalization of mesoporous material*

One of the approaches used for preparation composite material is to synthesis mesoporous precursor followed by an additional hydrothermal treatment with use of secondary template. This treatment is resulting in the formation of partially microporous crystalline walls of mesoporous matrix. This approach is also called "dual templating" and is shown in Fig.1.5.

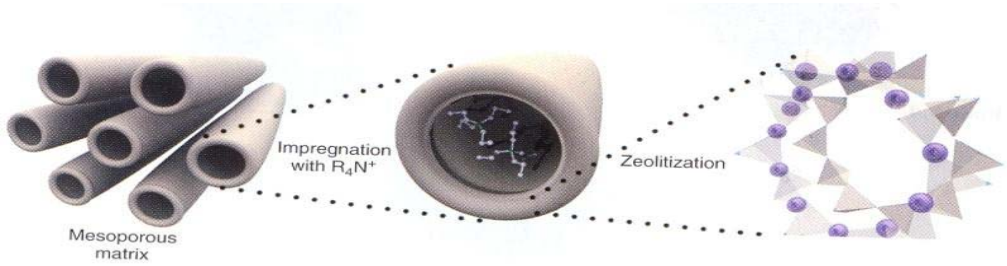

Fig. 1.5. Partial crystallization route for synthesis of micro/mesoporous composite material [191].

Karlsson et al. [186] reported the synthesis of composites containing both zeolite ZSM-5 as the zeolitic phase and the MCM-41 material using dual templating approach. In this approach, heat treatment (may be hydrothermal, microwave or by dry gel) to mesoporous material impregnated with tetra alkylammonium cation leads to formation of composite material. An amount and type of organic are the most important factors controlling the contribution of meso and micro material in composite material.

1.4.1.2. *Using seed of Microporous (zeolite) material.*

In this approach, Zeolite seeds are used to enhance the formation of micro/mesoporous composite. In this method, nanoparticles of zeolite are synthesized by shortening the synthesis time or at relatively low crystallization temperature [216]. These zeolitic particles can be further used as building blocks for self organization in mesoporous matrices (Figure 1.6). In such cases, various types of structure-directing agents functioning as micelles during the organization of building blocks can be used (Fig 1.6).

Another way to prepare composite material by this approach is to add powder of nano zeolitic material into initial gel before formation of mesosphere [192].

The main advantage of seeding method is the substantial increase hydrothermal stability and acidity of composite material when it is compared to mesoporous material [193-196].

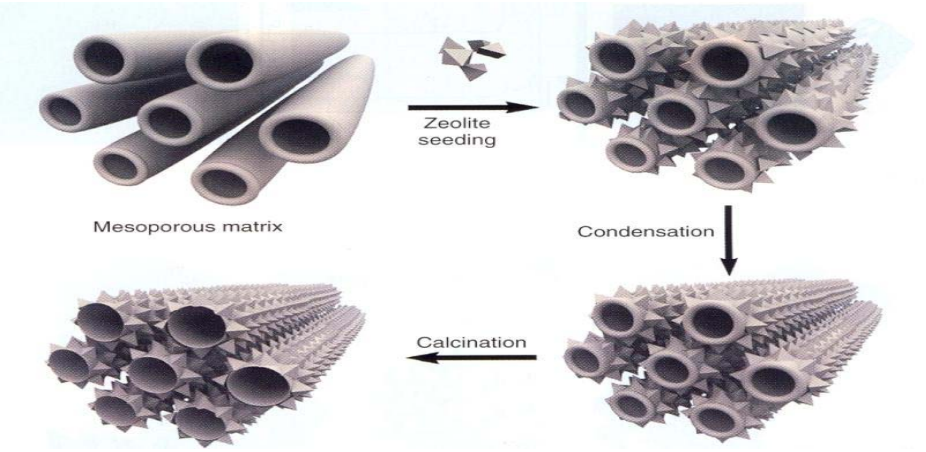

Fig. 1.6. Self organization of zeoite seeds into mesoporous matrix [191].

1.4.1.3. ***Post modification of zeolite.***

There are number of methods used for preparation of composite material by post treatment of zeolite. Few of them are discussed here.

a. Disilication of zeolite

This method is based careful removal of silica of zeolite structure, desilication of zeolite is performed in alkailine medium. Extraction of silicon atoms was proposed as an effective way to create a significant amount of pores inside zeolite crystal. It is also reported that the presence of high concentration of Al in zeolite prevent extraction of Si and hence only small amount mesopores is formed. On other hand, in siliceous zeolite, extraction of Si proceeds in non selective manner and this leads in the formation of large pore with broad distribution.

b. Dealumination

Dealumination of zeolites usually proceed in acidic media. In the Dealumination of zeolite, partial removal of Al from zeolite framework leads to formation of mesopore. Ivanova et al [197] reported dealumination of mordenite using oxalic or methanesulfonic acid and further recrystallization carried out in the presence of surfactants (hexadecyltrimethylammonium bromide) provided the

formation of mesoporous mordenite. The mesopore formed by this method is very similar to the one formed with pure mesoporous molecular sieves of M41S family.

c. Thermal treatment

Another method is heat treatment to zeolitic material. In this case [198], ZSM-5 is heated at 900-1000^{o}C in alumina tube in quartz tube furnace. The resulting material has not only bimodal porous structure and high crystallinity but also narrow pore size distribution

1.4.1.4. *Templating mesoporous zeolite*

By this method, mesopore in zeolite material is introduced by using solid template/supramolecule as template. In this method, solid template is mixed with reaction gel of zeolite. During crystallization, the reaction gel enables zeolite to grow around solid template. This results in the presence of a large number of solid template particles inside the individual zeolite crystals. Removal of solid template by combustion leads to the formation of mesopores. By this method, well-defined zeolite single crystals with mesopores, the size of which is close to the size of solid template, are prepared.

Carbon particles (carbon black) having sizes in the range 5–50 nm[199] , polystyrene beads [200] ion exchange resine [201] are used as solid template.

1.4.2. Isomorphous substitution in micro/mesoporous composite material

The incorporation of transition metals into silicate framework generates or moderates catalytically active sites in the porous material. Progress in composite material from 1990 to till date involved the syntheses of Al containing material. There very few report on Ti-, V- containing mesoporous silicates with zeolitic character (combined micro-mesoporous material or micro/mesoporous composites) addressing improved diffusion rates for transport in catalytic process [202], better hydrothermal stability [186], controlled leaching rates for a constant and gradual release of active component [203, 204]. In case of Sn containing composite material, Jinka et al. have reported mesoporous Sn-MFI by templating method.

1.5. PHYSICO-CHEMICAL CHARACTERIZATION

Characterization of the microporous, mesoporous and Micro/mesoporous composite molecular sieve by means of analytical techniques is far most important to identification of type material and to know its properties. A number of techniques have been used to characterize different types of molecular sieve materials. Each technique is unique by itself and provides important information for the understanding of different structural/compositional features. Among all, the most commonly used characterization techniques are as follows:

- Powder X-ray diffraction
- Surface area and porosity measurement by nitrogen adsorption
- Transmission electron microscopy (TEM)
- Scanning electron microscopy (SEM)
- Diffuse reflectance UV-Vis spectroscopy
- Fourier transform infrared (FTIR) spectroscopy
- X-ray photoelectron spectroscopy
- Nuclear magnetic resonance (NMR) spectroscopy
- Thermal gravimetric analysis (TGA)
- Thermal programmed desorption of ammonia (TPD-NH_3)
- Atomic absorption spectroscopy (AAS)

1.5.1. Powder X-ray diffraction

X-ray diffraction is one of the non-destructive techniques and does not require elaborative work for the sample preparation. For characterization of microporous material, Powder X-ray diffraction is the most important and commonly used tool to monitor structure, phase purity, degree of crystallinity and unit cell parameters of crystallite materials. Microporous solids generally show characteristic peaks in the 2 theta range of 5-50º. Isomorphous substitution of a heteroatom in the framework of the molecular sieves can be easily predicted by calculating the changes in the unit cell parameters and unit cell volume. This is one of the indirect ways to confirm isomorphous substitution [206].

Several important structural features of mesoporous molecular sieve are obtained from XRD data such as: identification of the phase/s, phase purity, unit cell

parameter and orderness of mesoporous molecular sieves. XRD patterns of mesoporous phase exhibit peaks in the low angle region, the most intense peak being the (100) for MCM-41 and (211) for MCM-48 reflection. The unit cell parameter 'a_o' can be calculated using the relation $2d_{100}/\sqrt{3}$ for MCM-41 and $d_{211}\sqrt{6}$ for MCM-48. The information on wall thickness of desired phase can also be deduced.

For characterization of Micro/mesoporous composite molecular sieve, similar information as discussed above is deducted.

1.5.2. N_2 adsorption/desorption

Molecular sieves possess uniform pores and channels with large void volume which is accessible to molecules of comparable size. Adsorptions of gaseous molecules or liquids at lower temperature and high pressure yield information about the hydrophilicity/hydrophobicity, surface area, pore dimensions and pore volume while desorption of the same gives information about pore size distribution of the mesoporous molecular sieves. The adsorption of nitrogen measured by Brunauer-Emmett-Teller (BET) equation at low pressure (10-4 Torr) and liquification temperature of N_2 (-196^{o}C) is the standard method for the determination of surface area, pore volume and pore size distribution of molecular sieves[207]. Relation between the amount adsorbed and the equilibrium pressure of the gas at constant temperature is defined by the adsorption isotherm. N_2-adsorption-desorption isotherms of microporous and mesoporous molecular sieve are of the type I and IV isotherm respectively. [4,121] BET surface area was calculated using the conventional BET equation. Mesopore size distribution and pore volume was calculated using Barrett-Joyner-Halenda (BJH) model and t-plot analysis were used to determine the micropore surface area and pore volume.

1.5.3. Transmission electron microscopy (TEM)

Transmission electron microscopy (TEM) is one widely used to evaluate the microstructure and pore structure of molecular sieve. HRTEM (High Resolution Transmission Electron Microscopy) can be successfully used to examine the microstructural feature of mesoporous molecular sieves [208]. TEM gives a direct, precise and simultaneous measurement of the orderness, pore diameter and pore

thickness. In addition to structural characterization, it can also be used to detect the location of metal clusters and heavy cations in the framework [208].

1.5.4. Scanning electron microscopy (SEM)

Scanning electron microscopy (SEM) is one of the most widely used techniques for characterization of size and morphology of the molecular sieve. SEM also provides information about not only topographical information like optical microscopes do, but also the presence of any amorphous phase in the samples and chemical composition near the surface. Electron microscopes are instruments, which uses beam of highly energetic electrons to create magnified images of tiny crystals or particles. An electron gun emits a beam of high energy electron that travels through a series of magnetic lenses, which focus the electrons to a very fine spot or sample. The main difference between SEM and TEM is that SEM sees contrast due to the topology of a surface, whereas TEM projects all information in a two dimensional image, which is of nanometer resolution.

1.5.5. Diffuse Reflectance UV-Vis Spectroscopy

The diffuse reflectance UV-Vis spectroscopy is known to be a very sensitive and useful technique for the identification and characterization of the metal ion coordination and its existence in the framework or extra-framework position of metal containing molecular sieves. UV-Vis Spectroscopy technique is specially used to determine the coordination state of transition metal (Ti, V and Sn) ions substituted in the silica matrix, involving ligand-to-metal charge transfer transitions. The position of "ligand-to-metal charge transfer" (L→M) band depends on the ligand field symmetry surrounding the metal center and the electronic transitions from ligand-to-metal require higher energy for a tetra-coordinated metal ion than for a hexa-coordinated one. For most of the isomorphously substituted microporous and mesoporous metallo-silicate (particularly Ti, Sn, V-containing) molecular sieves, transitions in the UV region (200-400 nm) are of prime interest.

1.5.6. Fourier-Transform Infrared (FTIR) Spectroscopy

Fourier transform infrared (FTIR) spectroscopy deals with the vibration of chemical bonds in a molecule at various frequencies depending on the elements and types of bonds

The FTIR spectroscopy in the framework region (400-1300 cm^{-1}) provides additional information about the structural details including isomorphous substitution in molecular sieves, whereas the hydroxyl region vibrations (3000-4000 cm^{-1}) help in the determination of different acid sites (Brönsted and Lewis) [209a] and silanol groups. [209b]. Acidic and basic properties as well as its strength in molecular sieves can also be determined by FTIR spectroscopy using CO_2, ammonia, pyridine, triphenylphosphine, etc. as probe molecules. [209 c]. IR spectroscopy along with powder XRD can be used as a supplementary tool for structure elucidation.

1.5.7. X-ray photoelectron spectroscopy

X-ray photoelectron spectroscopy (XPS) is widely used for probing the electronic structure of atoms, molecules and condensed matter. When an X-ray photon of energy $h\nu$ is incident on a solid matter, the kinetic energy (E_k) and the binding energy (E_b) of the ejected photoelectrons can be related as follows: $E_K = h\nu + E_b$

This kinetic energy distribution of the photoelectrons is fabricated by a series of discrete bands, which symbolizes for the electronic structure of the sample. The core level binding energies of all the elements (other than H and He) in all different oxidation states are unique, which provides instant detection of the chemical composition of the sample after a full range scan. However, to account for the multiplet splitting and satellites accompanying the photoemission peaks, the photoelectron spectra should be interpreted in terms of many-electron states of the final ionized state of the sample, rather than the occupied one-electron st ates of the neutral species [210-211].

1.5.8. Nuclear magnetic resonance (NMR) spectroscopy

Nuclear magnetic resonance spectroscopy, both in the liquid and the solid state, is a very important tool for understanding the structure of zeolites, for determining the active species formed at the molecular level during synthesis (*in situ*), and also to characterize the local environment of framework metal ions in solids. Lippama *et al*. showed that ^{29}Si MAS NMR spectra are very sensitive to the nature and chemical environment of the atoms. MAS NMR of ^{27}Al, ^{51}V, etc. has also been extensively studied to characterize the incorporation of heteroatom in the framework

by determining the local environment of Al, Ga, V, etc in corresponding metallosilicates

The main application of NMR studies in zeoltype material are as follows

Evaluation of the environment of the silicon framework atoms,

Determination of framework *n*Si/*n*Al ratio,

silicon and aluminium ordering,

Identification of framework and non-framework aluminium,

Incorporation of metals into molecular sieves and

Determination of acidity of hydroxyl groups.

1.5.9. Thermal gravimetric analysis (TGA)

Thermo gravimetry analysis is a technique measuring the variation in mass of a sample when it undergoes a temperature scanning in a controlled atmosphere. Thermal analysis is widely used to study the structural stability molecular sieves. It also provides information about temperature required for the removal of adsorbed water, decomposition of the occluded organic cations in the pores and channels of mesoporous molecular sieves and dehydroxylation at higher temperatures to produce Lewis acid sites. Data obtained from TG, DTA and DTG helps in evaluating the thermal properties of molecular sieves. The shape and splitting of the endotherms (low temperature) helps to identify the location of water molecules and also helps in studying the kinetics of dehydration. The temperature at which an exotherm appears in the DTA after the loss of water molecules, gives helpful information about the temperature required to remove the template molecules from the pores of the molecular sieves during calcinations. Phase transformations (if any) can also be understood from the exotherms obtained at higher temperatures. The amount lost in the given temperature range also gives the estimate of the concentration of that species.

1.5.10. Thermal programmed desorption of ammonia (TPD-NH_3)

The strength, the type and the amount of acidity can be determined using probe molecules by temperature programmed desorption (TPD) and infrared (IR) spectroscopy techniques.

In TPD of NH_3 technique, NH_3 is initially allowed to adsorb on an activated solid catalyst at a defined temperature. The adsorbed molecules are then allowed to desorbs in a flow of N_2 or Ar by heating the catalyst material in a programmed manner. The amount of ammonia desorbed from the catalyst estimated by a TCD close to the reactor outlet. Based on the amount of base molecules desorbed, the total acidity and the relative strength of the acid sites can be determined. This technique can be used to characterize the acid sites present in solids such as zeolites and mesoporous materials.

In a TPD spectrum, one or more peaks may be observed, the ones at low temperatures corresponding to NH_3 desorbing from the weaker acidic sites and the ones at higher temperatures corresponding to the stronger acidic sites. The areas under these peaks give information about the amount of acidic sites of different acidity, whereas the peak (–maximum–) temperatures give information about the relative acid strengths. The TPD curves can be deconvoluted into individual peaks and the areas under the peaks are converted into mmol of NH_3 per g catalyst based on injection of known volumes of NH_3 at similar conditions.

1.6. CATALYTIC APPLICATION OF Sn-CONTAINING MOLECULAR SIEVE.

Catalysts are substances that facilitate a chemical reaction by lowering the energy barrier of the reaction pathway and thus increasing the reaction rate. Heterogeneous acidic catalysts are of great importance for the environmentally benign synthesis of bulk and fine chemicals.

Acidic molecular sieves have been attracting great interest because they occupy a special place in the realm of heterogeneous catalysts and green chemistry as they have proved to be more economical, often produce products with better quality and provides clean environment when compared with conventional homogeneous catalysts. By virtue of higher electronegativity and atomic size, the incorporation of Sn (IV) in the tetrahedral silica frameworks of zeolitic material is expected to enhance the Lewis acidity of the material [15]. Tin containing molecular sieves have shown potential applications as sorbent [86] and catalyst for various reactions of commercial importance like Baeyer Villiger (BV) reaction [58], Meerwein-Ponndorf-Verley

(MPV) reactions [112], phenol hydroxylation [100,103], intramolecular carbonyl-ene reactions [18], oxidation of ethyl benzene [101] and vapor phase aniline alkylation [110].

Similarly, substitution of Sn in mesoporous silicate (MPS) offer a broad range of potential applications where adsorption/diffusion of bulky substrates have no limitations as observed in case of microporous molecular sieves. These material have shown excellent catalytic performance for reaction [166-176] such as hydroxylation of phenol and 1-napthol, epoxidation of norborne, MPV reaction , Mukaiyama-type aldol condensation, BV , transesterfications , synthesis of poly(L-lactic acid) [26], acylation of aromatics and heteroaromatics , selective oxidative dehydrogenation of cyclohexane , benzylation of aromatics and conversion of biomass products into fine chemicals .

1.7. OBJECTIVE OF RESEARCH

In the present work, the studies were aimed at synthesis, characterization and catalytic application of tin-containing microporous and mesoporous molecular sieves The data obtained by optimization of synthesis parameters and its influence on product quality represented a convenient vehicle for the preparation of tailor-made material for a particular application. The following important objectives were taken into consideration:

I. Synthesis of Sn containing molecular sieves with different topology :
   a. Microporous Molecular sieves : -
      - Synthesis of medium pore tin silicalite-1 (Sn-MFI) by Dry Gel Method.
      - Synthesis of Al^{3+} inserted Sn-MFI (Al-Sn-MFI).
      - Synthesis of large pore tridirectional Sn –BEA in fluoride medium from unseeded gels.
      - Optimization of synthesis parameters for Sn-MFI and Sn-BEA.
   b. Micro/Mesoporous composite material

- Synthesis of Micro-/meso-porous stannosilicate composites (Sn-MFI/MCM-41) via two-step crystallization process.
- Optimization of process parameters

II. Physico-chemical characterization by powder XRD, SEM/TEM, FTIR, UV-Vis, TG/DTG, TPD, XPS, N_2 adsorption/desorption , elemental analysis.

III. Catalytic applications :-

a. For microporous molecular sieve - Vapor phase methylation of aniline

b. For mesoporous and micro/meso composites - hydroxyalkylation of p-Cresol.

1.8. OUTLINE OF THESIS

The thesis describes the synthesis, characterization and catalytic application of tin-containing molecular sieves viz. Sn-MFI, Sn-BEA, Sn-MCM-41 and Sn-MFI/MCM-41 composite. The thesis would be presented in seven (7) chapters and a brief summary is given below.

CHAPTER 1: INTRODUCTION

Chapter 1 provides a general introduction related to synthesis routes, characterization techniques and catalytic applications of microporous, mesoporous and micro-/mesoporous composite molecular sieves with and/or without Sn. A review of the literature to date in these areas is included. The objectives and scope of the research work are outlined briefly at the end of this chapter.

CHAPTER 2: SYNTHESIS BY DRY GEL CONVERSION METHOD AND CHARACTERIZATION OF MICROPOROUS MEDIUM PORE Sn-MFI MOLECULAR SIEVES

Chapter 2 describes the synthesis of tin silicate –1 (Sn-MFI) molecular sieve by Dry Gel Conversion (DGC) method. The results obtained by varying the synthesis parameters such as crystallization time, temperature, water content at the bottom of

autoclave, molar ratios of $(TPA)_2O$/ SiO_2 and SiO_2/SnO_2 in dry gel are discussed on the basis of crystallization kinetics and physico-chemical properties of Sn-MFI. An *in-situ* high temperature X-ray diffraction studies were carried out to elucidate the thermal expansion properties of silica based MFI type molecular sieves with and without tin. The nature, strength and density of surface acid sites in Sn-MFI molecular sieve with different Sn-content were characterized by N1s XPS of chemisorbed pyridine and details are included in this chapter.

CHAPTER 3: CATALYTIC PERFORMANCE OF Sn-CONTAINING MICROPOROUS MEDIUM PORE Sn-MFI MOLECULAR SIEVES IN VAPOUR PHASE ANILINE N-METHYLATION

Chapter 3 gives an account of heterogeneously catalysed vapour phase N-methylation of aniline over Sn containing microporous molecular sieve synthesized during this investigation. This includes 1) comparison of catalytic performance of Sn-MFI with Al-MFI, Ti-MFI and Si-MFI, 2) optimization of reaction parameter and 3) comparison of catalytic performance of Sn microporous molecular sieves with different topology (Sn-MFI, Sn-MTW and Sn-BEA).

CHAPTER 4: SYNTHESIS, CHARACTREIZATION AND CATALYTI PERFORMANCE OF Al^{3+} INSERTED Sn-MFI (Al-Sn-MFI) MOLECULAR SIEVES IN VAPOUR PHASE ANILINE N- METHYLATION.

Chapter 4 deals with the synthesis and characterization of Al-Sn-MFI with different degree of isomorphous substitution of Al^{3+} in Sn-MFI framework. The samples containing both Lewis and Brønsted acid sites were studied for the investigating the synergy effect between Bronsted and Lewis acidity in alkylation's of aniline with methanol aiming at maximizing the aniline conversion and N-methylaniline selectivity.

CHAPTER 5: OXYANION INDUCED CRYSTALLIZATION , CHARACTERIZATION AND CATALYTIC APPLICATION OF MICROPOROUS LARGE PORE Sn-BEA MOLECULAR SIEVES

Chapter 5 presents the seedless synthesis of microporous stannosilicate molecular sieve with BEA topology (Sn- BEA) using fluoride route. It also describes the influence of molar ratios of TEA^+/ SiO_2 and SiO_2/SnO_2 in initial gel composition on the crystallization period, % crystallinity and physico-chemical properties of Sn-BEA. Various characterization was carried out by Powder XRD, AAS, IR, DRUV-Vis and SEM. The performance of Sn-BEA in BV oxidation reaction is also included in this chapter.

CHAPTER 6: SYNTHESIS , CHARACTERIZATION AND CATALYTIC APPLICATION OF MESOPOROUS Sn-MCM-41 and MICRO-/ MESOPOROUS COMPOSITE Sn-MFI/MCM-41

Chapter 6 describes the preparation and characterization of Sn-containing Micro-/meso-porous. It describes :

- Synthesis and characterization of Micro-/meso-porous stannosilicate composites (Sn-MFI/MCM-41) obtained via two-step crystallization process
- Optimization and establishing synthesis parameter-phase relationship for Sn-MFI/MCM-41 composites.
- Brief study of hydroxyalkylation of p-Cresol over Sn-MCM-41 and Sn-MFI/MCM-41

CHAPTER 7: SUMMARY AND CONCLUSIONS

Chapter 7 summarizes the conclusions reached in this thesis and gives suggestions for further research.

1.9. REFERENCES

[1] J. W. MacBain, The Sorption of Gases and Vapors by solids Rutledge and Sons, London (1932), Ch.5.

[2] K.S.W. Sing, D.H. Everett, R.A.W. Haul, L. Moscou, R. A. Pierotti, J.Rouquerol, T. Siemieniewska, Pure Appl. Chem.; 57 (1985) 603.

[3] F. Schuth, K. Sing, J. Weitkamp, "Handbook of Porous Solids", vol. I–V,Wiley-VCH, Weinheim, (2002).

[4] D. Breck, W. Zeolite Molecular Sieves; Wiley: New York, (1974). 2.

[5] R..M. Barrer, Hydrothermal Chemistry of Zeolites; Academic Press: London, (1982).

[6] R. Szostak, Molecular Sieves-Principles of Synthesis and Identification; Blackie: London, (1998).

[7] R. Szostak, Molecular Sieves-Principles of Synthesis and Identification; Blackie: London, (1984).

[8] E. M. Flanigen, R. L Patton, S. T Wilson, Stud. Surf. Sci. Catal. ; 37 (1988) 13.

[9] W. M. Meier, In Molecular Sieves; Soc. Chem. Ind.: London, 1968; p 10.

[10] Flanigen, E. M. Proc. 5th Int. Conf. Zeolites; Ress, L. V. C. Ed.; Heyden and Sons: London, 1980, p 760.

[11] L. B. Sand, Econ. Geol. (1967) 191.

[12] D. W. Breck, W.G. Eeversole, R. M. Milton, T.B. Reed, T.L.Titomas, J. Am.Chem. Soc.; 78 (1956) 5964.

[13] R.M. Milton, US. Pat. 2 882 244(1959).

[14] D.W. Breck US. Pat. 3 130 007(1964).

[15] D.W. Breck US. Pat. 3 216 789 (1965).

[16] US. Pat. 3 442 795

[17] R.M. Barrer, P.J. Denny, J. Am.Chem. Soc.; (1961) 971.

[18] G.T. Kerr, G.T. Kokotailo, J. Am.Chem. Soc.; 83 (1961) 4675.

[19] R.L. Wadlinger, G.T. Kerr, E.J. Rosinki, US Pat. 3 308 069(1967).

[20] R.J. Argauer, G.R. Landolf, US Pat. 3 702 886 (1972).

[21] P. Chu, US Pat. 3 709 979 (1973).

[22] E.J. Rosinki, M. K. Rubin US Pat. 3 832 449 (1974).

[23] J. Ciric US Pat. 3 972 983 (1976).

[24] C.J. Plank, E.J. Rosinki, M. K. Rubin, US Pat. 3 076 842 (1978).

[25] H.G. Dohety, E.J. Rosinki, C.J. Plank, US Pat. 15 702 (1980).

[26] G.H. Kuel US Pat. 4 495 303(1985).

[27] L.D. Rollman, E.W. Valyocsik, E. Pat. Appl. 15 132 (1981).

[28] P. Chu, J.C. Vartuti, A, J. Herbst, E. Pat. Appl. 127 399 (1984).

[29] J.L. Casci, B.M. Lowe, T.V. Whittam, E. Pat. Appl. 42 226 (1981).

[30] R. Kumar, Catalysis Principles and Application, Ed. B. Viswanathan, S. Sivasanker, A.V. Ramaswamy , Narosa Publishing House, Delhi, (2002) Ch 5

[31] W. Hoelderich, L. Marosi, W.D. Mross and M. Schwarzmann, E. Pat.005 1741 (1982).

[32] (a) Q. Huo, S. Feng and R. Xu, in Zeolites: Facts, Figures, Future, PA. Jacobs, R.A. Van Santen (Eds.), Elsevier, Amsterdam, Stud. Surf. Sci. Catal.; 49 (1989) 291., (b) Q. Huo, S. Feng and R. Xu, I. Chem. Soc. Chem. Commun.; (1988) 1486.

[33] D.M. Bibby and M.P. Dale, Nature; 317 (1985) 157.

[34] (a) E.R.Cooper, C.D. Andrew, P.S. Wheatley, P.B. Webb, P. Wormald R.E. Morries, Natue; 430 (1012) (b) E.R. parnham and R.E. Morries, J. Am. Chem. Soc.;128 (2006) 2204.

[35] Y. Xu, Z. Tian, S. Wang, Y. Hu, L. Wang, B. Wang, Y. Ma, L. Hou, I. Yu and L. Lin, Angew. Chem. tnt. Ed.; 45 (2006) 3965.

[36] EM. Flanigen and R.L. Patton, US Patent 4,073,865 (1978).

[37] H. Kessler, J. Patarin, C. Schott-Darie, Stud. Surf. Sci. Catal.; 85(1994) 75.: J. L Guth, H. Kessler, J.M. Higel, J.M. Lamblin, J. Patarin, A Seive, J. M. Chezeau, R. Wey, ACS Symp. Ser. ; 398(1989) 176.

[38] IL Goth, H. Kessler and R. Wey, in New Developments in Zeolites Science and Technology, Y. Murakami, A. lijima, 1W. Ward (Eds.), Elsevier, Amsterdam, Stud. Surf. Sci. Catal.; 28 (1986) 121.

[39] M.A. Camblor, L.A. Villaescusa and Ml. Diaz-Cabanns, Top. Catal.; 9 (1999) 59.

[40] (*a*) L. B.M. McCusker, C. Baerlocher, A. Merrouche, H. Kessler, Nature;352 (1991) 320. , (*b*) M. A. Camblor, L. A. Villaescusa, M. J. Diaz-Cabanas, Top. Catal.; (1999) 9., (c) J. L. Guth, H Kessler, J.M. Higel, J. M. Lamblin, J. Patarin, A Seive, J.M. Chezeau, R Wey, ACS Symp. Ser. 1989, 398, 176. (*d*) H. Kessler, Stud. Surf. Sci. Catal.; 52(1989) 17., (*e*) J.L. Guth, P. Caullet, A. Seive, J. Patarin, F. Delprato, In Guidelines for Mastering the Properties of Molecular Sieves In Barthomeuf, D.; Derouane, E. G.; Holderich, W. Eds.; NATO ASI Series, No. B221; Plenum: New York, 1990, p 69., (*f*) J.P. Gilson, In Zeolite Microporous Solids: Synthesis, Structure and Reactivity E.G. Derouane, F. Lemos, C. Naccache, F. Ribeiro, F. R. Ed. NATOASI Series, No. C352; Kluwer: Dordrecht, 1992, p. 19.

[41] W. Xu, J. Dong, J. Li, J. Li, F. Wu, J. Chem. Soc., Chem. Commun.; (1990) 755.

[42] M. Matsukata , M. Ogura, T. Osaki, P.R. Hari Prasad Rao, M. Nomura and E. Kikuchi, Top. Catal.; 9 (1999) 77.

[43] P.R.H.P. Rao, M. Matsukata, Chem. Commun.; (1996) 1441.

[44] A. Arnold, M. Hunger, J. Weitkamp, Chem. Eng. Tech.; 73(2001) 1588.

[45] M. Matsukata, K. Kizu, M. Ogura, E. Kikuchi, Cryst.Growth Des.; 1 (2001) 509.

[46] S.G. Thoma, D.E. Trudell, F. Bonhomme, T.M. Nenoff, Micropor. Mesopor. Mat.; 50 (2001) 33.

[47] S.G. Thoma, T.M. Nenoff, Micropor. Mesopor. Mat.; 41(2000) 295.

[48] S.I. Zones, Y. Nakagawa, R.A. van Nordstrand, L.T. Yuen, S.D. Toto, in: R. von Ballmoos, J.B. Higgins, M.M.J. Treacy (Eds.), Proceedings of the 9th international Zeolite Conference, Butterworth-Heinemann, Stoneham, MA, 1993, p. 163.

[49] P. Wu, T. Tatsumi, T. Komatsu, T. Yashima, J. Phys. Chem.B;105 (2001) 2897.

[50] A. Bhaumik, T. Tatsumi, Micropor. Mesopor. Mat.; 34 (2000) 1.

[51] S. Shen, F. Chen, P. S. Chow, P. Phanapavudhikul, K. Zhu, R. B. H. Tan, Micropor. Mesopor. Mat.; 92 (2006) 300.

[52] N.K. Mal, PhD Thesis submitted to University of Pune , 1995.

[53] Z. Gabelica, S. Valange, Micropor. Mesopor. Mat.; 30 (1999) 57.

[54] J.R. Goldsmith, Min. Mag.; 29 (1952) 952.

[55] R.M. Barrer, J.W. Baynham, F.W. Bultitride, W.M. Meier, J. Chem. Soc.; (1959) 195.

[56] E.M. Flenigen, B.M. Lok, R.L. Patton and S.T. Wilson, Proc. 7th Intern. Zeolite Conf.(Y. Murakami, A. Iijima and J.W. Ward, Eds.) Elsevier, Amsterrdam, 1986, p103

[57] A. Thangaraj, M.J. Eapen, S. Sivasanker, and P. Ratnasamy, Zeolite ; 12 (1992) 943.

[58] A. Corma, L. Nemeth, M. Renz and S. Valencia, Nature; 412 (2001) 423.

[59] Z. Wang, M.A. Al-Daous, E. R. Kiesel, F. Li, A. Stein, Micropor. Mesopor. Mat.;120 (2009) 351.

[60] (*a*) M.G. Clerici, Top. Catal.; 13(2000) 373., (*b*) A. Corma, P. Esteve, A. Martinez, J. Catal.;161 (1996) 11. (***c***) R. Hutter, T. Mallatt, A. Baiker, J. Catal.; 153 (1995) 177.

[61] J. C. Bailar, (Eds), Comprehensive Inorganic Chemistry, Pergamon Press, First Edition. 2, 44 (1973)

[62] J. C. Bailar, (Eds), Comprehensive Inorganic Chemistry, Pergamon Press, First Edition. 2, 45 (1973)

[63] J. C. Bailar, (Eds), Comprehensive Inorganic Chemistry, Pergamon Press, First Edition. 2, 46 (1973)

[64] Li, G. J.; Zhang, X. H.; Kawi, S. Sens. Actuators; B 60 (1999) 64.

[65] E.R. Leite, I.T. Weber, E. Longo, J.A. Varela, Adv. Mater.;12 (2000) 966.

[66] G. Sberveglieri, Sens. Actuators; 6 (1992) 239.

[67] D. Kotsikau, M. Ivanovskaya, D. Orlik, M. Falasconi Sens. Actuator B ;101(2004)199.

[68] J.Watson, K. Ihokura, G.S.V. Coles, Meas. Sci. Technol.; 4 (1993) 711.

[69] C.O. Park, S.A. Akbar, J. Mater. Sci.; 38 (2003) 4611.

[70] Y.W. Xiao, J. Y. Lee, A. S. Yu, Z. L. Liu, J. Electrochem. Soc.; 146 (1999) 3623.

[71] M. Behm, J. T. S. Irvine, Electrochim. Acta; 47(2002)1727.

[72] T Hayakawa, M Nogami, Sci Technol Adv Mater.; 6 (2005) 66

[73] S. Ferrere, A. B Zaban, A.J. Gregg, A. J. Phys. Chem. B; 101(1997) 4490.

[74] A. Kay, M. Grätzel, Chem. Mater. 14 (2002) 2930-2935

[75] A. Hultqvist, M. Edoff, T.Torndahl, Prog. Photovoltaics; 19(2011)478.

[76] D. Ruvini, W. K. Upul; T. A. Ali, J. Electroanal Chem.; 646 (2010)124.

[77] J. Minsung, K. Koichi, Mater. Lett.; 63 (2009)777.

[78] P.C.Tseng, M.H. Hsu, M.A, Tsai, C.W. Chu, H.C. Kuo, P. Yu, Org. Elecron.; 12 (2011) 886.

[79] C.H. Chang, M.S. Hsu, P.C. Tseng, P. Yu, W.L. Chang, W.C. Sun, W.C. Hsu, Opt. Express; 19 (2011) 219.

[80] A.M. Gheidari, E.A. Soleimani, M. Mansorhoseini, S. Mohajerzadeh, N. Madani, W. Shams-Kolahi, Mater. Res. Bull.; 40 (2005)1303.

[81] P.Veluchamy, M.Tsuji, T.Nishio, T. Aramoto, H. Higuchi, S. Kumazawa, S. Shibutani, J. Nakajima, T. Arita, H. Ohyama, A. Hanafusa, T. Hibino, K. Omura, Sol. Energ. Mat. Sol. C.; 67 (2001) 179.

[82] Francesco Fringuelli,* Ferdinando Pizzo, and Luigi VaccaroJ. Org. Chem. 2001, 66, 4719-4722

[83] H. Matsuhashi, M. Hino, K. Arata. Appl. Catal. A 59 (1990) 205.

[84] R. Unnikrishnan Pillai, S.D. Endalkachew, J. Mol.Cata. A: Chem.; 191 (2003) 93.

[85] N.K. Mal, M. Sasidharan, M. Matsukata, S. Sivasanker, A.V. Ramaswamy, Stud. Surf. Sci. Catal.; 154 (2004) 2403.

[86] E.W. Corcoran Jr., and D.E.W. Vaughan, US. Pat. 5,192,519 (1993).

[87] I.G.K. Anderson, E.K Anderson, N. Knudsen and E. Skou, Solid State Ionics; 46 (1991) 89.

[88] N. Knudsen, E.K Anderson, G.K. Anderson and E. Skou, Solid State Ionics; 35 (1989) 51

[89] E. Janiszewska, S. Kowalak, W. Supronowicz, F. Roessner, Micropor. Mesopor. Mat.; 117(2009) 423.

[90] B. Notari, Stud. Surf. Sci. Catal.; 47(1987) 413.

[91] F.G. Dwyer and E.E. Jenkins, US. Pat. 3, 941,871 (1976).

[92] G.W. Skeels and E.M. Flanigen, US Pat. Appl. 133 372 (1987).

[93] G.W. Skeels and E.M. Flanigen, EP 321 177 (1989).

[94] G.W. Skeels and E.M. Flanigen, Stud. Surf. Sci. Catal.; 49A (1989) 331.

[95] D.E.W. Vaughan and S.B. Rice, US Patent 4 933 161 (1990) assigned to Exxon.

[96] E.W. Corcoran, Jr. and D.E.W. Vaughan, US Patent, 5 192 519 (1993) assigned to Exxon.

[97] N.K. Mal, V. Ramaswamy, S. Ganapathy and A. V. Ramaswamy, J. Chem. Soc., Chem. Commun.; (1994) 1933.

[98] N. K. Mal, V. Ramaswamy, S. Ganapathy, A.V. Ramaswamy Appl. Catal. A-Gen; 125 (1995) 233.

[99] N.K. Mal, A. Bhaumik, R. Kumar, A.V.Ramaswamy, Catal. Lett.; 33 (1995) 387.

[100] N.K. Mal, A.V. Ramaswamy, J. Mol. Catal. A : Chem.;105 (1996) 149.

[101] N.K. Mal, A.V. Ramaswamy, Appl. Catal. A ;143 (1996) 75.

[102] N.K Mal, V. Ramaswamy, P.R. Rajamohanan, A.V. Ramaswamy, Micropor. Mater.; 12 (1997) 331.

[103] N.K. Mal, A.V. Ramaswamy, Chem. Commun.; 5 (1997) 425.

[104] S. Valencia, A. Corma, US Pat. 5 968 473 (1999).

[105] L. Nemeth, J. Moscoso, N. Erdman, S.R. Bare, A. Oroskar, S.D.Kelly, A. Corma, S. Valencia, M. Renz, Stud. Sur. Sci. Catal.; 154 (2004)2626.

[106] R. Grieken, C. Martos, M. Sánchez-Sánchez, David P. Serrano, J.A. Melero, José Iglesias, A.G. Cubero, Micropor. Mesopor. Mat.; 119 (2009)176.

[107] G. T. Kokotailo, S. L. Lawton, D. H. Olson and W. M. Meier Nature; 272 (1978) 437.

[108] D. H. Olson, G. T. Kokotailo, S. L. Lawton and W. M. Meier, J. Phys. Chem.; 85 (1981) 2238.

[109] www.IZC-structure.org

[110] P.S. Niphadkar, P. N. Joshi, H.R. Gaurav, S.S. Deshpande, V.V.Bokade, Catal. Lett.; 133 (2009) 175-184.

[111] A. Corma, M. T. Navarro, F. Rey, J. Rius, S. Valencia, Angew. Chem.; 113 (2001) 2337.

[112] A. Corma, M. E. Domine, S. Valencia, J. Catal.; 215 (2003) 294.

[113] A. Corma, M. Renz, Chem. Commun.; (2004) 550.

[114] R.K. Iler, The Chemistry of Silica, John Wiley & Sons, 1979.

[115] T.J. Pinnavaia, Science; 220 (1983) 365.

[116] T. Yanagisawa, T. Schimizu, Kuroda, C. Kato, Bull. Chem. Soc. Japan.; 63 (1990) 988.

[117] A. Corma, J. Pérez-Pariente, V. Fornés, F. Rey, D. Rawlence, Appl. Catal.; 63, (1990), 145.

[118] V. Chiola, J.E. Ritsko, C.D. Vanderpool, US Pat. No. 3 556 25 (1971).

[119] F. Di-Renzo, H. Cambon, R. Dutartre, Micropor. Mater.; 10 (1997) 283.

[120] J.S. Beck, C.T. Chu, I.D. Johnson, C.T. Kresge, M.E. Leonowicz, W.J. Roth, J.W. Vartuli, WO Patent 91/11390 (1991).

[121] C.T. Kresge, M.E. Leonowicz, W.J. Roth, J.C. Vartuli, J.S. Beck, Nature; 359 (1992) 710.

[122] J.S. Beck, J.C. Vartuli, W.J. Roth, M.E. Leonowicz, C.T. Kresge, K.D. Schmitt, C.T.W. Chu, D.H. Olson, E.W. Shepp- ard, S.B. McCullen, J.B. Higgins, J.L. Schlenker, J. Am. Chem. Soc.; 114 (1992) 10834.

[123] T. Yanagisawa, T. Shimizu, K. Kuroda, C. Kato, Bull. Chem. Soc. Jpn.; 63 (1990) 988.

[124] S. Inagaki, Y. Fukushima, K. Kuroda, J. Chem. Soc. Chem. Commun.; (1993) 680.

[125] S. Inagaki, A. Koiwai, N. Suzuki, Y. Fukushima, K. Kuroda, Bull. Chem. Soc. Jpn.; 69 (1996) 1449.

[126] A. Corma, Chem. Rev.; 97 (1997) 2373.

[127] U. Ciesla, F. Schuth, Micropor. Mesopor. Mat. ; 27 (1999) 131.

[128] M. Linden, S. Schacht, F. Schuth, A. Steel, K. Unger, J. Porous. Mater.; 5 (1998) 177.

[129] A. Tuel, Micropor. Mesopor. Mat.; 27 (1999) 151.

[130] P. Selvam, S.K. Bhatia, C.G. Sonwane, Ind. Eng. Chem. Res.; 40 (2001) 3237.

[131] Y. Liu, T.J. Pinnavaia, J. Mater. Chem.; 12 (2002) 3179.

[132] J.M. Thomas, Angew. Chem. Int. Ed.; 38 (1999) 3588.

[133] R. Anwander, Chem. Mater.; 13 (2001) 4419.

[134] J.Y. Ying, C.P. Mehnert, M.S. Wong, Angew. Chem. Int. Ed.; 38 (1999) 56.

[135] M. Morey, A. Davidson, H. Eckert, G.D. Stucky, Chem. Mater.; 8 (1996) 486.

[136] P. Xue, G. Lu, Y. Guo, Y. Wang, Y. Guo, J. Mol. Catal. B; 30, (2004), 75.

[137] C. Subrahmanyam, B. Viswanathan, T.K. Varadarajan, J. Mol.Catal. A-Chem.; 226, (2005) 155.

[138] M. Anpo, H. Yamashita, K. keue, Y. Fujii, S.G. Zhang, Y. Ichihashi, D.R. Park, Y. Suzuki, K Koyano, T. Tatsumi, Catal. Today; 44 (1998) 327.

[139] M.De bruyn, M. Limbourg, J. Denayer, G.V. Baron, V. Parvulescu, P.J Grobet, D.E. DeVo s, P.A. Jacobs, Appl. Catal. A-Gen.; 254 (2003) 189.

[140] N. Nishiyama, H. Saputra, D.-H. Park, Y. Egashira, K. Ueyama, J. Membr. Sci.; 218 (2003) 165.

[141] J.W. Lee, D.L Cho, W.G. Shim, H. Moon, Korean J.Chem.Eng.; 21 (2004) 246.

[142] M. Kruk, M. Jaroniec, R. Ryoo, S.H. Joo, J. Phys.Chem. B; 104 (2000) 7960.

[143] S. Shylesh, A.P. Singh, J. Catal.; 228 (2004) 333.

[144] K.K. Kang, W.S. Ahn, J. Mol. Catal. A: Chem.;159 (2000) 403.

[145] A. Michalska, M. Daturi, J. Saussey, I. Nowak, M. Ziolek, Micropor. Mesoporous Mat.; 90 (2006) 362.

[146] A. Y. Khodakov, V. L. Zholobenko, R. Bechara, D. Durand, Micropor. Mesopor.Mat.; 79 (2005) 29.

[147] A. Tuel, and S. Gontier, Chem. Mater.; 8 (1996) 114.

[148] A. Sayari, I. Moudrakovaski, C. Danumah, C.I. Ratcliffe, J.A. Ripmeester, K.F. Preston, J. Phys. Chem.; 99 (1995) 16373.

[149] U. Oberhagemann, I. Topalovic, B. Marler, H. Gies, Stud. Surf. Sci. Catal.; 98 (1995) 17.

[150] S. Liu, H. He, Z. Luan, Klinowski, J. Chem. Soc., Faraday Trans.; 92 (1996) 2011.

[151] C.F. Cheng, and J.J. Klinowski, Chem. Soc., Faraday Trans.; 92 (1996) 289.

[152] Z.Y. Yuan, S.H. Liu, T.H. Chen, J.Z Wang, H.X. Li, J. Chem. Soc., Chem. Commun.; (1995) 973.

[153] J.L Casci, Stud. Surf. Sci. Catal.; 85 (1994) 329

[154] A. Sayari, Chem. Mater.; 8 (1996) 1840.

[155] C.T. Kresge, M.E. Leonowicz, W.J. Roth, J.C. Vartuli, U.S. Patent 5 250 282 (1993).

[156] A. Corma, M.T. Navarro, J. Perez-Pariente, J.Chem.Soc.,Chem. Commun.; (1994) 147.

[157] K.M. Reddy, I.L. Moudrakovski, A. Sayari, J.Chem.Soc.Chem. Commun.; (1994) 1059

[158] Z. Luan J. Xu, H. He, J. Klinowski, L. Kevan, J. Phys. Chem.; 100 (1996) 19595.

[159] A. Corma, M.T Navarro, Perez-Pariente, F. Sanchez, Stud. Surf. Sci. Catal.; 84 (1994) 69.

[160] T.J. Pinnavaia, P.T. Tanev, J. Wang, W. Zhang, Mater. Res. Soc. Symp. Proc.; 371 (1995) 53.

[161] J.S. Reddy, P. Liu, A. Sayari, Appl. Catal. A-Gen.; 148 (1996) 7.

[162] W. Zhang, T.J. Pinnavaia, Catal. Lett.; 38 (1996) 261.

[163] W. Zhang, J. Wang, P.T. Tanev, T.J. Pinnavaia, T.J., Chem. Commun.; (1996) 979.

[164] N. Ulagappan, and C.N.R. Rao, J. Chem. Soc., Chem. Commun.; (1996) 1047.

[165] D. Zhao, and D.J Goldfarb, J. Chem. Soc., Chem. Commun.; (1995) 875.

[166] K. Chaudhari, T.K. Das, P.R. Rajmohanan, K. Lazar, S. Sivasanker and A.J. Chandwadkar, J. Catal.; 183 (1999) 281.

[167] P. P. Samuel, S. Shylesh and A.P. Singh, J. Mol. Catal. A: Chem.; 266 (2007) 11.

[168] U.S Taralkar, P Kalita, R. Kumar, P.N. Joshi, Appl. Catal. A-Gen.; 358 (2009) 88.

[169] A. Corma, M.T. Navarro, L. Nemeth, M. Renz, Chem. Commun.; (2001) 2190.

[170] V. Ramaswamy, P. Shah, K. Lazar and A. V. Ramaswamy, Catal. Surveys from Asia;12 (2008) 283.

[171] T.M. Abdel-Fattah, T.J. Pinnavaia, Chem. Commun.; (1996) 665.

[172] N. Candu, S. Coman, V.I. Parvulescu ,J. E. Haskouri , P. Amoros, D. Beltran, Top Catal.; 52 (2009) 571.

[173] K. Bachari , O. Cherifi Appl. Cata. A-Gen.; 319 (2007) 259.

[174] A. Corma , M.Renz ,M. Susarte, Top. Catal. 52 (2009) 1182.

[175] M. Renz, T. Blasco, A. Corma, V. Fornés, R. Jensen, L. Nemeth, Chem. Eur. J.; 8 (2002) 4708.

[176] T.R. Gaydhankar, P.N. Joshi, P. Kalita, R. Kumar, J. Mol. Catal. A: Chem.; 265 (2007) 306.

[177] M. Hartmann, Angew. Chem. 2004, 116, 6004-6006, Angew. Chem. Int. Ed.; 43 (2004) 5880.

[178] J. Perez-Ramirez, C. H. Christensen, K. Egeblad, J.C. Groen, Chem. Soc. Rev.; 37 (2008) 2530.

[179] M.E. Davis, Nature; 364(1993) 391.

[180] A. Corma, V. Fornes, M.T. Navarro, J, Perez-Pariente, J. Catal.; 148 (1994) 569.

[181] P.J. Branton, P.G. Hall, K. S.W. H. Sing, Reichert, F. Schuth, K.K. Unger, J. Chem. Soc., Farady Trans.; 90 (1994) 2965.

[182] M. J. Verhoef, J.A. Peters, H. van Bekkum, Micropor. Meesopor. Mat.; 27 (1999) 365.

[183] K. R. Kloetstra, H.W. Zandbergen, J.C. Jansen, H. van Bekkum, Microporous Mater.; 6, (1996) 287.

[184] K.R. Kloetstra, J.C. Jansen, H. van Bekkum, Am. Chem. Soc., Div. Pet. Chem.; 41(1996) 412.

[185] K.R. Kloetstra, H. van Bekkum.; J.C. Jansen, J. Chem. Soc., Chem. Commun.; (1997) 2281.

[186] A. Karlsson, M. Stocker, R. Schmidt, Micropor. Mesopor Mat.; 27 (**1999**) 181.

[187] L. Huang, W. Guo, D. Peng, X. Zhiyuan, L. Quanzhi, J. Phys. Chem. B.; 104 (2000) 2817.

[188] W. Guo, C, Xiong, L. Huang, Q. Li, J. Mater, Chem.; 11 (2001) 1886.

[189] (*a*) P. Prokesova, S. Mintova, J. Cejka, T. Bein, Micropor. Mesopor. Mate.; 64 (2003) 165., (*b*) Y.D. Xia, R. Mokayo, J. Mater. Chem.; 14(2004) 863., (*c*) S. Ramirez, J.M. Dominguez, L.A. Garcia, M.A. Mantilla, C.A. Flores, J. Salmones, D. Jeronimo, Petroleum Science Techanology; 22(2004) 119., (*d*) H. Gies, S. Grabowski, W. Grunert, Stud. Surf. Sci. Catal.; 154(2004) 2869.,(e) P. Prokesova, N. Petkova, J Cejka, S. Mintova, T. Bein, COLLECTION OF CZECHOSLOVAK CHEMICAL COMMUNICATIONS; 70(2005) 1829., (*f*) *M*. Mazaj, N. Z. Logar, G. Mali, N.N. Tusar, I. Arcon, A. Ristic, A. Recnik, V. Kaucic Micropor. Mesopor. Mate.; 99 (2007) 3., (*g)* Y. Wang, D. Cui, Q. Li, Micropor. Mesopor. Mate.; 142 (2011) 503., (*h*) J. Zhou,

Z. Hua, J. Zhao, Z. Gao, S. Zeng, J. Shi, J. Mater. Chem.; 20 (2010) 6764., (*i*) L. Liu, G. Xiong, X. Wang, J. Cai, Z. Zhao, Micropor. Mesopor. Mate.; 123 (2009) 221., (*J)* Z. Zhou, J. Lu, S.F. Wu, J.L. Zhou, J.Q. Wang, J. Inorg. Mater.; 24 (2009)325.

[190] J. Čejka, S. Mintova, Catal. Rev.; 49 (2007) 457.

[191] S. Mintova, J. Čejka, Stud. Surf, Scien. Catal.; 168 (2007) 301.

[192] A. Bordoloi, B.M. Devassy, P.S. Niphadkar, P.N. Joshi, S. B. Halligudi , J. Mol. Catal. A-Chem.; 253 (2006) 239.

[193] Y. Liu, W, Zhang and T. J. Pinnavaia, J. Am. Chem. Soc.; 122 (2000) 8791.

[194] Z. Zhang, Y. Han, F.-S. Xiao, S. Qiu, Y. wei, J. Am. Chem. Soc.; 123(2001) 5014.

[195] P. Prokesova, S. Mintova, J Cejka, T. Bein Micro. Meso. Mater.; 64 (2003)165.

[196] F.S. Xiao, Top. Catal.; 35(2005) 9.

[197] (a) I.I. Ivanova, A.S. Kuznetsov, V.V. Yuschenko, E.E. Knyazeva, Pure Appl. Chem.; 76 (2004) 1647. (*b*) I.I. Ivanova, A.S. Kuznetsov, O.A. Ponomareva, V.V. Yuschenko, E.M. Knyazeva, Stud. Surf. Sci. Catal. Elsevier: Amsterdam, 158 (2005) 121.

[198] C Zhang, Q. Liu, Z. Xu, K. Wan, Micropor. Mesopor, Mat.; 62 (2003)157.

[199] (*a.*) C.J.H. Jacobsen, C. Madsen, J. Houzˇvicˇka, I. Schmidt, A. Carlsson, J. Am. Chem. Soc.; 122 (2000) 7116., (*b*) A.H. Janssen, I. Schmidt, C.J.H. Jacobsen,A.J. Koster, K.P. de Jong, K.P. Micropor. Mesopor. Mat.; 65 (2003) 59.

[200] B.T. Holland, L. Abrams, A. Stein, J. Am. Chem. Soc.;121(1999) 4308.

[201] L. Tosheva , V. Valtch, J. Sterte, Micropor. Mesopor. Mat.; 35(2000) 621.

[202] J. Lee, Y. Park, P. Kim, J. Yi, J Mater. Chem.; 14 (2004) 1050.

[203] M. Kruk, M. Jarnoniec, S. H. Joo, R. Ryoo, J. Phy. Chem. B; 107 (2002) 2205

[204] P. Van der Voort, P.I. Ravikovitch, K. P. De Jong, M. Benjelloun, E. Van Bavel, A. H. Janssen, A. v. Neimark, B. M. weckhuysen, E. F. Vansant, J. Phy. Chem. B;106(2002) 5873.

[205] K.M. Jinka, S.C. Lee, S. E. Park, R.V. Jasra, Stud. Surf. Sci. Catal.; 174 B (2008) 1187.

[206] (*a*) R. C. Rau, In *Advances in X-ray Analysis*, Mueller, W. M. Ed: Sir Isaac Pitman and Sons Ltd.: London, 1962*, Vol. 5*, p 104., (*b*) L.S. Birks, H. Friedman, J. Appl. Phys.; 17 (1946) 687.

[207] S Brunauer, P.H. Emmett, E. Teller, J. Am. Chem. Soc.; 60 (1938) 309.

[208] V. Alfredsson, M. Keung, A. Monnier, G.D. Stucky, K.K. Unger, and F. Schüth, J. Chem. Soc., Chem. Commun.; (1994) 921.

[209] (*a*) P.A. Jacobs, W.y. Martier, Zeolites 2(1982) 226.: *b.* B. Notari, Stud. Surf. Sci. Catal.; 37(1987) 413., (*c*). Ryczkowski, J. Catal. Today; 68(2001) 263.

[210] C.S. Fadley, Electron Spectroscopy: Theory, Techniques and Applications, Vol. 2,Eds: C.R. Brundle, A. D. Baker, Academic Press, New York, 1978.

[211] W.N. Delgass, T.R. Hughes, C.S. Fadley, Catal. Rev.; 4 (1970) 179.

CHAPTER 2

SYNTHESIS BY DRY GEL CONVERSION METHOD AND CHARACTERIZATION OF MICROPOROUS MEDIUM PORE Sn-MFI MOLECULAR SIEVES

2.1. INTRODUCTION

MFI type molecular sieve is medium pore high silica zeolitic phase. Most common route for synthesis of isomorphously substituted MFI type zeolite is the hydrothermal crystallization. Hydrothermal route generally involves the preparation of reactant mixture (hydro gel) comprising source of silica, source of tri or tetravalent metal ions, an organic cation, an alkali metal hydroxide and water. Further, heating the hydro gel in the temperature range of 150-200^{o}C under autogenous pressure (Fig. 2.1). Because of high autogenous pressure, longer crystallization time and tedious downstream process, there is limitation for applying hydrothermal crystallization method to bulk scale preparation. The only method reported in the open literature for the preparation of Sn-MFI is the hydrothermal crystallization method [1-3].

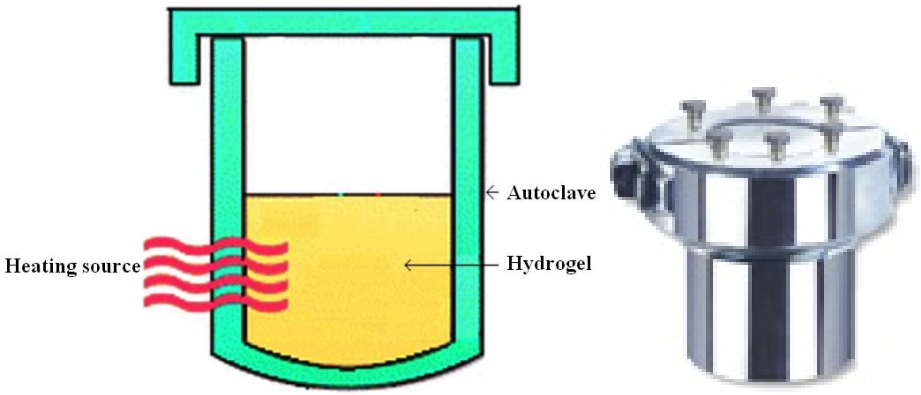

Fig. 2.1. Schematic diagram of stainless-steel autoclave for hydrothermal crystallization method.

Modification in existing conventional method or development a novel method for eco-friendly, cost-effective synthesis of zeolites and related molecular sieves is an interesting and challenging task for researchers. In 1990, Xu et al [4] developed an alternative technique of zeolite crystallization called as Dry Gel Conversion (DGC) Method (Fig. 2.2). A silicate or aluminosilicate hydrogel is dried and the resulting dry gel is converted to zeolite crystals in presence of vapor. The DGC method is classified into two separate methods, (1) a vapor-phase transport method in which a dry gel is crystallized in the vapor of water and structure-direct agent (SDA) like

ethylenediamine, and (2) a steam-assisted crystallization (SAC) method in which a dry gel containing non-volatile SDA molecules like tetrapropylammonium (TPA+) salts is crystallized in steam. Compared to the conventional hydrothermal route, DGC method is advantageous in respects of higher yield, low waste and more convenient procedure. Moreover, in DGC method, solid gels are in contact only with steam and therefore, solid-liquid phase separation phenomenon can be effectively avoided [5-8].

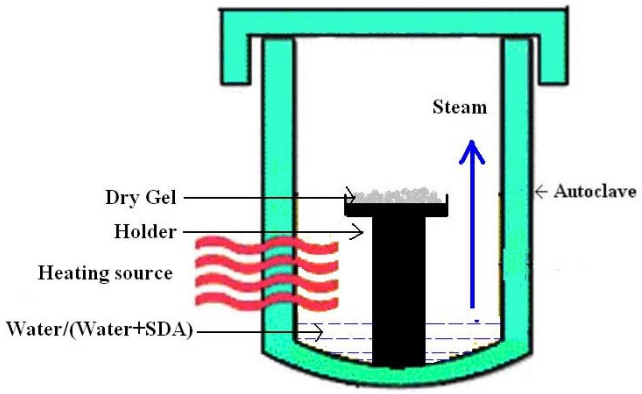

Fig. 2.2. Schematic diagram of the autoclave used for the dry-gel synthesis of molecular sieves.

DGC is one of the efficient routes to synthesize conventional zeolites, reported [8-11] literature on synthesis of zeolite confirmed that DGC method can be applied to synthesis of various zeolites such as ANA, FER, MFI, MOR, BEA, FAU and MWW. Synthesis of isomorphously substituted molecular sieve like B-BEA/MTW/MFI, Ti-BEA/MFI/MWW, Ga-BEA etc were also reported by DGC technique [12-16].

It is, however, noteworthy here that despite the significance of Sn-MFI catalysts, no much effort has been devoted to synthesize Sn-MFI by advantageous DGC route. This chapter describes the systematic studies on the synthesis of Tin Silicate–1 (Sn-MFI) molecular sieve by Dry Gel Conversion (DGC) method and optimization of synthesis parameters such as crystallization time, temperature, water content at the bottom of autoclave, molar ratios of $(TPA)_2O/ SiO_2$ and SiO_2/SnO_2 in dry gel. The results related to the physico-chemical properties of Sn-MFI molecular sieves are also presented and discussed in this chapter.

2.2. EXPERIMENTAL

2.2.1. Synthesis of Tin –silicalite-1 (Sn-MFI) by Dry Gel Conversion Method

Synthesis runs were carried out using dry gel of various composition in special setup of autoclave (Fig 2.2). The detail specifications of the reactants used in synthesis are given in Table 2.1.

Table 2.1. Specification of the reactants

Sr. No.	Chemical name	Chemical formula	Chemical composition	Company
1.	Tetra ethyl orthosilicate (TEOS)	$Si(OC_2H_5)_4$	98 % $Si(OC_2H_5)_4$	Aldrich
2.	Tetra propyl ammonium hydroxide (TPAOH)	$(C_3H_7)_4$ NOH	20 % TPAOH in aqueous solution	VP Chemical
3.	Tin Chloride	$SnCl_4.5H_2O$	98% $SnCl_4.5H_2O$	Loba

Tin Silicalite-1 samples were prepared from synthesis gel having the following general molar composition:

SiO_2: 0.0066-0.033SnO_2: 0.15-0.23 $(TPA)_2O$

In typical synthesis, 53.06 g of tetraethyl orthosilicate (TEOS) was slowly added to 116.7 g of tetra propyl ammonium hydroxide under vigorous stirring. The stirring was continued for 3 hours. To this, 0.89 g of $SnCl_4$ $5H_2O$ dissolved in 10 ml distilled water was added with constant stirring. The final mixture was further stirred for 2 hours. Then the gel was subjected to drying at 80^oC. A white solid powder obtained was ground into a fine powder. An appropriate quantity of this dry gel powder was weighed and poured into small Teflon cups. Each cup was then placed in a separate autoclave (Fig. 2.2). Appropriate quantity of water acting as a source of steam was placed at the bottom of each autoclave in such manner that dry gel never came into the direct contact with water. Each autoclave after being sealed was placed in an air-heated oven maintained at 170^oC. The time when autoclave attained the desired temperature was taken as a zero point in the crystallization process. The autoclaves were taken out of the oven one by one at scheduled time intervals,

quenched to room temperature and thus the extent of crystallization as a function of crystallization period was monitored. The sample was taken out from the cup, filtered, washed thoroughly with distilled water and dried at 110^{o}C followed by calcinations at 550^{o}C for 12 hour.

Similarly, Sn-free Silicalite-1 was prepared using dry gel having molar gel compositions SiO_2:0.23$(TPA)_2O$. For comparison purpose, Sn-MFI with molar ratio of SiO_2/SnO_2 =50 was prepared by employing conventional hydrothermal method described elsewhere [2].

2.2.2. Characterization

The samples prepared by DGC method were characterized by different characterization techniques.

2.2.2.1. *Powder X-ray Diffraction*

The powder X-ray diffractograms of as-synthesized and calcined samples were recorded on Rigaku Miniflex diffractometer using a Ni-filtered monochromatic Cu *K*α radiation (l = 1.5406 Å). The microporous materials were scanned between 5-60° (2θ) whereas the mesoporous materials were recorded in the 2θ range 1.5-10°. The samples were prepared as thin layers on glass/aluminum slides, prior to scanning. The degree of crystallinity of solid sample was estimated by the formula:

$$\% \text{ Crystallinity} = \left(\frac{\text{Peak areas of the peaks appearing at } 2\theta = 22.5 \text{ to } 25^{O} \text{ of the test sample}}{\text{Peak areas of the peaks appearing at } 2\theta = 22.5 \text{ to } 25^{O} \text{ in the most crystalline phase obtained during crystallization kinetics.}} \right) \times 100$$

To check the thermal expansion properties of Si-MFI and SnSi-MFI, Powder XRD patterns in the temperature range 100–700^{o}C were collected on the Philips X'Pert Pro 3040/60 diffractometer equipped with Anton Parr HTK 1600 attachment

under static air environment. Sample was mounted on a sample holder (platinum strip) which also served as the heating element. Temperature was monitored by a Pt/Rh – 13% thermocouple which was spot-welded to the bottom of the calibrated stage. XRD Data were collected in the 2θ region 5–60° in a continuous mode with step size of 0.017°, time per step was 20 s, using CuKα radiation and X'celerator as detector. Diffraction patterns were collected at every 50°C interval. A heating rate of 10°C min^{-1} and a soak time of 10 min were applied. Bragg–Brentano geometry was employed. The optics used in the incident beam (primary) were 0.04 radian soller slit, 1/2° divergence slit, 10 mm mask, and 0.02 radian soller slit in the secondary beam path. Collected HTXRD patterns were refined using the Rietveld method [17]. The unit cell parameters at each temperature were refined with the Rietveld method using the GSAS [18] package and the EXPGUI graphical interface [19]. The thermal expansion coefficient along the three crystallographic directions a, b and c were calculated for using the formulae $\alpha_a = \Delta a/(T - RT)a_{RT}$, $\alpha_b = \Delta b/(T - RT)b_{RT}$ and $\alpha_c = \Delta c/(T - RT)c_{RT}$, respectively. The lattice or volume thermal expansion coefficient was calculated using the formula $\alpha_V = \Delta V/(T - RT)V_{RT}$ where T and RT are the typical temperature of the scan and room temperature, respectively; Δa, Δb, Δc and ΔV are the differences in the values of the respective unit cell parameters of the scans at T and RT. The starting atomic coordinates for MFI in the orthorhombic phase were taken from Ref. [20] and framework atoms of the same element type were constrained to have the same isotropic thermal displacement parameters.

2.2.2.2. *Diffuse Reflectance UV-Vis Spectroscopy (DRUV-Vis)*

The detection of type and coordination state of Sn species was carried out using diffuse reflectance UV–vis spectroscopy. Diffuse reflectance UV–vis spectra were recorded in the range 200–600 nm with a Perkin-Elmer Lambda 6 spectrometer equipped with a diffuse reflectance attachment using $BaSO_4$ as the reference. The UV spectra were recorded in the 200-600 nm range.

2.2.2.3. *Scanning Electron microscopy*

The size and shape of particles in the Sn-MFI samples was examined using scanning electron microscope (JSM-5200-Model) after coating with Au-Pd evaporated film.

2.2.2.4. *Nitrogen Adsorption Measurements*

A conventional volumetric nitrogen adsorption apparatus (Micromeritics ASAP 2010 system/ NOVA-1200[Quanta chrome, USA]) was used for evaluating the textural properties. The calcined sample was degassed at 300^{o}C for 10 h at 0.00133 Pa, prior to the measurements. The sample was then cooled to –196^{o}C using liquid nitrogen and the sorption of nitrogen was carried out at different equilibrium pressures. The specific surface area of the sample was calculated using BET method.

2.2.2.5. *Chemical analysis*

Bulk SiO_2/SnO_2 molar ratio in final calcined samples was calculated by determining SiO_2 and SnO_2 contents in product by combination of gravimetric analysis and atomic absorption spectrometry (Varian SpectrAA 220 FS).

2.2.2.6. *X-ray Photoelectron spectroscopy*

Surface SiO_2/SnO_2 molar ratio in the samples and nature of tin in MFI structure was determined using X-ray Photoelectron Spectrometer [V. G. Scientific (UK) ESCA-3000). The X-ray source used was Mg Kα (hv = 1253.6eV). The spectrometer was operated at 12 mA and 12.5 kV and the analyzer at a constant pass energy mode (50 eV). The residual gas pressure in the spectrometer chamber during the data acquisition was less than $1.3X10^{-7}$ Pa.

The nature, strength and density of surface acid sites in Sn-MFI molecular sieves with different Sn-content were also characterized by XPS, in particular, N 1s high resolution photoelectron peak of chemisorbed pyridine. The detail experimental procedure for characterize of surface acidity by XPS is;

The calcined sample was first mounted on a stainless steel sample holder. Sample with holder were activated at 400^{o}C for 4 hour under high vacuum system and

then cooled down to room temperature under vacuum. After saturating the activated samples with pyridine vapors, desorption of pyridine was carried out under vacuum for 2 hour at desired temperature. When the experiment was over then sample was transferred into the introduction chamber of the spectrometer via a glove box/nitrogen blanket. The measurements were performed in the following sequence: Si 2p, Al 2p, O 1s, Sn $3d_{3/2}$, Sn $3d_{5/2}$ and N 1s.

The intensities of various XPS lines were determined by using linear background subtraction and integration of peak areas. N 1s peaks were deconvoluted into one, two, or three components by keeping the full width at half-maximum (FWHM) constant in a particular spectrum and assuming that each peak has a Gaussian shape. Deconvolution of N 1s peaks were carried out using XPS peak fitting program (XPSPEAK version 4.1). In this deconvolution operation, the FWHM value adopted for all component peaks of N 1s line was 2.2-2.4 eV on basis of FWHM values of Si 2p, Al 2p, O 1s, Sn $3d_{3/2}$ and Sn $3d_{5/2}$ in our studied and reported values used for deconvoluting N 1s peak [21,22].

The ratios of atomic concentration (Si/Sn and N/Sn) on the surface of the sample were calculated from the corresponding XPS peak area and sensitivity factor.

2.2.2.7. *Temperature Programmed Desorption of Ammonia*

The overall acidity and acid strength associated with sites were measured by Temperature Programmed Ammonia Desorption (TPAD) using a Micromeritics AutoChem (2910, USA) equipped with thermal conductivity detector. Prior to the measurements, sample was dehydrated at 500^{o} C in He (30 cm^3 min^{-1}) for 1 h. The temperature was then decreased to 50 ^{o}C and then NH_3 was allowed to adsorb by exposing sample to a gas stream containing 10% NH_3 in He for 1 h. It was then flushed with He for another 1 h. The NH_3 desorption was carried out in He flow (30 cm^3 min^{-1}) by increasing the temperature up to 450 ^{o}C with a heating rate of 10^{o} C min^{-1}.

2.2.2.8. *Pyridine Infrared spectroscopy*

The nature of acid sites (Bronsted and/or Lewis) in the catalyst was elucidated by ex-situ pyridine-FTIR. After activating a catalyst powder sample at 400 ^{o}C for 2 h, it was cooled down to room temperature under high vacuum. It was then exposed to pyridine vapors for 2 h. The physisorbed pyridine was driven off by activating at 150^{o}C for 2 h under high vacuum. The IR spectra were recorded on a Shimadzu (Model-820 PC) spectrophotometer under DRIFT (Diffuse Reflectance Infrared Fourier Transform) mode.

2.2.2.9. *Catalytic test reaction*

Al-free tin silicates with isolated Sn4+ ions were reported [23, 24] to be active in the hydroxylation of phenol with aqueous H2O2. In the same reaction, negligible activity has been shown by Sn-impregnated molecular sieves and pure SnO2. Therefore, in present studies, the dual purpose of selecting this reaction was to make use of this reaction as a useful characterizing tool for collecting more information on the tin species and investigating the catalytic performance of Sn-MFI catalysts prepared by dry gel conversion method.

Phenol hydroxylation reaction was carried out batch wise in a (25 ml capacity) glass vessel fitted with a condenser and a mechanical stirrer. In a standard run, 0.94 g phenol, 0.1 g of catalyst and 3.5 ml H2O were placed in the reaction vessel. After attaining 80oC, 0.85 g of H2O2 (20 % aqueous solution) was added to the glass vessel. The time at which this addition was completed was refereed to zero hour of the reaction. The total duration of each run was kept as 24 hours. The products were collected at regular interval of time, centrifuged and diluted with a solvent for analyses using a gas chromatograph (Chemito GC1000) equipped with a 30 m long capillary column(BPX-5, Forte).

2.3. RESULTS AND DISCUSSION

2.3.1. Synthesis

Unlike conventional hydrothermal crystallization route to synthesize Sn-MFI, there is no need to accomplish complete hydrolysis of TEOS in the DGC method. The

crucial step involved is to obtain the clear mixture containing sources of Si, Sn and TPAOH (with no formation of precipitate). After drying followed by steam-assisted conversion, the product exhibited no loss of Si and Sn irrespective of its crystallinity. Moreover, in present studies, tin in the dry gel and in the samples recovered at different crystallization periods exhibited tetrahedral coordination. Following section describe systematic study on the influence of synthesis variables on the physico-chemical characteristics of Sn-MFI molecular sieves.

2.3.2. Influence of synthesis parameters on the formation Sn-MFI

The influence of various parameters such as crystallizations time, temperature, water content at the bottom of autoclave, molar ratios of $(TPA)_2O$ / SiO_2 and SiO_2/SnO_2 in dry gel on the formation and physico-chemical properties of Sn-MFI with different SiO_2/SnO_2 molar ratio was investigated by varying one variable at a time.

2.3.2.1. *Crystallization time*

Conversion of dry gel having composition SiO_2: 0.01 SnO_2: 0.25$(TPA)_2O$ to crystalline Sn-MFI was carried out at 170^oC keeping 3.33 ml water at bottom of autoclave per gm of dry gel. Time dependent studies were conducted for investigating the progressive crystallization as a function of time. Fig. 2.3a shows progressive development of Sn-MFI phase with increasing crystallization period.

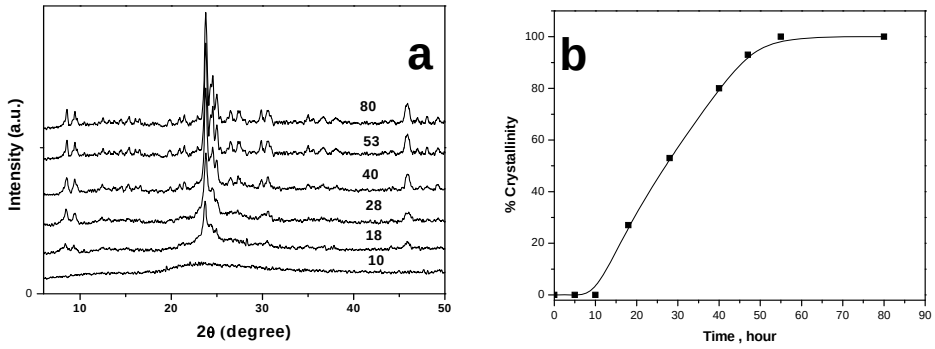

Fig. 2.3. (a) Powder XRD patterns of as-synthesized Sn-MFI samples showing progressive development as function of time (the synthesis time expressed in hours is shown on respective profile), (b) Crystallization kinetic curve.

The powder XRD pattern of sample obtained at 10 hour has shown an amorphous nature. The characteristic peaks of MFI phase start appearing after 18 hour and reach to maximum integrated intensity at 53 hour. Further extension of the crystallization period upto 80 hour has yielded no further improvement in MFI crystallinity or transformation into another phase/s. Hence the % crystallinity of the sample, which was obtained at 53 hour, was assigned as 100. The intermediate samples at 18, 28 and 40 hours have shown 30, 54 and 80 % relative crystallinity respectively. The powder XRD pattern of sample at 53 hours matches well with the reported one [1], confirming the well-crystalline MFI phase with no other impurity. Based on the values of % crystallinity and corresponding crystallization period, crystallization kinetic curve was established and illustrated as Fig. 2.3b**.** This curve exhibited a sigmoidal or S-type shape showing two distinct stages, namely: (i) an induction period when nuclei are formed and (ii) a crystal growth period when nuclei grow into crystals. The induction period may be defined as the time required for nuclei formation and crystal growth period as the time which is necessary for the growth of nuclei to Sn-MFI crystals. It is evident from Fig. 2.3b that, there are different rates of crystallization at different crystallization periods. Moreover, the rate of crystallization was found to decrease as the crystallization process approaches completion, indicated by constancy, i.e., 100% crystallinity.

Thus, the synthesis time was found to be a critical variable in the formation of Sn-MFI. Moreover, the meta-stability region was also found long enough favoring the continuous process for the large-scale production. Similar, time dependant studies were conducted to obtain the optimum synthesis period required for the formation of well crystalline and pure Sn-MFI phase under different synthesis conditions.

2.3.2.2. *Crystallization temperature*

The influence of crystallization temperature on crystallization time and percentage crystallinity was investigated by carrying out synthesis in the temperature range 100 to 200^{o}C using dry gel composition SiO_2: 0.01 SnO_2: 0.25$(TPA)_2O$ and 3.33 ml water at bottom of autoclave per gm of dry gel. Fig. 2.4 shows the crystallization kinetic curves as a function of crystallization temperature.

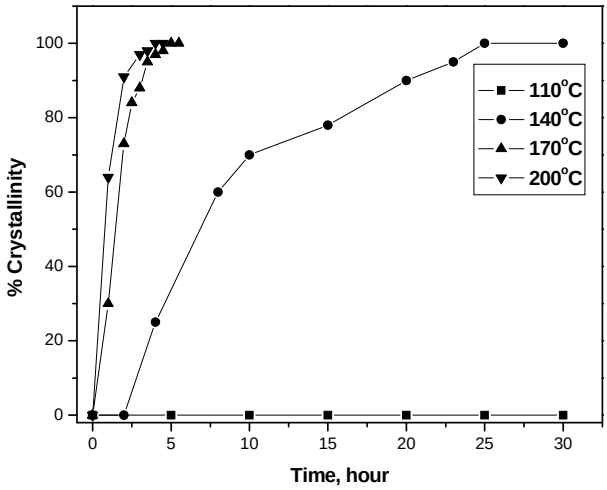

Fig. 2.4. Kinetics of crystallization of Sn-MFI at different temperatures.

The curve shows that the rate of crystallization significantly depends on the temperature, which influences the kinetics of the crystallization process. There was no indication of the formation of MFI phase even upto 30 hours at 110^{o}C. The XRD pattern showed amorphous nature. On increasing the crystallization temperature from 140 to 200^{o}C, there is decrease in both, the induction period and crystal growth period. The rate of any crystallization process is determined by the rate of nuclei formation and the rate of crystal growth. Thus, the formation of nuclei during the induction period is an energetically activated process and since nucleation is the rate determining step during the induction period, the apparent activation energy for nucleation (E_n) and crystallization (E_c) can be calculated from the Arrhenius equation. Fig 2.5 illustrates the Arrhenius plots for the rate of nucleation and crystallization of Sn-MFI by Dry Gel Conversion method.

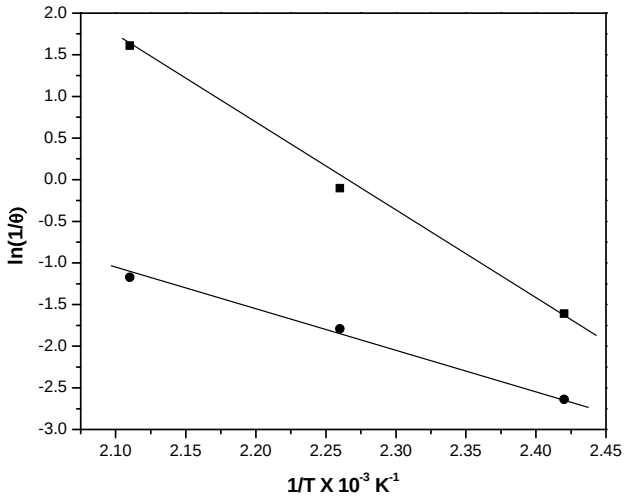

Fig. 2.5. Arrhenius plots for nucleation an crystallization

The calculated apparent activation energy for nucleation (E_n) and crystallization (E_c) are 15 and 9.9 kJ/mol respectively. It is interesting to note that, these values of E_n and E_c are lower than that of reported [25-30] ones for the crystallization of metallosilicate MFI molecular sieves by conventional hydrothermal routes. Thus, the reduction in the overall crystallization period might be due to lower activation energies for nucleation and crystallization in dry gel method.

Although, lower time is needed to obtain fully crystalline Sn-MFI phase at higher temperature, considering the marginal difference in crystallization time required at 170 and 200^{o}C, further investigations were carried out at lower temperature i.e. at 170^{o}C.

2.3.2.3. *Amount of water at the bottom of an autoclave*

In dry gel conversion, water at the bottom autoclave never comes into direct contact with dry gel but steam leads to transformation of amorphous gel into crystalline form by adsorptions and condensation of water on/in the dry gel [31]. On the contradictory, in the hydrothermal synthesis, water content in the hydro-gel plays an important role on the crystallization pathway and crystallinity of the zeolitic

material [32]. Therefore, it was thought that, it would be interesting to investigate the change in crystallization rate with change in amount of water at the bottom of the autoclave. Keeping other variables constant (dry gel composition: SiO_2: 0.009 SnO_2: 0.25$(TPA)_2O$, temp. = 170^oC), time dependent studies were conducted by varying the amount of water from 0 to 8 ml per gm of dry gel . The results in terms of crystallization time and % crystallinity of samples obtained from these runs are included in Table 2.2.

Table 2.2. The variation in crystallization time and percentage crystallinity as a function of the amount of the water at bottom of autoclave. Oxide molar composition of dry gel : SiO_2: 0.01 SnO_2: 0.23$(TPA)_2O$

Amount of water at bottom of autoclave (ml)	**Crystallization Temperature**	**Crystallization time (hour)**	**% Crystallinity**
0	170^oC	10	0[a]
0.66	170^oC	10	100
2.00	170^oC	8	100
3.33	170^oC	5	100
8.00	170^oC	10	0[a]

a : *amorphous sample*

Without addition of water at bottom of autoclave, dry gel was found to remain amorphous even upto 48 hour. When water content varied from 00.66 to 3.33 ml per gm of dry gel, the crystallization time to obtain most crystalline Sn-MFI phase was found to decrease from 10 to 5 hours. Further increasing the amount of water (8 ml per gm of dry gel), no formation of MFI phase was observed. Similar results were reported [31] on the dry gel conversion to zeolite, Al- beta.

2.3.2.4. *Molar ratio of $(TPA)_2O/SiO_2$ in dry gel*

Non-volatile structure directing agent is occluded in the dry gel. Amount of such expensive reagent plays a crucial role in the crystallization process. Keeping molar SiO_2/SnO_2 = 50 in dry gel, water per gm of dry gel = 3.33 ml and temp.= 170^oC fixed, the crystallization kinetic curves were established by varying $(TPA)_2O/SiO_2$

molar ratio in the range from 0.15 to 0.25 in dry gel. These curves are illustrated in Fig. 2.6.

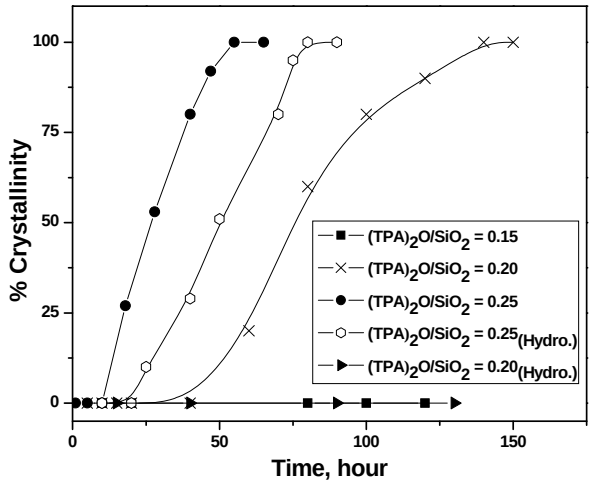

Fig. 2.6. Influence of $(TPA)_2O/SiO_2$ molar ratio on crystallization kinetics of Sn-MFI phases prepared by hydrothermal crystallization and DGC method.

It is clearly evident that, the dry gel containing molar $(TPA)_2O/SiO_2$= 0.15 did not yield Sn-MFI phase and remained amorphous up to 120 hours. However, with increase in $(TPA)_2O/SiO_2$ molar ratio from 0.2 to 0.25, there is a decrease in the time required for the formation of most-crystalline Sn-MFI. Thus, there exists a minimum $(TPA)_2O/SiO_2$ molar ratio needed for the formation of Sn-MFI. Since TPAOH is the most cost-bearing reagent, the experiments were also conducted using conventional hydrothermal method. Hydrothermal synthesis trials were conducted using hydrogels (i) SiO_2: $0.02SnO_2$: 0.25 $(TPA)_2O$: 32 H_2O and (ii) SiO_2: $0.02SnO_2$: 0.20 $(TPA)_2O$: 32 H_2O. These gels were subjected individually to 170^oC in order to carry out the time dependent studies for monitoring the progressive crystallization. Thus, in this case, except method, other synthesis conditions, in particular, composition of the initial reaction mixture and crystallization temperature was kept constant. The crystallization kinetics curves were established and depicted in Fig. 2.6. When compared with conventional hydrothermal route, faster crystallization was observed in case of DGC method at given gel molar $(TPA)_2O/SiO_2$ ratio (0.25). Moreover, at molar ratio of

$(TPA)_2O/SiO_2$ = 0.20, there was no any indication of occurrence of crystallization of any phase during hydrothermal synthesis, while in dry gel method, a well–crystalline Sn-MFI phase was formed. These results indicated that dry gel conversion method has added advantages of (1) use of less amount of structure directing agent and (2) faster crystallization resulting in the reduction of the overall crystallization period. The reduction in template quantity and faster crystallization in DGC method may be attributed to enhanced interaction of TPA^+ cations with siliceous species and high magnitude of stabilization of TPA^+ species [33].

2.3.2.5. *Molar ratio of SiO_2/SnO_2 in dry gel*

The catalytic application of metallosilicates depends on the concentration and coordination of heteroatom that is incorporated in the zeolitic structure. The degree of isomorphous substitution mainly depends on synthesis conditions, topology and characteristics of the heteroatom. In this regard, it becomes essential to investigate the pathway of crystallization as a function of amount of heteroatoms to be substituted isomorpously and degree of such substitution. In view of this, experiments were carried out to investigate the influence of molar ratio of SiO_2/SnO_2 in starting dry gel on the crystallization kinetics wherein the SiO_2/SnO_2 molar ratio in dry gel was varied from 30 to 150 keeping fixed $(TPA)_2O/SiO_2$ molar ratio = 0.25, crystallization temperature = 170^oC and 3.33 ml water at bottom of autoclave for 1 gm dry gel. Dry gel with SiO_2/SnO_2 molar ratio = 30 has not yielded MFI phase even up to 100 hour in present studies. Fig.2.7 represents crystallization kinetics curves of Sn-MFI samples obtained from dry gels having different SiO_2/SnO_2 molar ratios.

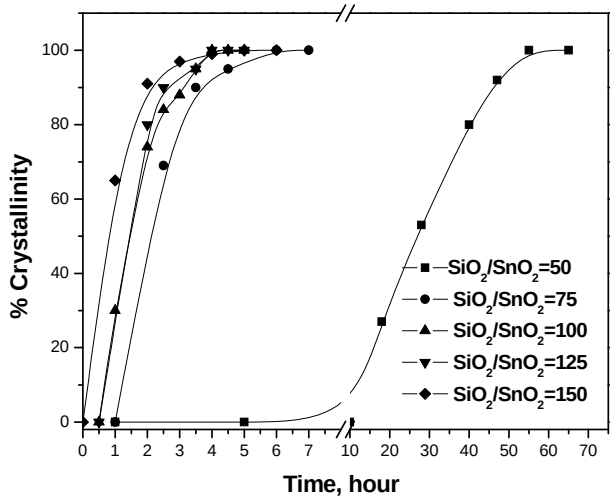

Fig.2.7. Crystallization kinetics curves of Sn-MFI samples obtained from dry gels having different SiO_2/SnO_2 molar ratios.

All kinetic curves exhibited sigmoidal shape indicative of different rates of nucleation and crystallization at different stages of crystallization. It can be seen clearly that, the increase in the SiO_2/SnO_2 in the dry gel caused the decrease in the induction period and shortened the overall crystallization period. The induction period is the time required for providing the condition for the formation of crystallization centers or nuclei. The maximum induction period of crystallization was to be 9 hour with dry gel having molar SiO_2/SnO_2 ratio of 50. In other words, lesser the amount of tin in the dry gel, faster is the crystallization.

2.3.3. Characterization of Sn-MFI samples.

The powder XRD of the well-crystalline Sn-MFI obtained from the dry gels having different SiO_2/SnO_2 molar ratios have illustrated in **Fig.2.8**. It is evident that, these materials possess all the characteristic peaks of MFI phase and contain no any contribution due to other phase/s.

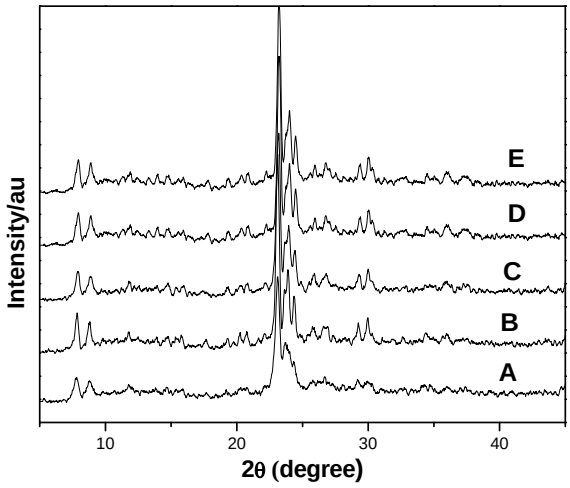

Fig. 2.8. Powder XRD of the well-crystalline Sn-MFI in as-prepared form obtained from the dry gels having different SiO_2/SnO_2 molar ratios. (A) SiO_2/SnO_2 = 50, (B) SiO_2/SnO_2 = 75, (C) SiO_2/SnO_2 =100, (D) SiO_2/SnO_2 =125 and (E) SiO_2/SnO_2 =150.

After being calcined, these samples were further subjected to detail characterization and the catalytic performance. The designation of these calcined samples is provided in Table 2.3.

Table 2.3. Designation, the chemical compositions and textural properties of calcined Sn-MFI samples.

Sample Designation	**SiO_2/SnO_2 molar ratio**			**Surface area m^2/g**
	Dry Gel	**Calcined Product**		
		XPS (Surface)	**$AAS_{(Bulk)}$**	
A	50	51	50.5	510
B	75	76	74.5	505
C	100	110.8	101.8	504
D	125	126.2	124.8	499
E	150	140	139.4	497

The chemical composition in terms of surface SiO_2/SnO_2 molar ratio was established by XPS. Similarly, SiO_2/SnO_2 molar ratio in bulk was determined by chemical analyses using gravimetric and AAS techniques. These results are summarized in Table 2.3. It is evident that, irrespective of the SiO_2/SnO_2 molar ratio in the dry gel, all the Sn-MFI samples have shown almost identical composition on the surface as well as in the bulk. This indicates that, there is a uniform distribution of tin in all the Sn-MFI samples under investigation. Moreover, a similar value of SiO_2/SnO_2 molar ratio in the dry gel and in the product suggesting no loss of Si or Sn during the crystallization and/or down-stream processes. Thus, SiO_2/SnO_2 molar ratio in the Sn-MFI increases linearly with the increase in SiO_2/SnO_2 molar ratio in the dry gel. The BET surface area has shown increasing trend with the increase of Sn content in the sample.

Further verification related to the incorporation of tin in MFI structure was carried out using diffuse reflectance UV-Vis spectroscopy. The DRUV–vis spectra of Sn-MFI with different Sn content prepared by DGC method are shown in **Fig. 2.9**.For comparison purpose, a Sn-impregnated Silicalite-1 sample is also included in the same figure.

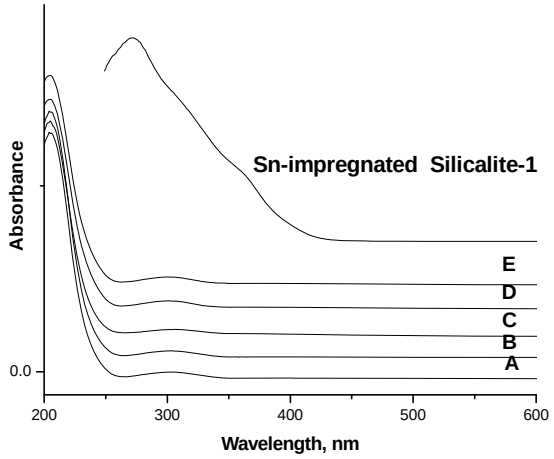

Fig. 2. 9. The DRUV–vis spectra of sample A, B,C, D, E and Sn-impregnated silicalite-1.

The Sn-impregnated sample shows strong adsorption at 280 nm which is assigned to hexacoordinated Sn-O-Sn type species [23,24, 34]. The spectra of all the Sn-MFI samples reveal absorption at ~ 220 nm. The absorption band at 220 nm can be assigned due to charge transitions (CT) from O^{2-} to Sn^{4+} in tetrahedral coordination [23,24,34]. Moreover, the intensity of this band was found to increase with the increase in the tin content. All Sn-MFI samples showed no bands typical for polymeric Sn–O–Sn type species at 280 nm [23,34]. This indicates that the isomorphous substitution of tetrahedral tin has been occurred in the MFI framework. At this juncture, identical spectral features of samples A, B,C,D and E suggest that, except synthesis times, the SiO_2/SnO_2 molar ratio in dry gel in the present studies has not influenced the extent of incorporation of tetrahedrally coordinated tin to the considerable extent. Although, spectra of all the Sn-MFI samples reveal absorption at ~ 220 nm with lack of absorption at ~ 280 nm suggesting occupancy of tin atoms in site-isolated positions in the silica framework, it is manifested by the broader character. We believe that site-isolated Sn in a distorted tetrahedral environment and/or in penta- or octahedral coordination sphere may be associated with such broadening character of Sn-MFI spectra.

The influences of SiO_2/SnO_2 molar ratio in the dry gel on the crystal morphology and size of pure and well crystalline Sn-MFI phases were investigated. Fig. 2.10 shows the SEM photograph of Sn-MFI samples with different SiO_2/SnO_2 molar ratio. Sample A, B and C exhibited uniform spherical shaped particles having size of approximately 0.3 μm and 0.8μm respectively. Further rise in SiO_2/SnO_2 molar ratio (sample D) resulted in a typical intergrown disc shaped morphology with 5-8 μm size. Sample E having still lower tin content than sample D, has shown irregular shaped morphology. The variations in the morphology and size might be associated with the differences in rates of nucleation and crystallization.

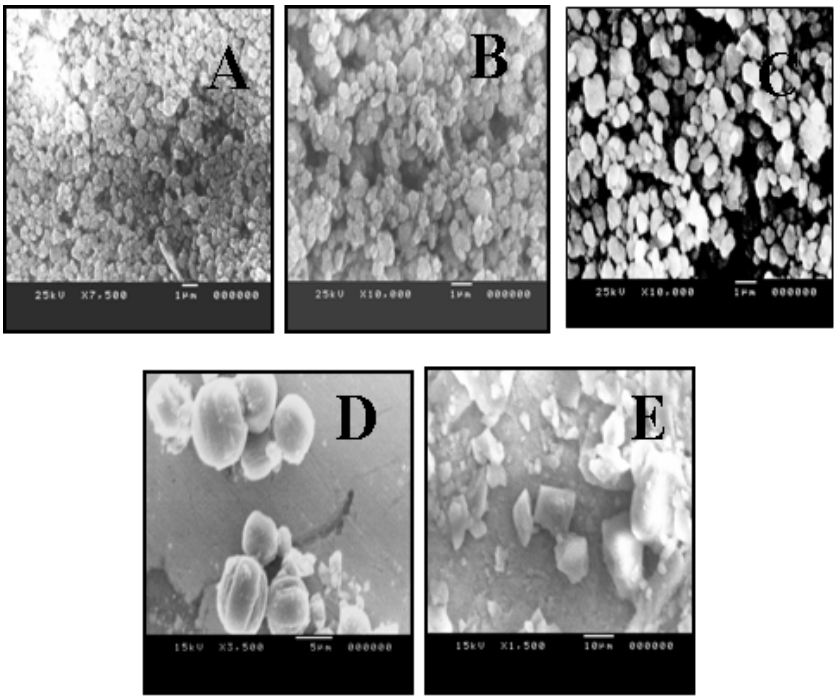

Fig.2.10. The SEM photograph of the samples A to E.

For the purpose of collecting more information on the tin species and investigating the catalytic performance of Sn-MFI catalysts prepared by dry gel conversion method, the phenol hydroxylation with H_2O_2 was selected as a test reaction. The dependency of conversion and efficiency of H_2O_2 on an environment of Sn species formed the basis for selecting this reaction as test tool. The catalytic performance of samples A, B, C, D and E was investigated in Phenol hydroxylation reaction with H_2O_2 as oxidant and water as a solvent at 80^oC for 8 and 24 hours. For comparison purpose, the sample designated as Sn-MFI $_{(Hydro)}$ was prepared by hydrothermal crystallization route having Sn content similar to sample A and screened under the identical set of reaction conditions. The activity data are presented in Table 2.4. After 8 hours of reaction time, all the catalysts have exhibited marginal enhancement of the magnitude 2-5% in phenol conversion when reaction time was extended to 24 hours. In case Sn-MFI catalysts obtained by DGC method (A to E), the phenol conversion and H_2O_2 efficiency were found to increase with an increase in the Sn content. This indicates that, there is a presence of isolated Sn^{4+} ions of whose

concentration increases with decrease in the molar SiO_2/SnO_2 ratio. This finding supports the earlier DRUV-vis results.

Table 2.4. Catalytic performance of Sn-MFI in the hydroxylation of phenol by H_2O_2[a].

Sample	Reaction time (hours)	Phenol conversion (mole %)	H_2O_2 Efficiency (mole %)	TON[b]	Product distribution (mole %)[c]		
					CAT	HQ	PBQ
A	8	26.1	52.2	75.6	57.7	40.1	2.2
	24	28.4	56.8	82.3	61.7	38.2	0.8
B	8	21.2	41.6	99.3	40.4	29.2	30.3
	24	24.6	48.3	115.2	46.6	25.5	27.7
C	8	19.4	38.8	127.6	34.4	24.4	41.1
	24	23.9	47.8	157.3	42.2	20.0	37.7
D	8	18.8	37.6	151.9	25.3	21.9	52.7
	24	23.6	47.2	193.1	31.1	18.8	50.0
E	8	18.1	37.2	195.2	24.3	20.1	55.6
	24	22.9	46.8	205.1	29.9	16.6	53.5
Sn MFI (Hydro)[d]	8	25.7	51.4	73.9	56.2	39.3	4.7
	24	28.1	56.2	80.9	61.1	37.7	1.1

[a]Reaction conditions: Catalyst/Phenol =10 g mol^{-1}, molar ratio of Phenol/H_2O_2 = 2, H_2O/Phenol = 20, Temperature = 353 K.

[b] Turnover number : number of molecules of phenol converted per atom of Sn.

[c]CAT - catechol; HQ-hydroquinone; PBQ- para-benzoquinone.

[d] Catalyst prepared by conventional hydrothermal crystallization route , used after calcination, SiO_2/SnO_2 molar ratio = 45.46 .

It can be clearly seen from Table 2.4 that, at 8 hours reaction time, the formation of catechol (CAT) was lower, whereas hydroquinone (HQ) and p-benzoquinone (PBQ) concentrations were higher as compared to product distribution

of 24 hours reaction time, in all the samples. Further, with the decrease in Sn content, there is an increase in the contribution of PBQ accompanied by the decrease in CAT and HQ contributions. The increase in PBQ selectivity might be associated with the fast oxidation of HQ in the reaction medium by large excess of H_2O_2 [24]. Nearly similar mole ratios (1.8 ± 0.2) of CAT to HQ at 24 hour also suggests that, all the Sn-MFIs possess excellent shape selective property and the presence of well-dispersed Sn^{4+} ions located within the cannels of MFI structure[8].

It is interesting to note that, the TON was found to decrease with the increase in tin content. The variation in the TON suggests that, there exists a possibility of presence of more than one types of Sn species that are different in their activeness. The proportion of less active Sn species might be increasing with the increase in tin content [35]. Thus, an incorporation of higher amount of tin in the MFI framework might be associated with the decrease in monoatomic dispersion of active Sn^{4+} ions in Sn-MFI samples. Although, not better but comparable activity has been exhibited by sample A (mole % H_2O_2 efficiency = 56.8, at 24 hours) when compared with Sn-MFI $_{(Hydro)}$ prepared by conventional hydrothermal crystallization method (mole % H_2O_2 efficiency = 56.2, at 24 hours) containing nearly identical tin content.

2.3.4. Thermal expansion properties of Sn-MFI

Microporous molecular sieves, especially zeolitic material, show specific catalytic properties in alkylation, isomerisation, oxidation and hydroxylation reactions. Many of such reactions are carried out at elevated temperature using catalysts. Mostly molecular sieves, used as catalyst/sorptive, are calcined more than 550^oC. In addition to this, it may need activation before use. During activation, one may need to heat these materials at a temperature of 750^oC. Hence zeolitic molecular sieves used as catalysts need to have the appropriate thermal and hydrothermal stability to withstand the extreme conditions frequently involved in their use and regeneration. Thus, the information regarding the stability of these materials is necessary. Apart from the thermal stability, Upon heating, zeolitic molecular sieve undergo different kinds of structural changes including: i) cell volume contraction due to the removal of water and/or templating organic molecules (dehydration and

calcination); ii) displacive or reconstructive phase transformation(s) to more or less metastable phase(s); iii) structural collapse; iv) structural breakdown (*i.e.* complete amorphization); v) negative thermal expansion (NTE). Materials having negative thermal expansion (NTE) properties are of great technological interest due to their potential applications in composites, which may facilitate the tailoring of thermal expansion coefficient and allow the design of materials with desired expansion coefficients. Thermal expansion matching is important to avoid cracks or separation at interfaces between two materials. Zero expansion is needed when exact positioning of electronic or optical components in a device is important.

Upon isomorphous substitution of Sn in MFI framework, it is expected that, the lattice dynamic effects might get perturbed. Since the negative thermal expansion (NTE) depends on lattice dynamic effect and in turn on chemical content and framework structure, it becomes essential to study the NTE behavior of this material to increase the knowledge about its thermal expansion behavior, for seeking its potential candidature for use in ceramic, optical and electronic applications. Different molecular sieves like ITQ-1[36], ZSM-5 [37], ITQ-5 [38], AlPO-5 [39], MAPO-17 [38] and faujasite [40] have exhibited negative thermal expansion on heating. Molecular sieves like CIT-5 and AlPO-31 have shown [41] positive thermal expansion upon heating.

This section describe the structural changes that occur in the representative Sn-MFI sample (Sample B) and its comparison with that of Sn-free Si-MFI sample as a function of temperature by *in-situ* high temperature X-ray diffraction (HTXRD) studies.

2.3.4.1. *An in-situ high temperature X-ray diffraction studies*

The method, type of the instrument, instrumental condition and software applied for data analysis for elucidating the thermal properties by *in-situ* high temperature X-ray diffraction are described in the section 2.2.2.1.

A multiple plot of temperature resolved powder XRD patterns collected at temperatures ranging from 100 to 700^{o}C in 50^{o}C intervals are depicted in Fig.2.11. The purity and crystallinity of both the phases were found to remain unchanged in the

entire temperature range. Thus, the incorporation of tin in the MFI framework seems to occur without creation of additional defects (destabilizing factor) in the orthorhombic MFI structure.

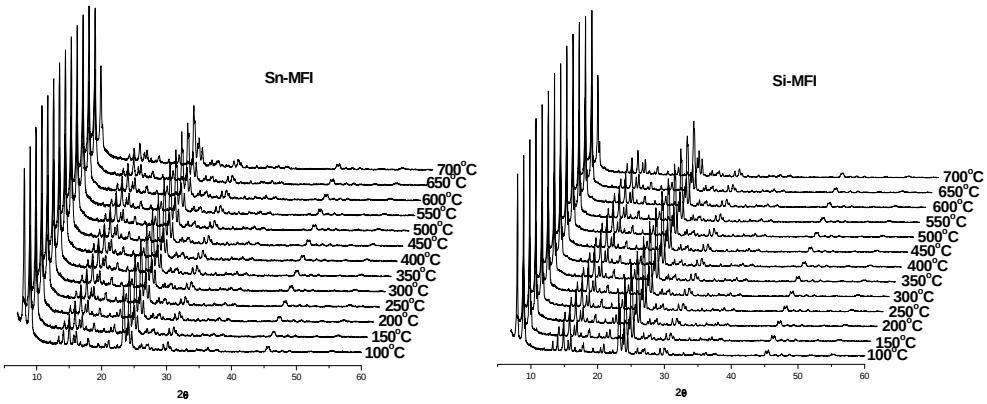

Fig. 2.11. Evolution of diffraction patterns in the temperature range 100 to 700°C.

In order to investigate the influence of an insertion of Sn^{4+} in place of Si^{4+} in MFI framework on the thermal expansion behavior, a variation in the unit cell parameters of tin-free Si-MFI and SnSi-MFI was studied over the temperature range of 100 to 700°C. The lattice parameters of both the samples were obtained by Rietveld refinement and used for calculating the thermal expansion. For Rietveld refinement, the conditions employed were $2\Theta = 10\text{-}60^{0}$, step size = 0.017°, number of data points > 2000, values for Rwp and Rp for all fits < 10 %, $\chi^2 < 5$, profile function = Pseudo-Voigt and background function = Shifted Chebyshev 16-coefficients. As an illustration, Fig. 2.12 illustrates the Rietveld refinement of powder XRD pattern collected at 100°C showing experimental, calculated and difference plots. The fit has shown Rwp= 7.06 %, Rp = 5.38 %, $\chi^2 = 1.32$ and number of data points were 2720.

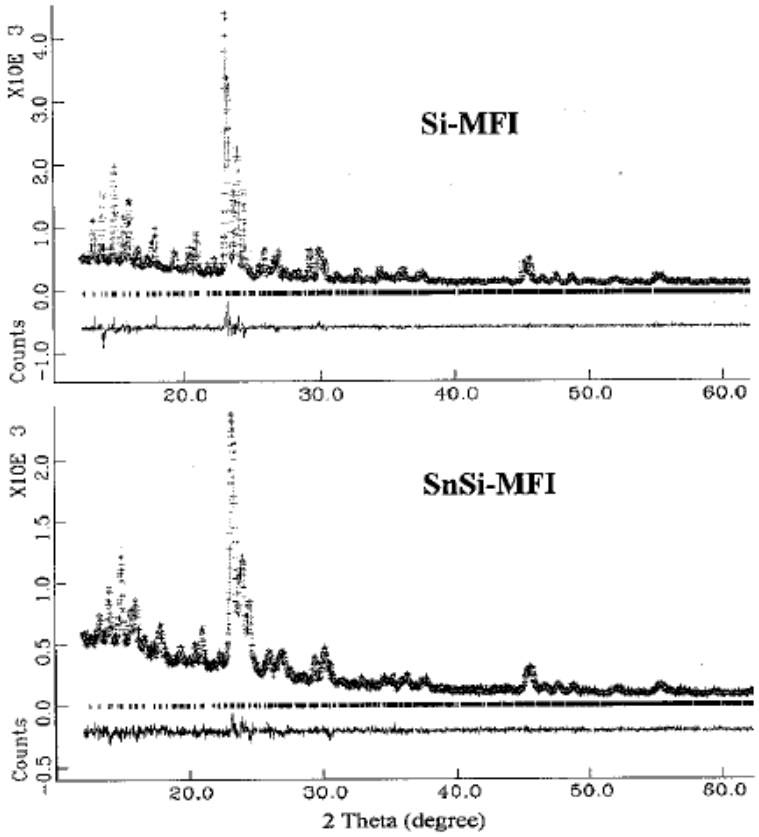

Fig. 2.12. Rietveld refinement of the powder XRD pattern collected at 100°C: observed (crosses), calculated (solid line) and the difference (lower trace).

The unit cell parameters deduced from this refinement are summarized in Table 2.5. The unit cell of SnSi-MFI was found to expand on account of the isomorphous substitution of Si^{4+} by Sn^{4+} possessing higher ionic radii in the MFI framework.

Table 2.5: Unit Cell parameters of Si-MFI and SnSi-MFI from 100°C scan

Sample	Unit cell parameters , Å			Unit Cell Volume, Å
	a	B	c	
Si-MFI	20.081(1)	19.904(1)	13.384(8)	5349.82
SnSi-MFI	20.085(1)	19.920(1)	13.396(1)	5359.91

In similar fashion, the unit cell parameters were obtained from Rietveld refinement of the all the powder XRD patterns scanned at different temperatures. The plots showing the influence of Sn^{4+} in place of Si^{4+} in MFI framework on the variations in unit cell parameters (a, b, and c), unit cell volume and the thermal expansion coefficients over a temperature range100-700^{o}C are shown in Fig. 2.13.

Both the samples, Si-MFI and SnSi-MFI have exhibited a negative thermal expansion (NTE), however, the behavior of variation in NTE with temperature was found to be different. All the unit cell parameters are higher in case of SnSi-MFI as compared to Si-MFI and were found to decrease in all the direction with increase in temperature. Interestingly, the extent of decrease was found to be 1.1± 0.1 times higher in SnSi-MFI as compared to Si-MFI. At all the temperatures, both the samples have shown the trend in the values of unit cell parameters as: a > c > b. In the temperature range of 100-700^{o}C, the extent of decrease in unit cell volume was observed to be 2.3 % and 2.6 % in case of Si-MFI and SnSi-MFI respectively.

The thermal expansion coefficient along 'a' (α_a) in the temperature range of 150 -700^{o}C in Si-MFI and SnSi-MFI were found to be -17.426 X $10^{-6}K^{-1}$ and -15. 354 X $10^{-6}K^{-1}$ respectively. The thermal expansion coefficients along 'b' and 'c' axis (α_b and α_c) were -12.299 X $10^{-6}K^{-1}$ (Si-MFI), -10.718 X $10^{-6}K^{-1}$ (SnSi-MFI) and -13.934 X $10^{-6}K^{-1}$ (Si-MFI), -12.751 X $10^{-6}K^{-1}$ (SnSi-MFI) respectively.

Fig. 2.13E shows that, the thermal expansion coefficients (α_v) decrease with increase in temperature for both the samples. The value for α_v for the 473–973 K for SnSi-MFI was found to be higher ($\alpha_V = -38.611\times 10^{-6}\ K^{-1}$) as compared to that of Si-MFI ($\alpha_V = -43.437 \times 10^{-6}\ K^{-1}$). Similar results were observed in many solids including molecular sieves and mixed oxides [41-46]. Thus, the isomorphous substitution of Sn^{4+} in MFI framework seems to be operative in enhancing the strength of the NTE coefficient which may be partly attributed to the transverse thermal vibrations of twofold coordinated oxygens and the intrinsic property of the framework [41, 47].

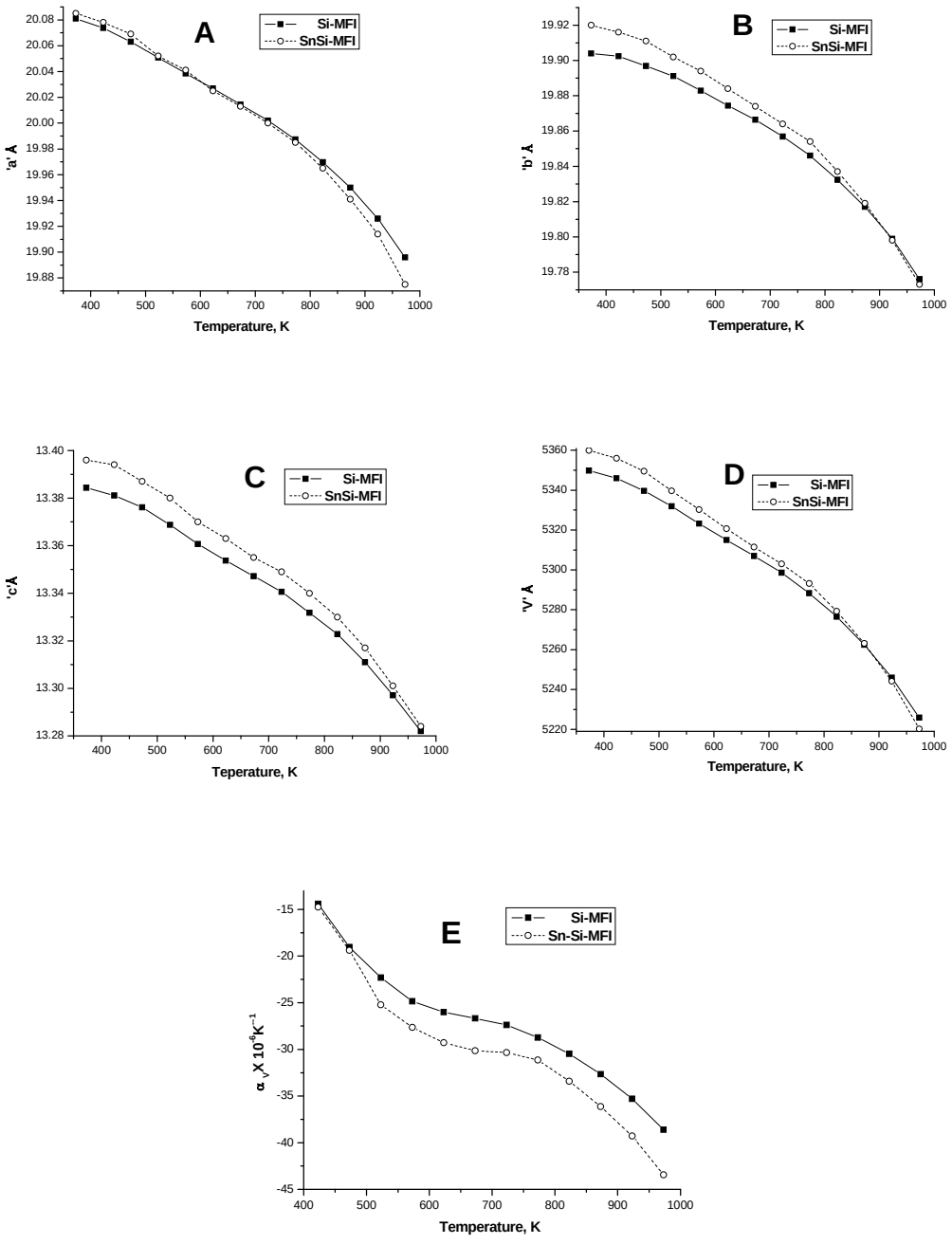

Fig. 2.13. Temperature dependence of (A) the unit cell dimensions 'a', (B) the unit cell dimensions 'b', (C) the unit cell dimensions 'c', (D) the unit cell volume and (E) αv in the temperature range 100-700^{o}C for Si-MFI and SnSi-MFI.

2.3.5. Surface acid sites in Sn-MFI molecular sieves

An understanding of type, concentration and strength of acid sites in solid acid catalyst is one of the bare necessities to understand their catalytic behavior as catalysts for several transformation reactions. An obvious goal of many researchers was to establish appropriate method for evaluating acidic properties of the materials possessing protonic and/or non-protonic acid sites and use it as a useful tool for establishing acidity-performance relationship. Although methods such as titration [48,49], microcolorimetry [50,51], magic angle spinning nuclear magnetic resonance (MASNMR) spectroscopy [52-55], temperature programmed ammonia desorption (TPAD) [56,57], infrared spectroscopy (IR) [48,57-59], sorption of basic molecules like n-butylamine [60] and X-ray photoelectron spectroscopy (XPS) [21,50,61-66] permit determination of type, concentration and strength of acid sites in solid catalysts, the most important and widespread used techniques are TPAD and IR. Although less used, XPS has a great power of detection and quantification of Bronsted as well as Lewis acid sites. In view of providing comprehensive information on catalyst surface acidity, the recent progress in this field has primarily involved the joint use of suitable techniques.

Uniform micropore size distribution, high thermal and hydrothermal stability, flexible framework to tune the surface properties and high internal surface area of Tin-silicalite-1 (Sn-MFI) make it attractive for potential applications. However, there is scanty information on its surface acidity [67,68]. The benefits of Sn-MFI molecular sieve and lack of adequate knowledge/method to measure the nature, type and strength of its acid sites have triggered our interest to employ XPS technique.

An attempt was made to find out the type and relative concentration of surface acidity of Sn-MFI samples by characterizing N1s XPS spectra of chemisorbed pyridine over Sn-MFI samples. The N1s XPS spectra of chemisorbed pyridine were recorded at room temperature using X-ray Photoelectron Spectrometer (V. G. Scientific (UK) ESCA-3000 and detail experimental condition and procedure has been stated in the section 2.2.2.6.

To acknowledge acid sites and find out its strength, the effect of pyridine desorption on N 1s spectra was studied in the temperature ranging from 50 to 300^{o}C using sample A (Sn-MFI, SiO_2/SnO_2 molar ratio = 50). The values for E_b of Si 2p, Al 2p, O 1s, Sn $3d_{3/2}$, Sn $3d_{5/2}$ and FWHM at every temperature match well with those of reported ones [2,21,63]. The most striking feature is that, at every temperature, N 1s peak was observed to be broader and asymmetric as compared to Si 2p, Al 2p, O 1s, Sn $3d_{3/2}$, Sn $3d_{5/2}$ peaks. The binding energy value corresponding to the maxima of broad N 1s envelop was found to vary between 400 and 400.5 eV which is also in close agreement with the reported one [21, 63]. The change in $(N/Sn)_s$ ratios and FWHM of broad N 1s peak as a function of pyridine desorption temperature is shown in Table 2.6.

Table-2.6. XPS data : Effect of pyridine desorption temperature on $(N/Sn)_s$, binding energy, FWHM and % relative intensity of N 1s components of sample A.

Pyridine desorption temp./^{o}C	**$(N/Sn)_s$**	**N 1s components/eV**				**% Relative intensity**	
		E_b	**FWHM**	**E_b**	**FWHM**	**Component at 399.5±0.2eV**	**Component at 401.5±0.2eV**
50	1.07	399.6	2.4	401.7	2.4	69.1	30.9
100	0.99	399.4	2.4	401.7	2.4	65.5	34.5
150	0.98	399.7	2.4	401.5	2.4	61.9	38.1
200	0.60	399.5	2.4	401.3	2.4	55.9	44.1
250	0.37	399.4	2.4	400.1	2.4	32.5	67.5

There is a decrease in $(N/Sn)_s$ ratio and FWHM of N 1s peak with the increase in pyridine desorption temperature. The complete desorption of pyridine was observed at 300^{o}C. The FWHM of N 1s peak varies in the range of 2.9 - 2.6 eV. However, this FWHM is not acceptable for one component i.e. for only one type of N species [63]. Temperature dependant variation in $(N/Sn)_s$ ratio and FWHM of N 1s peak suggest the presence of more than one type of acid site possessing different strength. Hence, N 1s peak obtained at different pyridine desorption temperatures was

further deconvoluted and depicted in Fig.2.14**.** Upon deconvolution, two peaks having reproducible binding energies of the magnitude 399.5±0.2 and 401.5±0.2 eV were emerged. The binding energy, FWHM and relative intensity of these two components at different pyridine desorption temperatures are summarized in Table 2.6.

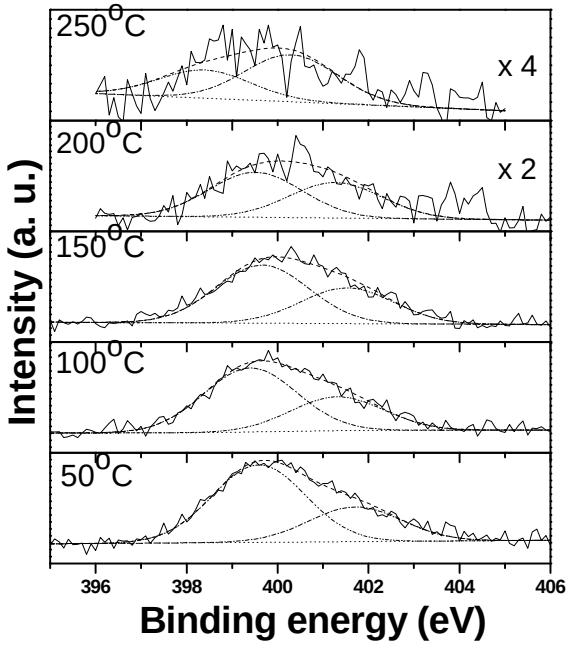

Fig. 2.14. N 1s XPS spectra recorded at different pyridine desorption temperatures using Sample A.

The assignment of components at 399.5±0.2 and 401.5±0.2 eV was the key issue in the present studies. The prior art discloses [21, 63] that, the N 1s binding energies at 398.7±0.3, 400±0.3 and 401.8±0.3 eV corresponds to chemisorption of pyridine in three different states on protonic forms of MFI type zeolites. The first peak at 398.7±0.3 eV was assigned to the N 1s level of pyridine adsorbed on Lewis site, whereas the second and third were assigned to the N 1s levels of pyridine adsorbed on relatively weak and strong Bronsted sites. Similarly, the peaks at 399.5 - 400.5 and 401.5 - 402.5 eV were assigned to the N 1s levels of pyridine/NH_3 adsorbed on Lewis and Bronsted acid sites, respectively, for metal-loaded MFI zeolites/amorphous silica-aluminas [50], supported binary oxides containing CuO

coupled with Ga_2O_3 and SnO_2 [61], silica – zirconia [64] and alumina/titania supported SnO_2 [65]. However, our Al-free Sn-MFI sample (A) is likely to possess no Bronsted acid sites, and hence the exploration of possible assignment of two components became essential. In view of this, ex-situ IR spectroscopy with chemisorbed pyridine was used for identification of Bronsted and Lewis acid sites in sample A. The temperature dependent study was conducted by desorbing the pyridine in the temperature ranging from 50 to 250^oC. The IR spectra collected at different pyridine desorption temperatures are shown in Fig 2.15.

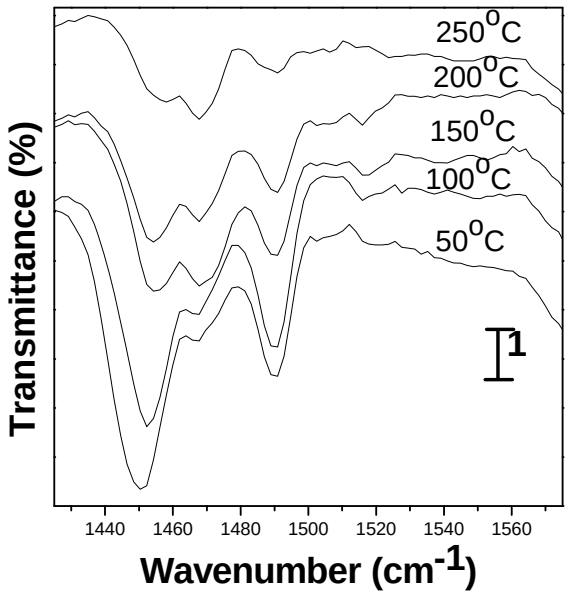

Fig. 2.15. IR spectra recorded at different pyridine desorption temperatures using Sample A.

Each IR spectrum revealed the appearance of bands at 1455 and 1490 cm^{-1}. Based on earlier reported literature [69, 71], the bands at 1455 and 1490 cm^{-1} can be assigned to pyridine coordinated to Lewis acid sites. A significant shift of a position of the band at 1455 cm^{-1} was observed with an increase of the desorption temperature indicating a stronger interaction between the pyridine and the acid sites on account of higher strength of the interacting Lewis acid sites. Moreover, the intensities of these

two bands were found to decrease with the increase in pyridine desorption temperature which is in excellent agreement with the trend observed in the N 1s spectra (Fig 2.14) and in the atomic N/Sn ratios (Table 2.6). An absence of band at 1545cm^{-1} assigned to Bronsted–bound pyridine (pyridinium ion) showed that our sample is free from Bronsted acid sites that are able to interact pyridine. In view of above, two peaks obtained at 399.5±0.2 and 401.5±0.2eV by deconvoluting N 1s spectra were assigned to chemisorbed pyridine on weak and relatively strong Lewis sites respectively. Thus, it seems that there are minimum two different types of framework Sn sites in Sn-MFI molecular sieves. The origin of these sites might be attributed to the partially hydrolyzed and nonhydrolyzed framework Sn sites. Based on the theoretical and experimental evidences, similar two Sn Lewis acid centers were reported for Sn-Beta zeolite [71].

In view of establishing the co-relationship between the relative percentages of strong Lewis acid sites with respect to total acidity and the framework Sn content in the sample, two more samples viz. B and D were also subjected to the similar studies keeping pyridine desorption temperature fixed at 150 ^{o}C.

The N1s high resolution photoelectron peak recorded under identical conditions are illustrated Fig. 2.16. Like sample A, samples B and D also showed two peaks after deconvolution and components also had the same binding energy values. In other words, no shift of components at 399.5±0.2 and 401.5±0.2 eV was observed with the change in surface atomic Si/Sn ratio. However, the intensities of these two components were found to decrease with the increase of Si/Sn atomic ratio. The values of % relative intensity and ratio of N1s components are provided in Table 2.7. It is clearly evident that, the Sn content in the sample is responsible for altering the overall Lewis acidity. More interestingly, the relative intensity ratio of peak at 399.5±0.2 to 401.5±0.2 eV i.e. ratio of weak to strong Lewis acid sites was found to decrease with increase in the Si/Sn molar ratio. Thus, it can be concluded that, the relative percentage of strong Lewis acid sites with respect to total acidity increases with the decrease of framework Sn content in the sample.

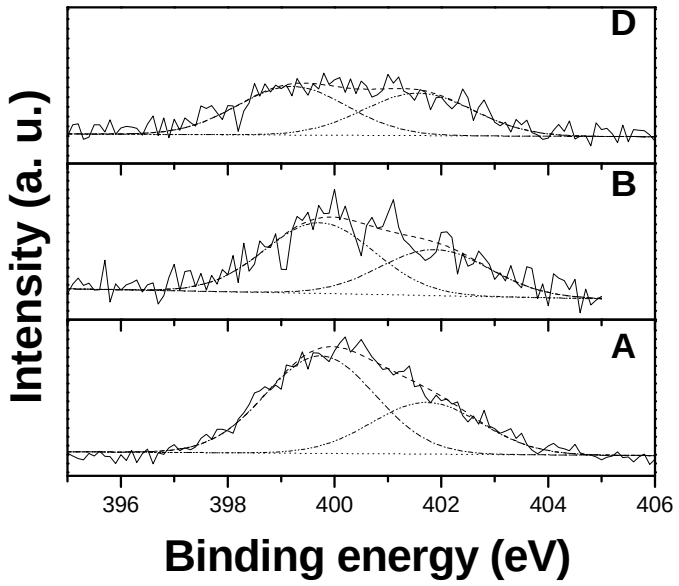

Fig. 2.16. N 1s XPS spectra of samples A, B and D after exposing to pyridine desorption temperature of 150^{o}C.

Table 2.7. Comparison of XPS and TPAD data with respect to density and ratio of weak and strong acid sites.

Sample	XPS			TPAD		
	% Relative Peak Intensity		Ratio of (Weak/Strong) Lewis acid sites	mmoles of NH_3 Desorbed /g		Ratio of (Weak/Strong) Lewis acid sites
	399.5±0.2eV (weak site)	401.5±0.2eV (strong site		Weak 177±15^{o}C	Strong 272±15 ^{o}C	
A	61.9	38.1	1.63	2.4	1.4	1.71
B	60.5	39.5	1.53	2.1	1.3	1.61
D	53.5	46.5	1.15	1.1	1.0	1.10

Since TPAD technique measures the number and strength of acid sites, samples A, B and C were subjected to TPAD evaluation. All samples exhibited similar TPAD profile which on deconvolution, resulted into three desorption peaks with maxima at 108±04^{o}C, 177±15^{o}C and 272±15 ^{o}C. These peaks can be assigned to desorption of physisorbed NH_3, weak Lewis acid sites and strong Lewis acid sites, respectively [68, 72]. The TPAD data for samples A, B and D are shown in Fig. 2.17

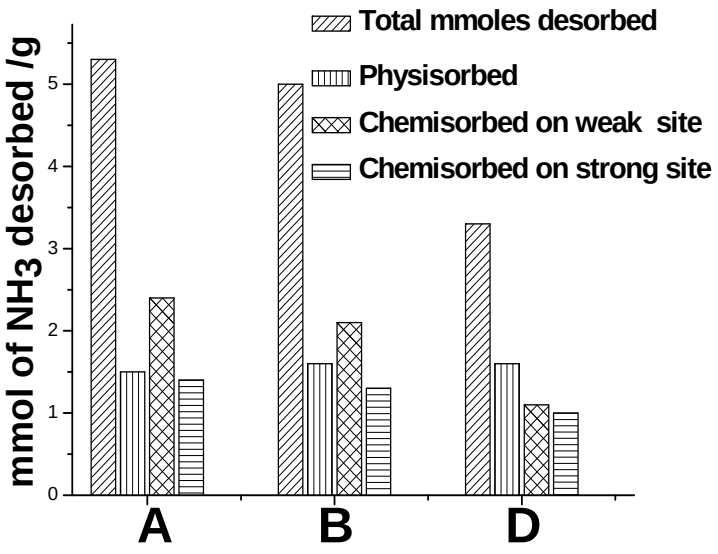

Fig. 2.17. TPAD data for samples A, B and D.

The amount of NH_3 desorbed from weak and strong acid sites and their ratios are summarized and compared with XPS data in Table 2.7. The close agreement between ratios of weak Lewis acid sites to strong Lewis acid sites obtained from XPS and TPAD supports our assignment of N 1s peak components at 399.5±0.2 and 401.5±0.2 eV to weak Lewis acid sites and strong Lewis acid sites respectively.

2.4. CONCLUSION

Tin-silicalite-1 (Sn-MFI) has been successfully synthesized by converting dry gels having compositions: SiO_2: 0.0071-0.02 SnO_2: 0.2- 0.25 $(TPA)_2O$. Crystallization time, temperature, water content at the bottom of autoclave, molar

ratios of $(TPA)_2O$/ SiO_2 and SiO_2/SnO_2 in dry gel have shown their influence on the crystallization kinetics and physico-chemical properties of Sn-MFI materials. No any phase transformation / amorphization/ appearance of impurity were observed when crystallization time was prolonged after achieving maximum crystallinity. Time dependent studies revealed that, increase in the crystallization temperature, water content at bottom of autoclave, $(TPA)_2O/SiO_2$ and SiO_2/SnO_2 molar ratios in dry gel resulted in the lowering of overall crystallization period. In comparison with conventional hydrothermal route, higher rates of crystallization and requirement of reduced amount of TPAOH in dry gel were observed in the DGC method. Nearly identical SiO_2/SnO_2 molar ratios estimated by XPS and AAS, indicated the uniform distribution of Sn^{4+} ions. DRUV-Vis spectra of Sn-MFI with SiO_2/SnO_2 molar ratio from 50 to 140 showed a single, sharp absorption band at ~220nm, indicative of isomorphous substitution of Sn in the frame work as tetrahedral species. The change in SiO_2/SnO_2 molar ratio in dry gel changes the nucleation and crystallization rates which might be responsible for changing the morphology and size of Sn-MFI. Although, not better but comparable activity has been shown by Sn-MFI prepared by dry gel conversion method with Sn-MFI prepared by conventional hydrothermal crystallization method in the hydroxylation of phenol reaction. Increase in concentration of isolated Sn^{4+} ions led to increase in phenol conversion and H_2O_2 efficiency. Nearly similar mole ratios (1.8 ± 0.2) of CAT to HQ suggested that, all the Sn-MFIs possess excellent shape selective property and the presence of well-dispersed Sn^{4+} ions located within the cannels of MFI structure. The turnover number was found to decrease with the increase in tin content. However, the variation in the TON suggested that the incorporation of higher amount of tin in the framework might be associated with the decrease the monoatomic dispersion of active Sn ions in Sn-MFI samples.

The thermal expansion properties and structural changes occurring in Si-MFI and SnSi-MFI molecular sieves as a function of temperature were studied by *in-situ* high temperature X-ray diffraction technique. An isomorphous substitution of Si^{4+} by Sn^{4+} possessing higher ionic radii in the MFI framework found to expand the unit cell. At all the temperatures, ranging from 100 to 700^oC both the samples have shown the

trend in the values of unit cell parameters as: a > c > b. The value for α_v for the 473–973 K for SnSi-MFI was found to be higher ($\alpha_V = -38.611 \times 10^{-6}\ K^{-1}$) as compared to that of Si-MFI ($\alpha_V = -43.437 \times 10^{-6}\ K^{-1}$). The isomorphous substitution of Sn^{4+} in MFI framework seems to be operative in enhancing the strength of the NTE coefficient which may be partly attributed to the transverse thermal vibrations of twofold coordinated oxygens and the intrinsic property of the framework.

The characterization of surface acid sites was carried out using N 1s high resolution photoelectron peak of chemisorbed pyridine in combination with pyridine-IR and TPAD. Two peaks emerged at 399.5±0.2 and 401.5±0.2eV by deconvoluting N 1s high resolution photoelectron peak were assigned to chemisorbed pyridine on weak and relatively strong Lewis acid sites respectively. The temperature dependent pyridine-IR studies revealed that, the intensity of the two bands appearing at 1455 and 1490 cm^{-1}, assigned to pyridine coordinated to Lewis acid sites, decreases with the increase in pyridine desorption temperature. Such behavior is in excellent agreement with the trend observed in intensities of N 1s components and in atomic N/Sn ratios. The ratios of weak Lewis acid sites to strong Lewis acid sites obtained from XPS match well with that of obtained by TPAD. Minimum two different types of framework Sn sites are expected in Sn-MFI molecular sieves and might be attributed to the partially hydrolyzed and nonhydrolyzed framework Sn sites.

2.5. REFERENCES

[1] N.K Mal, V. Ramaswamy, P.R. Rajamohanan, A.V. Ramaswamy, Microporous Mater.; 12 (1997) 331.

[2] N.K. Mal, V. Ramaswamy, S. Ganapathy and A. V. Ramaswamy, J. Chem. Soc., Chem. Commun.; (1994) 1933

[3] R.V. Grieken, C. Martos, M. Sanchez- Sanchez, D. P. Serrano, J. A. Melero, J. Iglesias, A. G. Cubero, Micropor. Mesopor. Mat.; 119 (2009) 176.

[4] W. Xu, J. Dong, Jinping Li, Jianquan Li and F. Wu, J. Chem. Soc., Chem. Commun.; (1990) 755.

[5] M. Matsukata, N. Nishiyama and K. Ueyama, Microporous Mater.; 7 (1996) 109.

[6] S. P. Naik, A. S. T. Chiang and R. W. Thompson, J. Phys. Chem. B; 107 (2003) 7006.

[7] M. B. Yue, L. B. Sun, T. T. Zhuang, X. Dong, Y. Chun and J. H. Zhu, J. Mater. Chem.; 18 (2008) 2044.

[8] M. Matsukata, N. Nishiyama, K. Ueyama, Microporous Mater.;1 (1993) 219.

[9] S. Inagaki, K. Kamino, M. Hoshino, E. Kikuchi, M. Matsukata, Bull. Chem. Soc. Jpn.; 77 (2004) 1249.

[10] N. Nishiyama, K. Ueyama, M. Matsukata, Micropor. Mat.; 7 (1996) 299.

[11] XW. Cheng, J. Wang, H. Yu, J. Guo, HY. He, YC. Long, Micropor. Mesopor. Mat.; 118 (2009) 152.

[12] J. Wang, SW Cheng, J. Guo, XW. Xu, Micropor. Mesopor. Mat.; 96 (2006) 307.

[13] S.K. Saha, P.K. Komura, Y. Kubota, Y. Sugi , Mater. Transactions ;46 (2005) 2651.

[14] P. Wu, T. Miyaji, Y.M. Liu, M.Y. He, T. Tatsumi, Catal. Today; 99 (2005) 233.

[15] M.H. Kim, H.X. Li, M.E. Davis, Microporous Mater.; 1(1993) 191.

[16] (*a*) A. Arnold, S. Steuernagel, M. Hunger, J. Weitkamp, Micropor. Mesopor. Mat.; 62 (2003) 97., (*b*) P.R. Hari Prasad Rao, K. Ueyama, M. Matsukata, Appl. Catal. A ; 166 (1998) 97., (*c*) M. Matsukata, T. Osaki, M. Ogura, E. Kikuchi, Micropor. Mesopor. Mat.; 56 (2002) 1., (*d*) Q-H. Xia, T. Tatsumi, Mater. Chem. Phys. 89 (2005) 89 (*e*) M. Matsukata, M. Ogura, T. Osaki, P. R Rao, M. Nomura, E. Kikuchi, Topics in Catalysis 9 (1999) 77.

[17] H.M. Rietveld, Acta Crystallogr. 22 (1967) 151.

[18] A.C. Larson, R.B. von Dreele, GSAS Generalized Structure Analysis System, Laur 86-748, Los Alamos National Laboratory, Los Alamos, New Mexico, 1999.

[19] B. Toby, J. Appl. Crystallogr.; 34 (2001) 210.

[20] H. van Koningsveld, H. van Bekkum, J.C. Jansen, Acta Cryst. B; 43 (1987) 127.

[21] R.B. Borade, A. Adnot, S. Kaliaguine, J. Catal.; 126 (1990) 26.

[22] R.B. Borade, A. Adnot, S. Kaliaguine, J. Phys. Chem.; 94 (1990) 598.

[23] K. Chaudhari, T.K. Das, P.R. Rajmohanan, K. Lazar, S. Sivasanker, A.J. Chandwadkar, J. Catal.; 183 (1999) 281.

[24] N.K. Mal, A.V. Ramaswamy, J. Mol. Catal. A: Chem.; 105 (1996) 149.

[25] N.J. Chao, T.C. Tasi, N.S. Chen, I. Wang, J. Chem. Soc., Faraday Trans. I; 77 (1981) 547

[26] A. Erdem and L.B. Sand, J. Catal.; 60 (1979) 241.

[27] D.J. Kong, W Zou, J.L. Zheng, X.L. Qi, D.Y. Fang, Acta Phys-Chim. Sin.; 25 (2009) 1921.

[28] Y. Zhang, Y. Li and Yi Zhang, J. Cryst. Growth; 254 (2003) 156.

[29] S.V. Awate, P.N. Joshi, V.P. Shiralkar and A.N. Kotasthane, J. Inclus. Phenom. Mol.; 13:207 (1992) 218.

[30] A. Thangaraj, Ph.D. Thesis, University of Pune, (1991)

[31] M. Matsukata , M. Ogura, T. Osaki, P.R. Hari Prasad Rao, M. Nomura and E. Kikuchi, Top. Catal.; 9 (1999) 77.

[32] S.D. Bhat, P.S. Niphadkar, T.R. Gaydhankar, S.V. Awate, A.A. Belhekar, P.N. Joshi, Micropor. Mesopor. Mat.; 76 (2004) 81.

[33] M. Matsukata, T. Osaki, M. Ogura, E. Kikuchi, Micropor. Mesopor. Mat.; 56 (2002) 1.

[34] X. Wang, H. Xu, X. Fu, P. Liu, F. Lefebvre, J.M. Basset, J. Mol. Catal. A: Chem.; 238 (2005) 185.

[35] P. Wu, T. Tatsumi, T. Komatsu, T. Yashima, J. Phys. Chem. B; 105 (2001) 2897.

[36] D.A. Woodcock, P. Lightfoot, P.A. Wright, L.A. Villaescusa, M.J. Draz-Cabanas, M.A. Camblor, J. Mater. Chem.; 9 (1999) 349.

[37] B.A. Marinkovic, P.M. Jardim, A. Saavendra, L.Y. Lau, C. Baehtza, R.R. de Avillez, F. Rizzo, Micropor. Mesopor. Mat.; 71 (2004) 117.

[38] P. Lightfoot, D.A. Woodcock, M.J. Marple, L.A. Villaescusa, P.A. Wright, J. Mater. Chem.; 1 (2001) 212.

[39] S.H. Park, R.W. Große-Kunstleve, H. Graetsch, H. Gies, Stud. Surf. Sci. Catal.; 105 (1997) 1989.

[40] M.P. Attfield, A.W. Sleight, J.Chem.Soc. Chem.Commun. ; 5 (1998) 601.

[41] D.S. Bhange, V. Ramaswamy, Micropor. Mesopor. Mat.; 130 (2010) 322.

[42] D.S. Bhange, V. Ramaswamy, Mater. Res. Bull.; 42 (2007) 851.

[43] P.M. Forster, A. Yokochi, A.W. Sleight, J. Solid State Chem.; 140 (1998) 157.

[44] B.A. Marinkovic, P.M. Jardim, R.R. de Avillez, F.Rizzo, Solid State Sci.; **7** (2005) 1377.

[45] J.S.O. Evans, T.A. Mary, A.W.Sleigh, J. Solid State Chem.; 133 (1997) 580.

[46] K.W. Chapman, P.J. Chupas, C.J. Kepert, J. Am. Chem. Soc.; 128 (2006) 7009.

[47] S. Sen, R.R. Wusirika, R.E. Youngman, Micropor. Mesopor. Mat.; 87 (2006) 217.

[48] L. Forni, Catal. Rev.; 8 (1974) 65.

[49] K. Wang, X. Wang, G. Li, Catal. Commun.; 8 (2007) 324.

[50] A. Auroux, A. Gervasini, C. Guimon, J. Phys. Chem. B; 103 (1999) 7195.

[51] D.T. Chen, S.B. Sharma, I. Filimonov, J.A. Dumesic, Catal. Lett.; 12 (1992) 201.

[52] H.M. Kao, C.P. Grey, K. Pitchumani, P.H. Lakshminarasimhan, V. Ramamurthy, J. Phys. Chem. A; 102 (1998) 5627.

[53] J.P. Osegovic, R.S. Drago, J. Phys. Chem. B; 104 (2000) 147.

[54] H.M. Kao, C.Y. Yu, M.C. Yeh, Micropor. Mesopor. Mat.; 53 (2002) 1.

[55] H. Pfeifer, D. Freude, M. Hunger, Zeolite ;5 (1985) 274.

[56] M. Niwa, S. Nishikawa, N. Katada, Micropor. Mesopor. Mat.; 82 (2005) 105.

[57] B.M. Lok, B.K. Marcus, C.L. Angell, Zeolite; 6 (1986) 185.

[58] B.L. Su, V. Norberg, Zeolite; 19 (1997) 65.

[59] E. P. Parry, J. Catal.; 2 (1963) 371.

[60] S.V. Awate, P.N. Joshi, M.J. Eapen, V.P. Shiralkar, J. Phy. Chem.; 97 (1993) 6042.

[61] A. Gervasini, B. Bennici, A. Auroux , C. Guimon, Appl. Catal. A-Gen.; 331 (2007) 129.

[62] L. Dussault, J.C. Dupin, E. Dumitriu, A. Auroux, C. Guimon, Thermochim. Acta; 434 (2005) 93.

[63] R. Borade, A. Sayari, A. Adnot, S. Kaliaguine, J. Phys. Chem.; 94 (1990) 5989.

[64] A. Gervasini, C. Messi, D. Flahaut, C. Guimon, Appl. Catal. A-Gen.; 367 (2009) 113.

[65] C. Guimon, A. Gervasin, A. Auroux, J. Phy. Chem. B; 105 (2001) 10316.

[66] M. Stocker, Micropor. Mater.; 6 (1996) 235.

[67] N.K. Mal, A.V. Ramaswamy, Appl. Catal. A: Gen.; 143 (1996) 75-85.

[68] P.S. Niphadkar, P.N. Joshi, H.R. Gurav, S.S. Deshpande , V.V. Bokade, Catal. Lett.; 133 (2009) 175.

[69] X. Ma, H. Guo, S. Wang, Y. Sun, Fuel Process. Technol.; 83 (2003) 275.

[70] D. Srinivas, R. Srivastava, P. Ratanasamy, Catal. Today; 96 (2004) 127.

[71] M. Boronat, P. Concepcion, A. Corma, M. Renz, S. Valencia, J. Catal.; 234 (2005) 111.

[72] Y.K. Park, K.Y. Park, S. Woo, Catal. Lett.; 26 (1994) 169.

CHAPTER 3

CATALYTIC PERFORMANCE OF Sn-CONTAINING MICROPOROUS MEDIUM PORE Sn-MFI MOLECULAR SIEVES IN VAPOUR PHASE ANILINE N-METHYLATION

3.1. INTRODUCTION

The alkylations are among the most important reactions in organic chemistry. It is widely used in the synthesis of the fine chemicals and valuable synthetic intermediates[1]. Alkylation of aniline is a industrially important reaction due to the fact that the numerous uses of various substituted anilines like N-methyl aniline (NMA), N-N-dimethyl aniline (NNDMA) and toluidines [2,3]. N-methyl anilines are the basic raw materials for the synthesis of organic chemicals, chemical intermediates and/or additives in dyes, synthetic rubbers, explosives, herbicides and pharmaceuticals etc [4-11].

The products of methylation of aniline are complex (**Scheme 1**) in nature. N-methylation of aniline always yields poor product selectivity due to the presence of chemically equivalent protons attached to the nitrogen atom. The high nucleophilicity of the amine nitrogen results in the formation of mixture of N-methyl and N,N dimethylated products [12]. However, the selectivity also depends strongly on the experimental conditions and the nature of the catalyst. In particular, it is very difficult to control the reaction for obtaining selectively NMA.

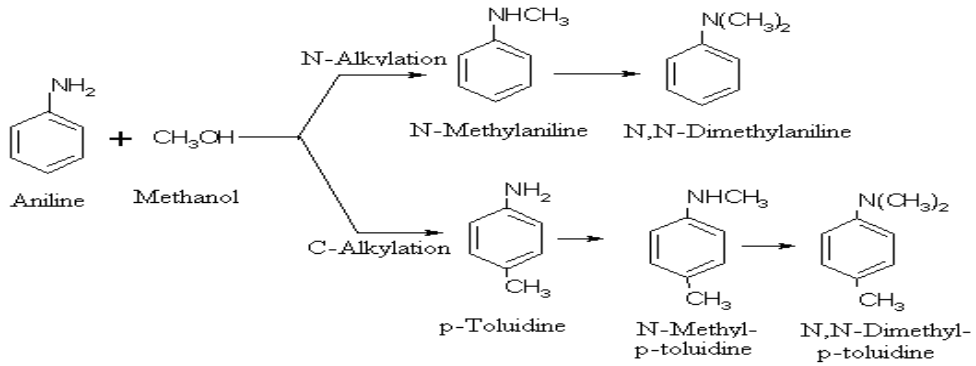

Scheme 1. Reaction scheme

The aniline methylation has been carried out in both liquid and vapour phase. The selective liquid phase mono-N-alkylation over zeolites was reported [13] in the aniline alkylation with dialkyl carbonate. Although liquid phase provides higher yield, it has restricted due to disadvantages such as very large ratio of dialkyl carbonate to aniline substrates (up to 70:1) employed, high capital cost, corrosion problems and formation of byproduct.

Vapor phase alkylation of aniline with methanol was studied over varieties of catalyst such as metal oxide (gamma Al_2O_3, MgO, Fe_2O_3-ZnO i.e. spinel structure) [14-16], zeolites (X,Y,L and ZSM-5) [17-19], alumina phosphate [20], modified clay[21], vanadium[22,23] and Mesoporous material (Al-MCM-41)[24]. In the reported literature [4-27], the aniline conversion in the range of 10 to 70 % and the selectivity of the N-methyl aniline ranging from 40 to 90 % was achieved at higher reaction temperatures (300-500^oC). The main factors influencing activity and selectivity are number and strength of acid site, shape selectivity of catalyst and reaction conditions. However, it was reported [17, 25-27] that, the use of strong solid acids with high concentration of Bronsted acid sites may not be suitable for this reaction. Weak to moderate strength of acid sites have been agreed to be involved in the reaction mechanism and the process being favored by the presence of Lewis acid sites. Lewis acidity in microporous molecular sieve, such as zeolites and aluminophosphates (AlPOs) has been extensively debated [28-31]. The transition metal ions (Ti, V and Zr) incorporated into all silica zeolite framework is associated to the Lewis acidity and used for aniline alkylation reaction [17]. By virtue of higher electronegativity, atomic size and strong acidity [30], the incorporation of Sn (IV) in the tetrahedral silica frameworks of zeolite material is expected to exhibits higher Lewis acidity than Ti and Zr incorporated all silica zeolite. Metallosilicate, in particular, tin-silicalite-1 (Sn-MFI) was reported as a promising catalyst for liquid phase hydroxylation of phenol [32] and ethyl benzene [33]. However, there is no study on catalytic application of Sn containing silicate for vapor phase aniline alkylation.

This chapter gives an account of heterogeneously catalysed vapour phase N-methylation of aniline over Sn containing microporous molecular sieves. This includes 1) comparison of catalytic performances of Sn-MFI with Al-MFI, Ti-MFI and Si-MFI, 2) optimization of reaction parameters viz; SiO_2/SnO_2 molar ratio, reaction temperature, weight hourly space velocity, molar ratio of aniline to methanol, reaction temperature and residence time, Sn-MFI catalyst stability and kinetics of the reaction.

3.2 EXPERIMENTAL

The details regarding the syntheses and characterization of Sn-MFI molecular sieves with different molar SiO_2/SnO_2 ratios ranging from 50 to 150 are provided in earlier Chapter 2. To compare the catalytic performance of Sn-MFI, TS-1(Ti-MFI, SiO_2/TiO_2= 50) and H-ZSM-5 (H-Al-MFI, SiO_2/Al_2O_3 = 60) were procured from Catalyst Pilot Plant, Catalysis & Inorganic Division of National Chemical Laboratory, Pune, India.

Vapor phase aniline alkylation with methanol was carried out in a down flow tubular SS316 (40 cm length x 2 cm internal diameter) reactor (Fig. 3.1). The reactor was heated to the required temperature with an electrical tubular furnace having digital temperature controller cum indicator. About 4 g of the catalyst (20–40 mesh size) was sandwiched at the centre by inert ceramic beads. Before start of the reaction, catalyst was activated in a N_2 flow (50ml/min) at 400^oC for 2hr. After catalyst activation, the catalyst temperature was reduced to desired reaction temperature. A molar mixture of aniline and methanol was fed at a required rate. The product was collected at a regular interval of time. The liquid mass balance for all the reactions was observed to be 98 ± 2%.

The feed and product were collected at regular interval of time and was analyzed by Gas Chromatography (Shimadzu, HP 5890A) using a flame ionization detector (FID) and carbowax column (30 m length x 0.3mm diameter). The products were confirmed by GC-MS. The *Weight Hourly Space Velocity, the %* conversion and selectivity are calculated as follows:

A. ***Weight Hourly Space Velocity*** (WHSV) = W/F

= weight of catalyst / weight of flow rate

B. % Conversion of Aniline and selectivity of products:

% Aniline conversion = (M_{AN} F- M_{AN} P / M_{AN} F) x100

M_{AN} F = Molar concentration of Aniline in feed

M_{AN} P = Molar concentration of Aniline in liquid product

% Selectivity of NMA = [C_{NMA}/ (C_{NMA}+ C_{NNDMA}+$C_{Oth.}$)] X 100

C_{NMA} = Concentration of NMA in liquid product

C_{NNDMA} = Concentration of NNDMA in liquid product

C_{Oth} = Concentrations of other products in liquid product

% Selectivity of NNDMA = $[C_{NNDMA}/ (C_{NMA}+ C_{NNDMA}+C_{Oth.})]$ X 100

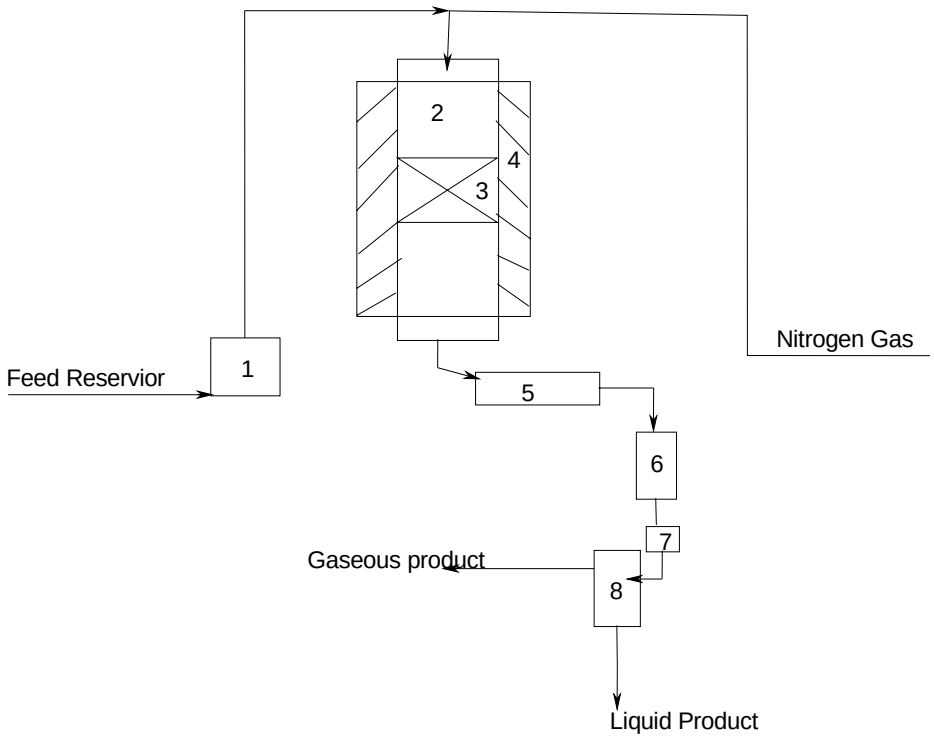

Fig. 3.1. Reaction Set Up

1: Feed Pump; 2: Fixed Bed Reactor (20cc); 3: Catalyst Bed; 4: Electrical Furnace; 5: Condenser; 6: High Pressure Product Receiver; 7: Back Pressure Valve; 8: Atmospheric Product Receiver.

3.3. RESULTS AND DISCUSSION

It is well-known that the N-alkylation corresponds to a nucleophilic SN2 mechanism. In SN2 mechanism, the rate of the reaction depends on the nucleophilicity of aniline and the "removability" of the OH group of methanol. Since the acidity of the catalyst aid the removal of the OH group and increase the nucleophilicity of the NH_2 group. In a similar mode, N, N-dimethyl aniline is produced from the methylation of N-methyl aniline by a consecutive reaction.

However, the conversion of aniline and secondary reaction pathway is depending on the reaction conditions and characteristics of the catalyst. Thus, the detail reaction studies on Sn-MFI sample were carried out to investigate application of Sn-MFI in aniline methylation.

3.3.1. Catalytic performances of Sn-MFI , H-ZSM-5 and TS-1

Aniline methylation is an acid driven reaction, thus a Sn-MFI (SiO_2/SnO_2 = 50) sample showing maximum Lewis acidic was chosen for the catalyst screening and its comparison study with H-ZSM-5 and TS-1. From **Table 3.1**, the trend of aniline conversion was found to be: Sn-MFI (39 %) ≅ H-ZSM-5 (41 %) >TS-1 (22%). Comparable aniline conversion and higher NMA selectivity was achieved with Sn-MFI (56 % NMA selectivity) sample as compared to H-ZSM-5 (46 % NMA selectivity).

Table 3.1. Catalytic performance over Sn-MFI,TS-1, H-ZSM-5 and Sn impregnated samples.

Performance (%)	**Thermal**	**Catalyst**			
		H-Al-ZSM-5	**TS-1**	**Sn-MFI**	**Sn impregnated MFI**
$Conv._{Aniline}$	3	41	22	39	5
$Sel._{NMA}$	92	46	69	56	90
$Sel._{N,N\text{-}DMA}$	8	52	30	41	9
$Sel._{Other}$	-	2	1	3	1

Reaction Condition: - Catalyst: 4g; Temperature: 240^0C; WHSV: 3 h^{-1}; Molar ratio (aniline: methanol): 1:6; Time on stream: 5h.

This comparable conversion could be attributed to almost identical acid density between Sn-MFI (5.31mmol/gm) and H-ZSM-5(5.01 mmol/gm). This indicates that, aniline conversion is directly proportional to the acidity irrespective of its origin (Bronsted or Lewis).Difference in NMA selectivity could be related to the nature of acidity i.e. Bronsted and Lewis acidity induced by H-ZSM-5 and Sn-MFI,

respectively. Even though Sn-MFI and TS-1 has equal SiO_2/MO_2 (M=Sn and Ti) molar ratio, TS-1 was found to be low aniline conversion than Sn-MFI. This may be due to more acidic nature of Sn-MFI (5.31mmol/gm) generated due to higher electronegative and atomic size of Sn than Ti in TS-1 (3.8mmol/gm). Thermal reaction (Table 3.1) at the identical reaction conditions with no catalyst, shows negligible aniline conversion (3 %). Pure silica MFI impregnated with $SnCl_4$ (Table 3.1) was observed to be less active. This may be due to hexacoordinated Sn-O-Sn type species in impregnated sample is inactive for aniline alkylation. These results indicate that, tin in tetrahedral coordination is the bare necessity for aniline conversion.

3.3.2 Effect of SiO_2/SnO_2 molar ratio

The effect of SiO_2/SnO_2 molar ratio in Sn-MFI on aniline alkylation with methanol were carried out at 200^oC, atmospheric pressure, weight hourly space velocity of 3 h^{-1} and methanol to aniline molar ratio of 6. The results obtained are presented in Table 3.2.

Table 3.2. Effect of SiO_2/SnO_2 molar ratio in Sn-MFI sample on catalytic performance

Performance (%)	**Molar ratio (SiO_2/SnO_2)**				
	50	**75**	**100**	**125**	**150**
Conv.$_{Aniline}$	55	54	37	27	25
Sel.$_{NMA}$	60	61	62	67	72
Sel.$_{DMA}$	38	38	36	30	27
Sel.$_{Other}$	2	2	2	3	01

Reaction Condition: - Catalyst: 4g; Temperature: 200^0C; WHSV: 3 h^{-1}; Molar ratio (aniline: methanol): 1:6; Time on stream: 5h.

It was found that conversion of aniline decreases with the increase of SiO_2/SnO_2 molar ratio. Maximum aniline conversion of 55% was observed with SiO_2/SnO_2 molar ratio of 50. This may be due to higher acidity, lower particle size and more surface area as compared to other studied samples. The cumulative effect of these catalyst properties, increases aniline conversion and reduces marginally NMA

formation, due to more rate of NMA alkylation as compared to rate of aniline alkylation.The further investigation on process parameters were carried out on Sn-MFI (SiO_2/SnO_2 = 50) catalyst.

3.3.3. Effect of Reaction Temperature

The effect of temperature on aniline conversion and product selectivity over Sn-MFI sample was carried out, keeping other process parameters identical. The results are tabulated in Table 3.3. As temperature increases from 200 to 260 ^oC, the aniline conversion was found to increase and remains constant above 260^oC. As a result of increase in temperature, N-methyl aniline selectivity was found to decrease with increase in NN dimethylaniline and others formation. This may be due to further alkylation of NMA to NNDMA and others [17]. The temperature of 240^oC was observed to be the optimum temperature. The study was further extended to see the effect of residence time.

Table 3.3. Effect of reaction temperature on catalytic performance

Performance (%)	**Temperature (^oC)**				
	200	**220**	**240**	**260**	**280**
Conv.$_{Aniline}$	40	51	55	60	62
Sel.$_{NMA}$	84	78	60	49	45
Sel.$_{N,N\text{-}DMA}$	15	21	38	47	50
Sel.$_{Other}$	1	1	2	4	5

Reaction Condition: - Catalyst (Sn-MFI): 4g; WHSV: 3 h^{-1}; Molar ratio (aniline: methanol): 1:6; Time on stream: 5 h.

3.3.4. Effect of Weight Hourly Space Velocity (WHSV), h-1

The effect of residence time i.e. WHSV was studied at 240^oC, keeping other process parameters identical. The results are presented in Table 3.4. The aniline conversion was found to be increased up to 71%, as WHSV decrease from 5 to 1h^{-1}. As decrease in WHSV (more contact time), NMA selectivity decreases by increasing

NNDMA and other formation. This may be partly attributed to higher contact time of reactants in catalyst environment and increased the NMA alkylation rate. The study was further extended to see the effect of concentration of methanol on catalytic activity.

Table 3.4. Effect of WHSV on catalytic performance

Performance (%)	**WHSV, h^{-1}**				
	1	**2**	**3**	**4**	**5**
Conv.$_{Aniline}$	71	66	55	46	41
Sel.$_{NMA}$	39	50	60	50	47
Sel.$_{N,N\text{-}DMA}$	58	47	38	46	49
Sel.$_{Other}$	3	3	2	4	4

Reaction Condition: - Catalyst (Sn-MFI): 4g; Temperature: 240^{O}C; Molar ratio (aniline: methanol): 1:6; Time on stream: 5 h

3.3.5. Effect of Aniline to Methanol Molar Ratio

Different molar ratio of aniline to methanol viz. 1:2, 1:4, 1:6, 1:8 and 1:10 were investigated at 240^{o}C, atmospheric pressure and WHSV of 3h^{-1}. Table 3.5 illustrates the influence of aniline to methanol molar ratio on aniline conversion and product distribution. It was observed that, increase in aniline to methanol molar ratio, increases the aniline conversion and decreases NMA selectivity with increase in NNDMA formation. The increased in methanol concentration enhanced alkylation of NMA to NNDMA over aniline.

Table 3.5. Effect of aniline : methanol molar ratio on catalytic performance

Performance	**Molar ratio (aniline : methanol)**				
(%)	**1:2**	**1:4**	**1:6**	**1:8**	**1:10**
Conv.$_{Aniline}$	43	49	55	58	60
Sel.$_{NMA}$	65	60	60	54	52
Sel.$_{N,N\text{-}DMA}$	33	39	38	44	48
Sel.$_{Other}$	2	1	2	2	

Reaction Condition: - Catalyst (Sn-MFI): 4g; Temperature: 240^{O}C; WHSV: 3 h^{-1}; Time on stream:5

3.3.6. Effect of Reaction Temperature and Residence Time

The effect of reaction temperature at different space velocity (residence time) on catalytic performance was investigated, keeping other process parameters identical. The results are presented in Fig. 3.2.

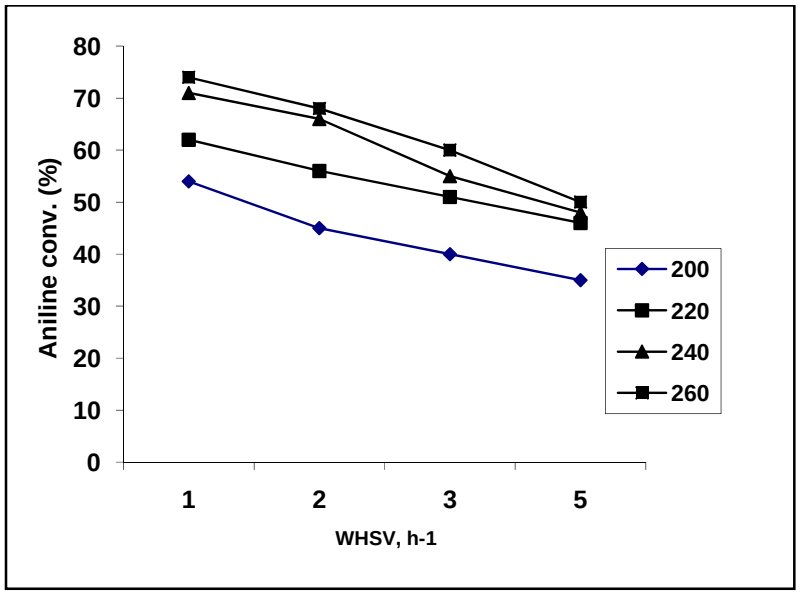

Fig. 3.2. Reaction Temperature and Residence Time over Sn-MFI (SiO_2/SnO_2 = 50).

The aniline conversion was found to decrease with the increase in space velocity. This may be due to less contact time of reactants in catalyst environment, at higher WHSV. As the temperature increases, aniline conversion also increases, for all the studied space velocities. This may be due to cumulative effect of the properties of Sn-MFI. The study was further extended to investigate the stability of Sn-MFI (SiO_2/SnO_2 = 50) at identical process parameters.

3.3.7. Catalyst stability

The stability of Sn-MFI (SiO_2/SnO_2 = 50) for aniline alkylation with methanol was studied at identical process parameters: 240^oC, WHSV of 3h^{-1}, molar ratio (aniline: methanol) of 1:6. The aniline conversion was found to be stable at 50-54% for a period of 10h (Fig. 3.3).

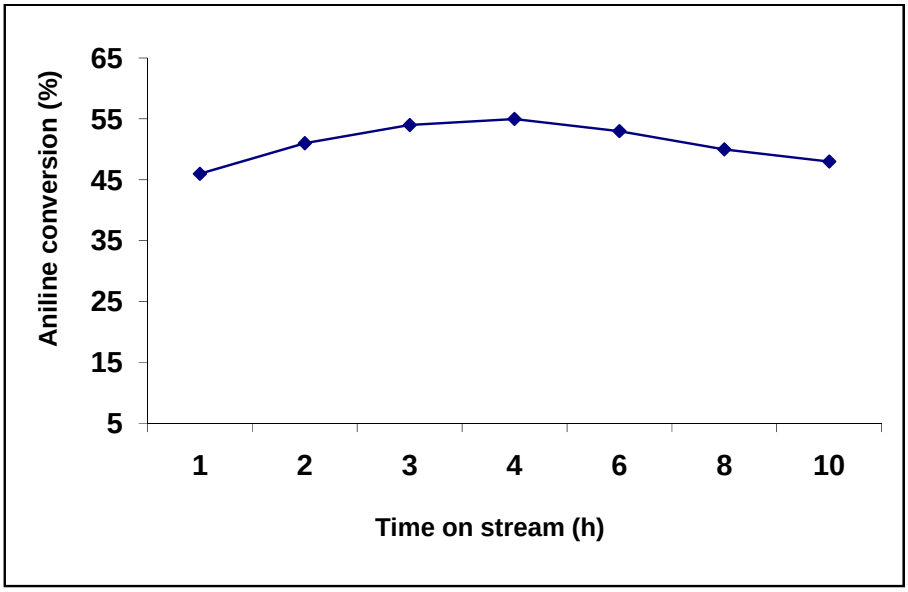

Fig. 3.3. Catalyst Stability over Sn-MFI (SiO_2/SnO_2 = 50).

Reaction Condition: - Catalyst: 4g; Temperature: 240^0C; WHSV: 3 h^{-1}; Molar ratio (aniline: methanol): 1:6

3.3.8. Reaction Kinetics

In the absence of both external and internal resistance to mass transfer, it is possible to determine the kinetics. Accordingly, for a pseudo first order reaction,

$$-d[A]/dt = k_{R1}\, w\, [A_o] \quad (1)$$

$$= k_1\, [A_o] \quad (2)$$

Where $k_1 = k_{R1}\, w$

Integrating equation 2, we get:

$$-\ln [A_o]/[A_o]_i = k_1\, t \quad (3)$$

Or $$-\ln (1-X_A) = k_1\, t \quad (4)$$

Or $$-\ln (1-X_A) = k_1\, (1/WHSV) \quad (5)$$

Where X_A is the fractional conversion of A i.e. aniline given as follows:

$$X_A = \{[A_o]_i - [A_o]\}/ [A_o]_i\} \quad (6)$$

Thus a plot of $-\ln(1-X_A)$ against time t or (1/WHSV) will give slope which represents k_1 and from which k_{R1} can be determined.

As can be seen from Fig. 3.4, the reaction follows the pseudo first order kinetics. From the slope, k can be found out and dividing with catalyst loading, w (g/cm^3), the k_R can be calculated.

Thus, $k = A\, e^{-Ead/RT}$

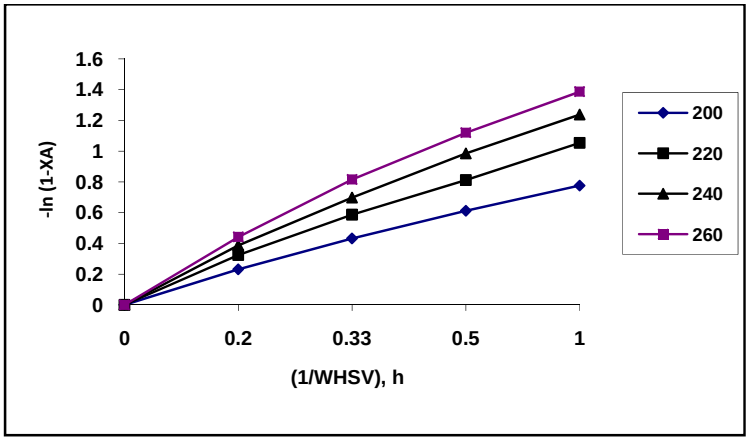

Fig. 3.4. Psuedo first order kinetics over Sn-MFI (SiO2/SnO2 = 50)

The surface adsorption constant obeys an Arrhenius type of equation. The Arrhenius plot of -ln k_1 against 1/T (Fig. 3.5**)**, with a slope equal to activation energy value of 7.3 kcal/mol**.**

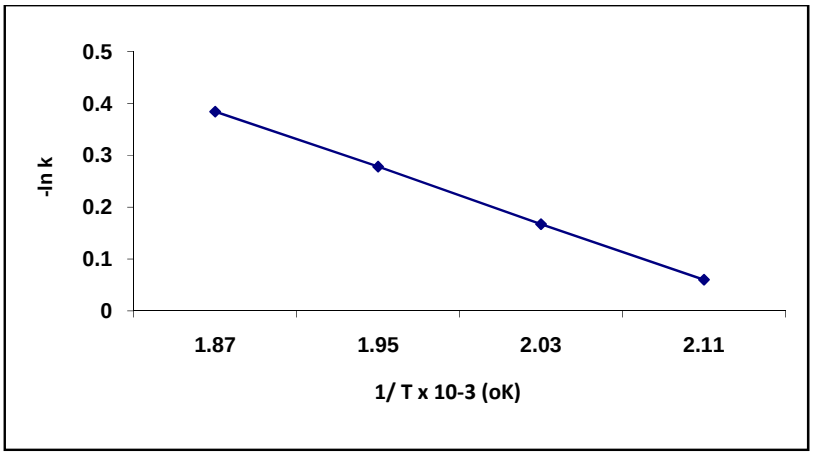

Fig. 3.5. Arrehenius plot over Sn-MFI (SiO_2/SnO_2 = 50).

3.4. CONCLUSION

Vapor phase methylation of aniline over Sn-MFI was systematically studied and optimizations of process parameters were carried out. The Sn-MFI (SiO_2/SnO_2 = 50) was found to be the optimum catalyst composition with 55% aniline conversion and 60% N-methylaniline selectivity at milder operating conditions of 240^oC, WHSV of 3h^{-1} and aniline to methanol molar ratio of 1:6. At lower WHSV of 1h^{-1}, aniline conversion was observed to be increased to 71% at the cost of reduction in NMA selectivity to 39% and enhancement in NNDMA selectivity to 58%. The reaction follows the pseudo first order kinetics with respect to aniline having activation energy of 7.3 kcal/mol.

3.5. REFERENCES

[1] Industrial Organic Chemicals, Ullmann's Encyclopedia, Wiley- VCH, 1 (1999).

[2] S. Narayanan, V. Durgakumari, A.S. Rao, Appl. Catal. A-Gen.; 111 (1994) 133.

[3] J. Santhanalakshmi, T. Raja, Appl. Catal. A-Gen.; 147 (1996) 69.

[4] S. Sunwanprasop, T. Nhujak, S. Roengsumran, A. Petsom, Ind. Eng. Chem. Res.; 43 (2004) 4973.

[5] S.R. Stauffer, J.F. Hartwig, J. Am. Chem. Soc.; 125 (2003) 6977.

[6] J.S. Kim, O.J. Shon, J.A. Rim, S.K. Kim, J. Yoon, J. Org. Chem.; 67 (2002) 2348.

[7] S. Narayanan, K. Deshpande, Appl. Catal.; 199 (2000) 1.

[8] F.M Baustista, J.M Campelo, G.D. Luna, J.M Marinas, A.A. Romero, M.R. Urbano, J. Catal.; 172(1997)103.

[9] F.M. Baustista, J.M. Campelo, G.D. Luna, J.M. Marinas, A.A. Romero, Appl. Catal. A-Gen.; 166(1998) 39.

[10] L.J. Garces, V.D. Makwana, B. Hincapie, A. Sacco, S.L. Suib, J. Catal.; 217 (2003) 107.

[11] I.I. Ivanova, E.B. Pomakhina, A.I. Rebrov, M. Hunger, Y.G. Kolyagin, J. Weitkamp, J. Catal.; 203(2001) 375.

[12] J. March, Advanced Organic Chemistry, Wiley, New York, 4th edn. (1991).

[13] M. Selva, P. Tundo, T. Foccardi, J. Org. Chem.; 70 (2005) 2476.

[14] A. Ko, C.Yang, W. Zhu, H.lin Appl. Catal. A-Gen.; 134 (1996) 53.

[15] M. Vijayaraj, C.S. Gopinath, J. Catal.; 241 (2006) 83.

[16] K. Sreekumar, T. Raja, B.P. Kiran, S. Sugunan, B.S. Rao, Appl. Catal. A-Gen.; 182 (1999) 327.

[17] Y. K. Park, K. Park, S.Woo ,Catal. Lett.; 26 (1994) 169.

[18] C. Yang, N. He , Q. Xu, J. Incl. Phen. Macro.; **35(**1999) 123.

[19] B. L. Su, D. Barthomeuf, Appl. Catal. A-Gen.; 124 (1995) 73.

[20] S.P. Elangovan, C. Kannan, B. Arabindoo, V. Murugesn, Appl. Catal. A-Gen.; 174 (1998) 213.

[21] G. D. Yadav, N. S. Doshi, J. Mol. Catal. A : Chem.; 194(2003) 195.

[22] S. Narayanan, K. Deshpande, J. Mol. Catal. A : Chem.; 104 (1995) L109.

[23] S. Narayanan, B. P. Prasad, J. Mol. Catal. A : Chem.; 96 (1995) 57.

[24] R. Luque, J. M. Campelo, D. Luna, J. M. Marinas, A. A. Romero, J. Mol. Catal. A : Chem.; 269 (2007) 190.

[25] S.I. Woo, J.K. Lee, B.S. Hong, Y.K. Park, Y.S. Uh, Stud. Surf. Sci.Catal.; 49B (1989) 1095.

[26] P.Y. Chen, M.C. Chen, H.Y. Chu, N.S. Chang, T.K. Chuang, Stud. Surf. Sci. Catal. 28 (1986) 739.

[27] J.M. Campelo, F. Lafont, J.M. Marinas, Zeolites; 15 (1995) 97.

[28] H. G. Karge, V. Dondur, J. Phys. Chem. 94 (1990) 765.

[29] H. G. Karge, V. Dondur, J. Weitkamp, J. Phys. Chem.; 95 (1991) 283.

[30] H. Jing, S.K. Edulji, J.M. Gibbs, C.L. Stern, H. Zhou, S.T. Nguyen, Inorg. Chem.; 43 (2004) 4315.

[31] M.R. Bryce, Chem. Soc. Rev.; 20 (1991) 355.

[32] N.K. Mal, V. Arumugamangalam, A.V. Ramaswamy, J. Mol. Catal. A: Chem. 105 (1996) 149.

[33] N.K. Mal, V. Arumugamangalam, A.V. Ramaswamy, Appl. Catal. A: Gen. 143 (1996) 75.

CHAPTER 4

SYNTHESIS, CHARACTREIZATION AND CATALYTIC PERFORMANCE OF Al^{3+} INSERTED Sn-MFI (Al-Sn-MFI) MOLECULAR SIEVES IN VAPOUR PHASE ANILINE N- METHYLATION.

4.1. INTRODUCTION

Beside reaction parameters, the factors contributing significantly to the performance and product distribution of the acid-catalysed organic transformation reaction are the type, number and the strength of acid sites in the solid catalyst. An influence of Lewis and Brønsted acid sites on conversion of aniline to alkylated aniline products has already been reported [1-4]. The use of strong Brønsted acid sites leads to increase the aniline conversion with more formation of byproducts such as N-dimethyl aniline (NNDMA), C-alkylated products and the coke. On other hand, the use of Lewis acid sites leads to increase the selectivity of N-alkylated products at the cost of aniline conversion. The simultaneous increase in both the Lewis and Brønsted acid sites has been reported [5] to improve the aniline conversion over vanadia-impregnated montmorillonite K-10. However, so far, there is no report on systematic studies on the investigating the synergy between Lewis and Brønsted acid sites to maximize the aniline conversion as well as N-methyl aniline (NMA) selectivity.

Because of the Brønsted/Lewis acid synergy, a remarkable increase in the acid strength of dealuminated HY zeolite is reported [6]. Similarly, mixed Al-Zr-TUD-1 catalyst demonstrated the synergy for Brønsted acid catalysed Prins cyclisation reaction [7]. An incorporation of Zn or Fe into Al-MCM-41 was also reported [8] for the generation of strong Brønsted acid sites, which lead to increase the toluene conversion in toluene isopropylation. The creation/enhancement of new redox and acidic sites in multi-metallic molecular sieve were observed as compared to monometallic counterpart [9-17]. A combination of Brønsted and Lewis acid sites on the catalyst surface was reported [18] to favor the aniline alkylation reaction. Moreover, in Al-Zr-beta catalyst, it is reported [19] that, presumably Zr^{4+} may strengthen the Brønsted acid sites and hence influence the isomerization of m-xylene. The information on prerequisites and eco-friendly considerations has triggered our interest in undertaking the research work on the synergy between Lewis and Brønsted acid sites for maximizing the aniline conversion and NMA selectivity.

As discussed in earlier chapter, Sn-MFI, a Lewis acid solid catalyst, has exhibited promising results in aniline alkylation with methanol. The simultaneous incorportion of Al^{3+} along with Sn^{4+} in the MFI framework can lead to the formation of Brønsted as well as Lewis acid sites. Such combination might play a prominent role in governing the specific catalytic property needed for enhancement in both, the conversion and product selectivity. Therefore, in view of maximizing the aniline conversion and NMA selectivity, we have investigated the synergetic effect of Lewis and Brønsted acid sites keeping total number of acid sites identical in Sn-MFI catalyst.

This chapter deals with the synthesis and characterization of Al-Sn-MFI with different degree of isomorphous substitution of Al^{3+} in Sn-MFI framework. The samples containing both Lewis and Brønsted acid sites were studied for the investigating the synergy effect between Brønsted and Lewis acidity in alkylation of aniline with methanol aiming at maximizing the aniline conversion and N-methylaniline selectivity .

4.2. EXPERIMENTAL

The synthesis of Al-Sn-MFI molecular sieve was carried out using TEOS (tetraethyl orthosilicate , 98%, Silbond), TPAOH (tetraethylpropyl ammonium hydroxide, aq. 20% solution, V.P. Chemicals), Tin(IV) chloride ($SnCl_4.5H_2O$, 98%, Loba Chem), aluminum isopropoxide (98%, Acros), distilled water, aniline (99.5 %, Rankem), and methanol (99.9% Rankem).

4.2.1 Preparation of Al-Sn-MFI molecular sieves

Keeping overall molar Si/(Al+Sn) ratio of 50 fixed, catalysts with varying molar Sn : Al ratios (ca. 1:0, 1:0.33, 1:1, 1:3, 0:1) were synthesized by DGC and hydrothermal crystallization method. The molar compositions used for preparation Initial hydrogel was: SiO_2: x SnO_2 : y Al_2O_3: 0.23 $(TPA)_2O$: 35H_2O, where x ranges from 1/0 to 1/200 and y from 1/0 to 1/400. The well crystalline Sn-MFI phases with no amorphous or impurity phase/s was obtained by establishing kinetics of crystallization. Upon calcination, the final products were designated as M100, M75,

M50, M25 and M0, where the numbers indicate the percentage of Sn moles in total (Sn+Al) moles present in the initial hydrogel.

A. Preparation by dry gel conversion method.

In a typical synthesis procedure for M50, 21.2 g of TEOS was added under stirring to a solution containing 0.21g of aluminum isopropoxide dissolved into 46.69 g of aq. TPAOH solution. To this, a solution of 0.35 g $SnCl_4.5H_2O$ in 25.6 ml distilled water was added with constant stirring. The clear solution formed was further stirred for 30 minutes. After drying at 80^oC, a white solid powder was obtained which was ground into a fine powder. This fine powder was charged into Teflon cup and placed in an autoclave (Fig. 2.2). The autoclave after being sealed was placed in an air-heated oven maintained at 160^oC for 15 hour. The autoclave was then quenched with cold water. The solid product was recovered, filtered and washed thoroughly with distilled water. After drying at 110^oC, it was calcined at 550^oC for 12 hour in air. Similar attempts were also made to synthesize M100, M75, M25, M0 samples.

B. Preparation by hydrothermal crystallization method.

In another approach to synthesize sample M50, conventional hydrothermal crystallization method was employed. The initial hydrogel was prepared by mixing 1) a solution containing 0.21g aluminum isopropoxide dissolved into 46.69 g of aq. TPAOH , and 2) a solution prepared by addition of aqueous solution of $SnCl_4.5H_2O$ (0.35 g $SnCl_4.5H_2O$ in 15 ml distilled water) to 21.2 g of TEOS under constant stirring. Then, the stirring was further continued till desired weight loss was achieved due to liberation of ethanol. Finally, 10.6 g distilled water was added to above mixture and stirring was continued for another 15 minutes. A clear gel thus obtained was then transferred to an autoclave and placed in an oven for crystallization at 160^oC for desired period (up to 40 h). The autoclave was then removed from the oven and quenched with cold water. The solid was recovered by filtration, then washed thoroughly with distilled water, dried at 120^oC and finally calcined at 550^oC for 12 h. Similar attempts were made to synthesize M100, M75, M25, M0 samples.

4.2.2 Characterization

The samples prepared by hydrothermal crystallization and DGC methods were characterized by powder X-ray diffraction, DRUV–vis spectroscopy, NH_3-TPD, pyridine-FTIR, elemental analysis and N_2 adsorption measurement. The details of these techniques are provided in Chapter 2, section 2.2. . Solid state ^{27}Al MASNMR spectra were obtained on a Bruker MSL-300 NMR spectrometer at 78.2 MHz with 3.0 kHz spinning speed, 1.5 μs excitation pulses (solution π /2 = 9 μs) and 0.25 s recycle times. Chemical shifts were referred to external $Al(H_2O)_6^{+3}$ in aqueous $AlCl_3$ solution.

4.2.3 Aniline Alkylation

Vapor phase aniline alkylation with methanol over M100, M75, M50, M25 and M0 was carried out according to the procedure described in Chapter 3.

4.3. RESULTS AND DISCUSSION

4.3.1. Preparation

A. Dry gel conversion method

The powder XRD patterns of all the samples prepared by DGC method have shown crystalline MFI phase without any impurity (figure not shown). However, samples M25 and M0 have shown poor crystallinity as compared to M100, M75 and M50. The DRUV-vis spectra of all the samples have shown presence of an absorption at ~ 220 nm and no band typical of polymeric Sn–O–Sn type species at 280 nm [21-23]. These spectral features indicated the occupancy of tetrahedrally coordinated Sn^{4+} species in MFI framework. However, ^{27}Al MAS NMR spectra of samples M25 and M0 exhibited signal (peak) at 0 ppm due to octahedrally coordinated aluminium species along with a signal at 50 ppm due to tetrahedrally coordinated aluminium species. Thus, this method seems to be unsuitable to achieve aluminous crystalline MFI phases comparable with that of others under present synthesis conditions. Since , it was desired to have samples with comparable characteristics having different combinations of Al^{3+} and Sn^{4+} in MFI framework [keeping overall molar Si/(Al+Sn) ratio ~ 50] for investigating the synergy effect between Brønsted and Lewis acidity

in alkylation of aniline with methanol, the set of samples obtained from DGC method was not further studied .

B. Hydrothermal crystallization method

The samples M100, M75, M50, M25 and M0 were prepared by hydrothermal crystallization method using hydrogel having molar gel composition SiO_2: x SnO_2 : y Al_2O_3: 0.23 $(TPA)_2O$: 35H_2O, where x ranges from 1/0 to 1/200 and y from 1/0 to 1/400 at 160^oC. Fig. 4.1 shows the typical crystallization kinetic curves for samples M100, M75, M50, M25 and M0. These curves exhibit typical sigmoid nature which is characteristics of processes involving nucleation and crystal growth respectively. As can be seen from the figure that, with increase in the Al content in the gel , there is a decrease in the rate of nucleation and crystal growth. Such reduction in rates might be due the higher concentration of aluminate species which may block the silica monomers which are needed for nucleation [20].

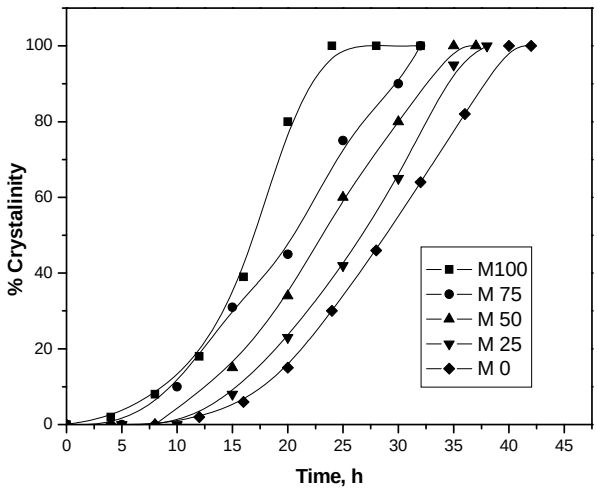

Fig. 4.1. Influence of molar SiO_2/ Al_2O_3 and SiO_2 /SnO_2 ratio in gel on the crystallization kinetics of M100, M75, M50, M25 and M0.

4.3.2. Characterization

4.3.2.1. *Powder X-ray diffraction*

The powder XRD patterns of M100, M75, M50, M25 and M0 in their as-prepared form are depicted in **Fig.4.2**. All samples have shown well crystalline nature and their XRD data match well with that of reported MFI phase [18]. No any contributions due to amorphous phase or other crystalline phase/s (impurity) were observed.

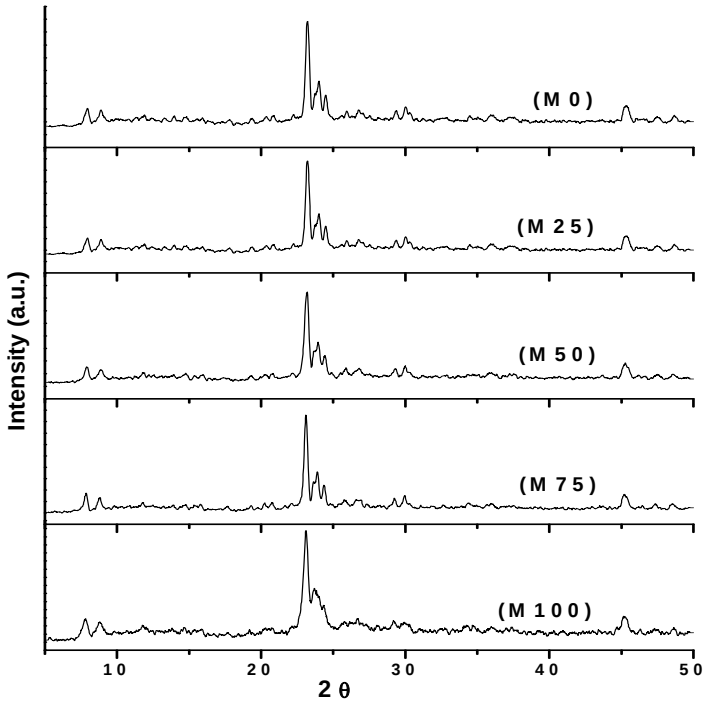

Fig. 4.2. Powder XRD patterns of M100, M75, M50, M25 and M0 samples in their as prepared form.

4.3.2.2. *Diffuse Reflectance UV-Vis Spectroscopy (DRUV-Vis)*

The DRUV–vis spectra of M100, M75, M50 and M25 were recorded for the verification of the framework occupancy of Sn^{4+}. All these spectra are presented in **Fig. 4.3**. Each sample has shown an absorption at ~ 220 nm which has been assigned to charge transitions (CT) from O^{2-} to Sn^{4+} in tetrahedral coordination [21-23].

Moreover, the intensity of this band was found to decrease with the decrease in the tin content from M100 to M25. All spectra showed no bands typical of polymeric Sn–O–Sn type species at 280 nm [21-23] indicating the absence of extra-framework occluded tin oxide. The identical spectral features in all these samples suggest the occupancy of Sn^{4+} species in MFI framework is in tetrahedral coordinated irrespective of presence of Al in variable proportion.

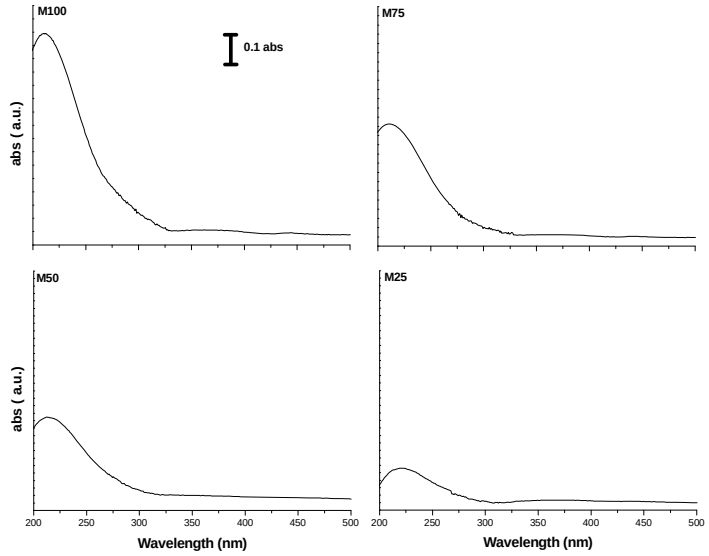

Fig. 4.3. Diffuse reflectance UV-vis spectra of M100, M75, M50 and M25

4.3.2.3. *^{27}Al MAS NMR*

^{27}Al MAS NMR spectra of M75, M50, M25 and M100 sample containing different proportion of Al and Sn are shown in Fig. 4.4. All the samples have exhibited a peak at 50 ppm assigned to tetrahedral aluminum. The absence of a signal (around zero ppm) due to octahedrally coordinated aluminum species confirms the fact that there is no dealumination from the crystalline framework occurring during calcinations (removal template) of material. However, the extent of broadening of NMR lines was found to decrease with the decreases Al content in initial gel composition, suggesting reduced distribution of aluminum with atoms having lower average coordination symmetry [24].

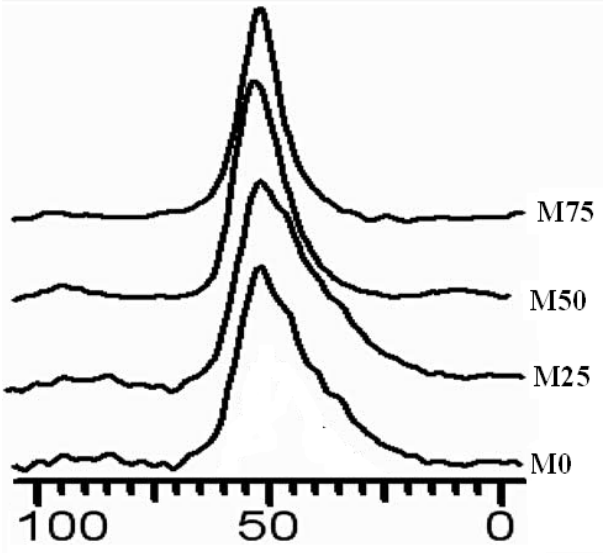

Fig. 4.4. ^{27}Al MAS NMR spectra of M75, M50, M25 and M0.

4.3.2.4. *Compositional and textural characteristics*

The chemical composition expressed as unit cell composition of all the samples is provided in Table 4.1.

Table 4.1. Unit cell composition, BET surface area and acidity data of all the samples.

Sample designation	**Unit cell composition (dry basis)**	**BET Surface area, m^2/g**	**mmol of NH_3 desorbed /g**		
			weak	**Rel. strong**	**Total**
M100	$(SiO_2)_{93.96}(SnO_2)_{2.04}$	431	0.53	-	0.53
M75	$(SiO_2)_{94.02}(SnO_2)_{1.46}(AlO_2)_{0.52}$	429	0.35	0.19	0.55
M50	$(SiO_2)_{93.83}(SnO_2)_{1.00}(AlO_2)_{1.17}$	415	0.38	0.21	0.59
M25	$(SiO_2)_{93.8}(SnO_2)_{0.48}(AlO_2)_{1.72}$	405	0.42	0.23	0.65
M0	$(SiO_2)_{93.4}(AlO_2)_{2.6}$	390	0.45	0.28	0.73

The Al and Sn was found to be absent in the sample M100 and M0 respectively. The Al content in the samples showed the trend as M0 > M25 > M50 > M 75 > M100 which is in close agreement with their initial gel molar compositions. Similar but reverse trend was observed in case of Sn content. The BET surface area of all the samples is tabulated in Table 1 and they are in the range of 390-431 m^2/g, which agreed well with those of zeolites with the MFI structures.

4.3.2.5. *Temperature Programmed Desorption of Ammonia (TPAD)*

An understanding of type, concentration and strength of acid sites in solid acids is one of the bare necessities to understand their synergetic effect on catalytic efficiency and behavior. Hence, all the samples were subjected to TPAD evaluation. Fig. 4.5 exhibits deconvoluted TPAD profiles of all samples. The deconvolution was performed using origin 8 software.

Upon deconvolution, M100 showed two desorption peaks. The maximum of first peak appeared at 111^oC and second peak maximum was at 209^oC. Except M100, all other samples exhibited three peaks in their respective deconvoluted patterns appearing at 109±7^oC, 189±4 ^oC and 381±21 ^oC. First and second peaks in all the samples can be assigned to desorption of physisorbed NH_3 and to desorption of NH_3 from weak acid sites, respectively [21]. All the samples, except M100, showed the existence of 3rd peak which can be assigned to relatively stronger acid sites. The area under this peak was found to increase with the increase in Al concentration. Thus, the origin of the relatively stronger acid sites in these samples might be the framework occupancy of Al^{3+}. Furthermore, the peak maximum was found to shift to higher temperature with the increase of Al. Thus, it seems that, with the increase in Al concentration, not only the population but also strength associated with these sites also increases. On the other hand, with the decrease in the Sn content, the only decrease in the area of the 2nd peak was observed in M75 as compared to M100. Surprisingly, with the further decrease in Sn content, the area of this peak was found to increase. Probably, higher degree of Al insertion in the framework might be responsible for the creation of stronger as well as weaker acid sites. It is evident from

Table 1 that, the total acidity increases with the increase in the Al content with simultaneous decrease in Sn content.

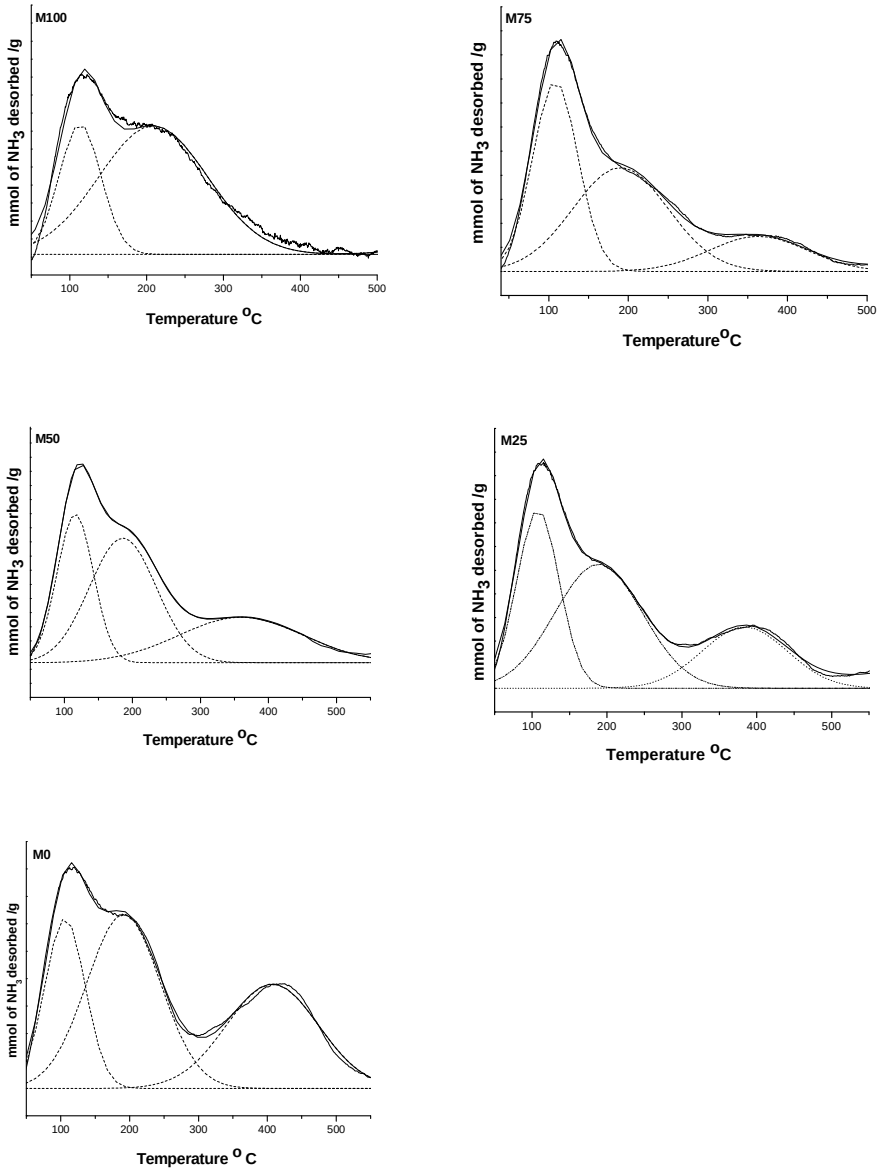

Fig. 4.5. Deconvoluted Temperature Programmed Ammonia Desorption profiles of M100, M75, M50, M25 and M0.

4.3.2.6. ***Pyridine Infrared spectroscopy***

The bands appearing at 1545 and/or 1455 cm^{-1} in pyridine-FTIR are assigned to pyridine coordinated to Brønsted and Lewis acid site respectively [25]. In present studies, the nature of the acid sites in all the samples was characterized by ex-situ FTIR spectroscopy with chemisorbed pyridine. The pyridine-FTIR spectra of all the samples are illustrated in Fig. 4.5.

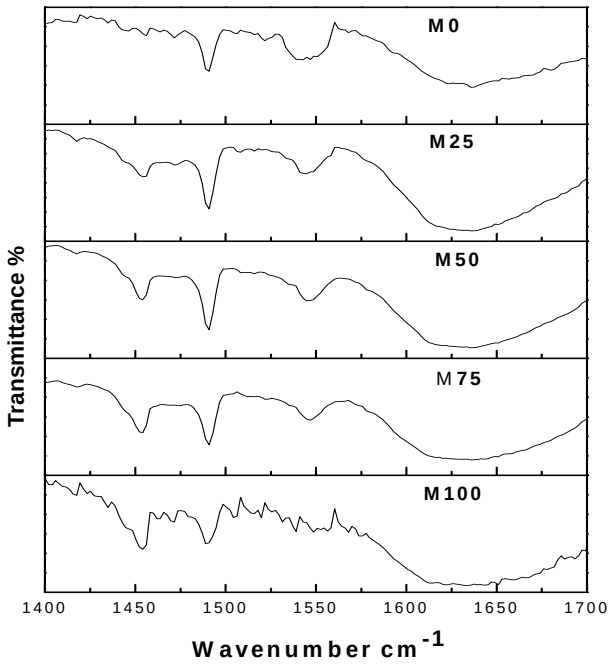

Fig. 4.6. Pyridine FTIR spectra of M100, M75, M50, M25 and M0.

The M100 sample showed two bands, one at 1455 cm^{-1} for Lewis acid site and another at 1490 cm^{-1}. The sample M0 also exhibited two bands, one at 1545cm^{-1} due to Brønsted–bound pyridine (pyridinium ion) and another at 1490 cm^{-1}. The common band at 1490 cm^{-1} in both M100 and M0 might be due to the contribution of Lewis and/or Brønsted acid sites. The bands at 1545 ,1455 and 1490 cm^{-1} due to Bronsted, Lewis and contribution of Brønsted and Lewis acid site respectively were appeared in spectra of samples M75, M50 and M25. Moreover, an intensity of band at 1445 cm^{-1} was found to decrease with the decrease in Sn concentration. Similar trend was

observed with the Al content in case of a band at 1545cm^{-1}. Based on the intensities of the bands appearing at 1545 and 1455 cm^{-1}, the Al-Sn-MFI samples viz. M75, M50 and M25 have shown the Brønsted/Lewis acidity ratio as 0.67, 0.91 and 1.27 respectively. Thus, a range of materials were successfully prepared for investigating the existence of synergy between Lewis and Brønsted acid sites in Al-Sn-MFI in acid catalyzed aniline N-methylation reaction to maximize the aniline conversion and N-methyl aniline (NMA) selectivity.

4.3.3. Aniline alkylation

Aniline alkylation is an acid catalyzed reaction. Beside reaction parameters, the characteristics of catalyst, in particular, the type, concentration and strength of acid sites in the catalyst are the main factors, which influence the activity and selectivity on N-alkylation of aniline. Using catalysts with different acidic properties, the synergetic effect of Brønsted/Lewis acid sites and strength on the catalytic performance was investigated systematically.

4.3.3.1. *Catalytic performance*

In order to improve the activity and to investigate an influence of Al^{3+} insertion in stannosilicate MFI structure, vapor phase N-methylation of aniline reaction was performed under optimized process parameters established in our earlier N-methylation of aniline study [21]. Fig.4.7a shows time on stream (TOS) data for methylation of aniline at temperature = 240 ^{O}C, WHSV = 3 h^{-1} and 1: 6 molar ratio of aniline to methanol. TOS study indicated that, the aniline conversion increases with increase in TOS up to 2 hour and then decreases with further increase of TOS. Steady state was apparently reached from 4th hour. Moreover, aniline conversion with M100 and M0 is found to be lower than other samples (M75, M50 and M25) having combination of Sn and Al. Thus, lower aniline conversion over sample M100 or M0 than sample M75, M50 and M25 suggest that presence of Sn and Al combination in a sample has distinct influence on aniline conversion. Data obtained at 4th h on all catalysts is selected for comparison and presented in Fig. 4.7b.

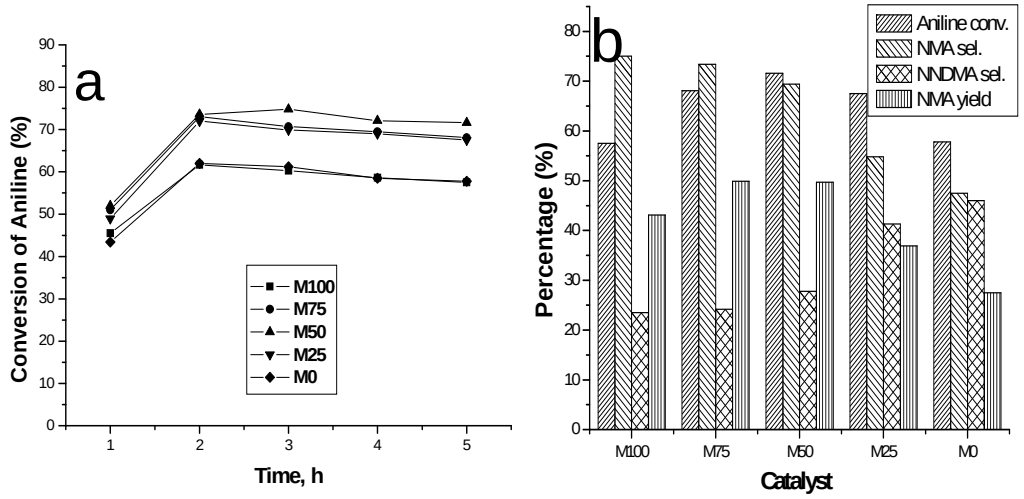

Fig. 4.7. Aniline methylation over samples M100, M75, M50, M25 and M0 (a) Aniline conversion with time on stream, and (b) comparative data at stable 4^{th} h.

It is evident from Fig.4.7b that, the aniline conversion increases from M100 to M50, reaches to maximum at M 50 and then further decreases from M50 to M0. In samples M100, M75 and M50, Al per unit cell increases from 0 to 1.17 (Table 4.1). As a result, the total acidity increases from 0.53 to 0.59 mmol of NH_3 per g (Table 4.1). Therefore, the aniline conversion increases from M100 to M50, reaches to maximum at M50. It is interesting to note that, with further increase in Al per unit cell (samples M25 and M0), decrease in aniline conversion was observed. Thus, in spite of having higher total acidity, M25 and M0 have shown lower aniline conversion. Probably, an increase in the stronger acid sites might be responsible for drop in the aniline conversion. Similar observations were reported by Narayanan et al [26] on alkylation of aniline over H-ZSM-5 with SiO_2/Al_2O_3 molar ratio from 30 to 280.

Fig.4.7b also exhibits the increases of NNDMA formation at the cost of NMA with the increase of Al per unit cell in sample M100 to M0 and the formation of other products (Toluidine, N-Methyl toluidine and N-Dimethyl touidine, in the range of 2-6 %). Woo et al [21] suggested that, the weak acidity helps to N-alkylation; medium acidity helps to NN-dialkylation and strong acidity to C-alkylation. The high

selectivity to NMA with M100 is because of the presence of a number of weak acid sites and increasing selectivity to NNDMA and others in M75-M0 samples is due to increasing trend of relatively strong acid site (medium acid site) with increasing Al.

Maximum NMA yield over M75 (49.9%) and M50 (49.7%) was found, while other samples showed lower NMA yield. An optimum number of weak (0.35 to 0.38 mmol of NH_3 desorbed per g) and relative strong (0.19 to 0.21 mmol of NH_3 desorbed per g) acid sites in M75 and M50 were found to maximize the NMA yield. In these samples, the weak acid sites are originated from framework Sn and Al, whereas; the relative stronger acid sites are induced by framework Al alone (**Fig. 4.5**). Generally, Al in zeolite framework induces Brønsted, while Lewis acid site imparted by tetrahedral substitution of Sn in the MFI framework. In conclusion, combination of Brønsted and Lewis acid sites with 0.67 to 0.91 B/L ratio in the samples M75 and M50 are found to be optimum for maximum NMA yield. Similar influence of Brønsted and Lewis acid sites combination (synergy between Brønsted and Lewis acid site) in Al-Zr-TDU-1 catalyst was reported by Telalovic [7] for Prins cyclisation reaction.

To optimize the reaction, the further studies on optimization of process parameters were carried out on optimum catalyst M50.

4.3.3.2. *Process parameters optimization*

4.3.3.2.1. Temperature

The effect of temperature on aniline conversion and product selectivity over M50 sample was carried out, keeping other process parameters identical. The results are tabulated in **Fig. 4.8**. As temperature increases from 220 to 260 ^oC, although, the aniline conversion was found to increase; there was a decrease in the selectivity towards N-methyl aniline. The drop in NMA selectivity is associated with the formation of undesired products such as NN dimethylaniline and others due to the further alkylation of NMA to NNDMA and others [1]. Thus, in the present studies, the optimum reaction temperature with respect to highest aniline conversion (65 %) and selectivity of NMA (80%) was identified as 220^oC.

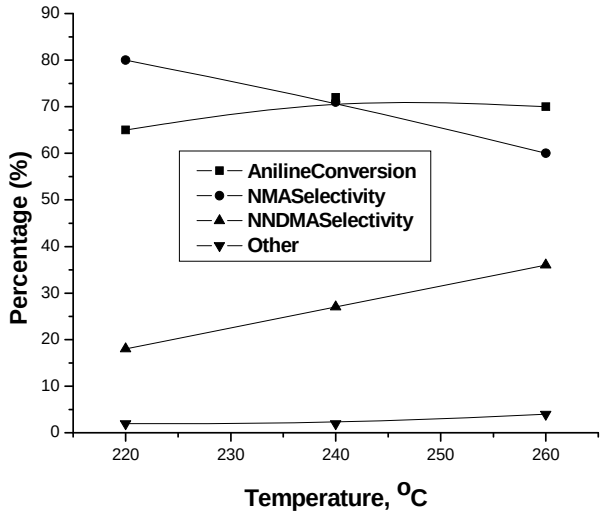

Fig. 4.8. Effect of temperature on the aniline conversion and selectivity over M50 (Mole Ratio Aniline to Methanol : 1:6, and WHSV: $3h^{-1}$)

4.3.3.2.2. Aniline to Methanol Molar Ratio

At optimum reaction temperature, different reactions were carried out with different molar ratios of aniline to methanol viz. 1:4, 1:6, 1:8 and 1:10 at atmospheric pressure and with WHSV of 3 h^{-1}. Fig. 4.9 illustrates the influence of aniline to methanol molar ratio on aniline conversion and product distribution.

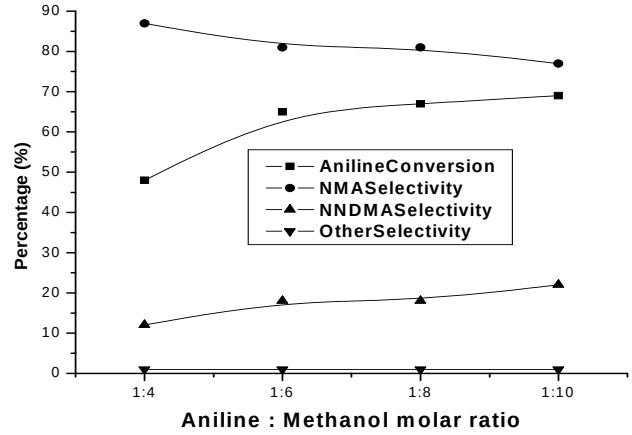

Fig. 4.9. Effect of mol ratio on the aniline conversion and selectivity over M50 (Temperature: 220^oC, and WHSV: $3h^{-1}$)

It was observed that, an increase in aniline to methanol molar ratio, the aniline conversion was increased from 48 to 69 %. However, the NMA selectivity was decreased from 87 to 77% with increase in NNDMA selectivity from 12 to 22 %. An increase in methanol concentration enhanced the rate of forward reaction leading to increase in the aniline conversion. At high conversion level, the NMA formed further reacts with available methanol to yield more NNDMA. The molar ratio of 1:8 was found to be the optimum molar ratio, which gave maximum aniline conversion (67 %) with 81% NMA selectivity. The study was further extended to optimize the contact time to maximize the NMA yield.

4.3.3.2.3. Weight Hourly Space Velocity (WHSV)

To optimize yet another reaction parameter, in particular WHSV, reactions with variable WHSV (from1 to 4 h^{-1}) were carried out at optimum reaction temperature (220^{o}C) and with aniline to methanol molar ratio of 1:8. The product distribution at 4th h for all these WHSVs are presented as Fig. 4.10.

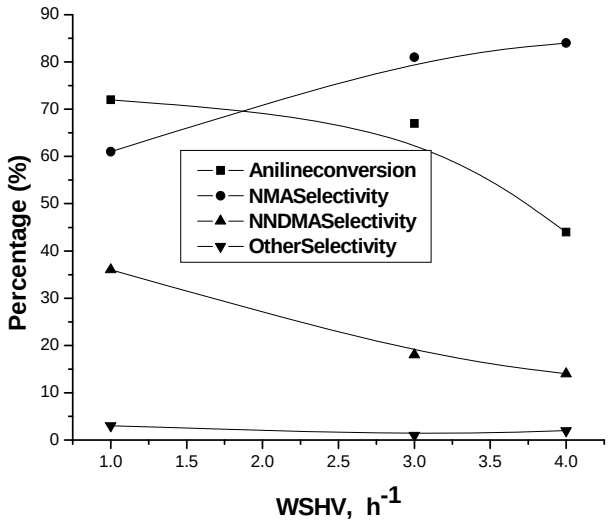

Fig.4.10. Effect of WHSV on the aniline conversion and selectivity over M50

(Temperature: 220^{o}C and Mole ratio: 1.8)

The aniline conversion was found to decrease with the increase in WHSV. The maximum aniline conversion (72 %) was obtained at WHSV =1 h^{-1}. In case of WHSV

= 4 h^{-1}, the aniline conversion was the least (44%), but the NMA selectivity was maximum (84%). There was an inverse proportion between the aniline conversion and NMA selectivity. The higher contact time (lower WHSV) increases NMA alkylation rate over aniline with the increase in aniline conversion. Considering the NMA yield, WHSV = 3 h^{-1} was found to be optimum which gave the maximum aniline conversion (67 %) and NMA selectivity (81 %) in the present studies.

4.3.4. Catalyst stability

In order to test the stability of the optimum catalyst and to examine the dependence of stability on the synergy between Lewis and Brønsted acid sites, M50 and M25 catalysts were subjected to the stability test under optimum reaction conditions. The alkylation of aniline with methanol was carried out at 220^{o}C with WHSV = 3h^{-1} using feed containing aniline and methanol in the molar ratio of 1:8. The results with regard to product distribution as a function of reaction time up to 10 h are shown in **Fig. 4.11**.

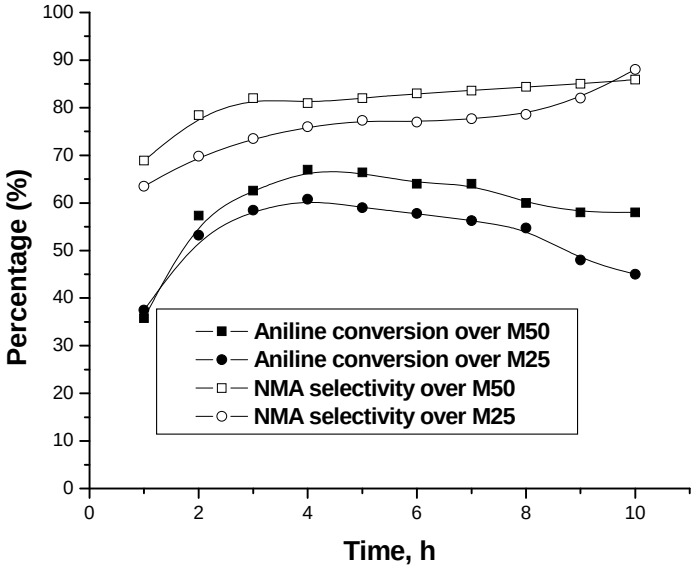

Fig.4. 11. Stability test for M50 and M25 catalysts under optimum reaction conditions. (Temperature: 220^{o}C, Mole ratio: 1.8, and WHSV: 3h^{-1})

M50 catalyst was found to be stable up to 10 h and has shown the stable aniline conversion and NMA selectivity of the order 36-67 % and 69-86 % respectively. As compared to M50, M25 has shown less stability, which has reflected in the drop in conversion from 8^{th} h. This phenomenon may be attributed to the higher Brønsted/Lewis acidity ratio of M25 as compared to M50. Thus, it seems that, there exist a synergy between Lewis and Brønsted acid sites in Al-Sn-MFI in aniline N-methylation reaction and catalyst stability as well.

4.4. CONCLUSION

Different degree of isomorphous substitution of Al^{3+} in the stannosilicate framework with MFI topology was achieved by hydrothermal crystallization. These catalysts were synthesized by hydrothermal crystallization of gels having molar compositions SiO_2: x SnO_2: y Al_2O_3: 0.23 $(TPA)_2O$: 35H_2O, where x ranges from 0 to 200 and y from 0 to 400. Although, Sn: Al ratio was varied (ca. 1:0, 1:0.33, 1:1, 1:3, 0:1), the overall molar Si/ (Al+Sn) ratio was kept constant as 50. It was evident from the TPAD results that, the framework tin species create the weak acid sites whereas insertion of Al lead to the creation of both the weaker as well as relatively stronger acid sites. With an increase in Al^{3+} insertion in Sn-MFI molecular sieves, there is an increase in the Brønsted/Lewis acidity ratio as well as the total acidity. Based on Brønsted/Lewis acidity ratio, the Al-Sn-MFI samples followed the trend as M75 < M50 < M25. These samples showed higher aniline conversion than the samples containing either Al or Sn alone. Interestingly, an increase in stronger acid sites with an increase in framework Al^{3+} leads to decrease in aniline conversion. Thus, synergy between Brønsted and Lewis acid sites in Al-Sn-MFI catalysts was demonstrated to exist in aniline N-methylation reaction. Upon process parameter optimization, Al-Sn-MFI with Si/Al = 50.2 , Si/Sn= 93.8, Si/(Al+Sn) = 43.2 showed the maximum aniline conversion (67 %) and NMA selectivity (81 %) at reaction temperature = 220^oC, WHSV = $3h^{-1}$, molar ratio (aniline to methanol) = 1:8 and TOS = 4 h. On account of higher Brønsted/Lewis acidity ratio, M25 (1.27) was found to be less stable as compared to M50 indicating the dependence of stability on a synergy between Lewis and Brønsted acid sites in Al-Sn-MFI .

4.5. REFERENCE

[1] Y. K. Park, K. Park, S.Woo ,Catal. Lett.; 26 (1994) 169.

[2] S.I. Woo, J.K. Lee, B.S. Hong, Y.K. Park, Y.S. Uh, Stud. Surf. Sci.Catal.; 49B (1989) 1095

[3] P.Y. Chen, M.C. Chen, H.Y. Chu, N.S. Chang, T.K. Chuang, Stud. Surf. Sci. Catal.; 28 (1986) 739.

[4] J.M. Campelo, F. Lafont, J.M. Marinas, Zeolites; 15 (1995) 97.

[5] S. Narayanan, K. Deshpande, Appl. Catal. A-Gen.; 199 (2000) 1.

[6] S. Li, A. Zheng, Y. Su, H. Zhang, L. Chen, J. Yang, C. Ye, F. Deng, J. Am. Chem. Soc.; 129 (2007) 11161.

[7] S. Telalović, J.F. Ng, R. Maheswari, A. Ramanathan, G.K. Chuah, U. Hanefeld, Chem. Commun.; (2008) 4631.

[8] R. Savidha,_ A. Pandurangan, M. Palaichamy, and V. Murugesan, Catal. Lett.; 91 (2003) 49.

[9] V. Parvulescu, C. Anastasescu, and B.L. Su, J. Mol. Catal. A: Chem.; 211 (2004) 143.

[10] V. Parvulescu, C. Anastasescu, C. Constantin, and B.L. Su, Catal.Today; 78 (2003) 477.

[11] V. Parvulescu, Cr. Tablet, C. Anastasescu, and B.L. Su, Catal. Today; 93–95 (2004) 307.

[12] V. Parvulescu, C. Constantin, and B.L. Su, J. Mol. Catal. A: Chem. ; 202 (2003) 171.

[13] R. Savidha and A. Pandurangan, Appl. Catal. A: Gen.; 276 (2004) 39.

[14] S. Vetrivel and A. Pandurangan, J. Mol. Catal. A: Chem. ; 217 (2004) 165.

[15] M. Selvaraj, B.R. Min, Y.G. Shul, and T.G. Lee, Micropor. Mesopor. Mat. ; **7**4 (2004) 143.

[16] V. Parvulescu and B.L. Su, Stud. Surf. Sci. Catal.;143 (2000) 575-584.

[17] V. Parvulescu, C. Anastasescu, and B.L. Su, J. Mol. Catal. A: Chem. ; 198 (2003) 249.

[18] S. Narayanan, K. Deshpande, J. Mol. Catal. A: Chem.; 104 (1995) 109.

[19] B. Rakshe, V. Ramaswamy, A.V. Ramaswamy , J. Catal.; 188 (1999) 252.

[20] R.B. Borade, Ph.D.Thesis, submitted to University of Pune, (1983)

[21] P. S. Niphadkar, P. N. Joshi, H. R. Gurav, S. S. Deshpande and V. V. Bokade, Catal. Lett.; 133 (2009) 175.

[22] K. Chaudhari, T.K. Das, P.R. Rajmohanan, K. Lazar, S. Sivasanker, A.J. Chandwadkar, J. Catal.; 183 (1999) 281.

[23] P.S. Niphadkar, A.C. Garade, R.K. Jha, C.V. Rode, P.N. Joshi, Micropor. Mesopor. Mat. 136 (2010) 115.

[24] I. Kiricsi, C. Flego, G. Pazzuconi, W.O. Parker Jr., R. Millini, C. Perego, G. Bellusi, J. Phys. Chem.; 98 (1994) 4627.

[25] P.S. Niphadkar, K.R. Patil, P.N. Joshi, Micropor. Mesopor. Mat.; 141(2011) 236.

[26] S. Narayanan, V. Durga Kumari, A. Sudhakar Rao, App. Catal.; 111 (1994) 133.

CHAPTER 5

OXYANION INDUCED CRYSTALLIZATION, CHARACTERIZATION AND CATALYTIC APPLICATION OF MICROPOROUS LARGE PORE Sn-BEA MOLECULAR SIEVES

5.1. INTRODUCTION

Zeolite beta (BEA) is a wide-pore and high-silica microporous molecular sieve whose structure consists of an intergrowth of two or more polymorphs comprising a three-dimensional system of 12-membered ring channels [1,2]. Due to its high thermal and chemical stability, strong acid sites, hydrophobicity and large pore size, zeolite Beta has demonstrated its potential as one of most important catalytic materials for variety of industrially important organic transformation reactions [3-5]. These catalytic performances of beta zeolite depends upon acid site like Bronsted and Lewis acid of Beta zeolite which can be tuned by isomorphous substitution of metal group IIIA (Al,B), IVA (Ge) and transition metal (Ti,V, Sn, Zr) [6-11]. In recent year, it has been shown that the isomorphous substitution of Ti and Sn into the all silica Beta zeolite framework provides a useful catalyst for hydroxylation [13], epoxidation [12], Baeyer-Villiger Oxidation [6, 14] and Meerwin-Ponndorf-Verley reaction (MPVO) [15]. Moreover, crystalline microporous stannosilicate molecular sieve with BEA topology (Sn- BEA) has shown better catalytic performance than Ti-BEA because of higher atomic size and electronegativity of Sn than the Ti atom, giving rise to stronger Lewis acid sites [12, 16]. Although, Sn-BEA has exhibited excellent performance in catalytic heterogeneous organic reactions where Lewis acid site plays a major role, more emphasis has been given to its catalytic applications rather than its synthesis. The lack of state-of-art, more defined synthesis conditions and need of longer crystallization period might be some of the probable reasons for negligible efforts that have been devoted for synthesis of Sn-BEA.

In 1997, Mal et al. first reported [12] the synthesis of Al-free-Sn-BEA from basic reaction medium. They have reported two routes for the synthesis of Sn-BEA viz. (1) crystallization of a Al-free gel containing dealuminated BEA seed, and (2) crystallization of Al-Sn-BEA from a gel comprising sources of aluminium, tin and silicon but contains no seed (synthesis time : about 10 days at 415 K) followed by dealumination treatment to Al-Sn-BEA molecular sieve. However, the synthesis in the conventional basic medium usually results in the formation of connectivity defects which affects the sorption, hydrophilic/hydrophobic properties and thermal stability [17]. In view of improving the hydrophobicity and thermal stability, Corma et al.

reported [6, 13, 17, 18] the synthesis of Sn-BEA in fluoride medium at neutral pH using dealuminated Beta as a seed (synthesis time: ~ 20 days at 413 K). In these prior arts, the seed used is prepared by dealumination method that involves repetitive leaching of aluminum from the framework. It is likely that, the aluminum leached may reside/occlude in the seed crystals and structural features of the seed crystals may get damaged due to severe treatments. Use of such crystals may lead to the detrimental effect of Sn-BEA formed for its catalytic performance. One can not also rule out the possibility of removal of Sn from the BEA framework while dealuminating Al-Sn-BEA. Moreover, preparation of seed or dealumination of Al-Sn-BEA also makes the process complex and add to cost and overall process time. Until now, no route has been reported for the synthesis of Sn-BEA from a gel containing no seed and/or no aluminium source.

In view of above, the development of a facile and cost-effective route for the synthesis of Sn-BEA is needed. Attempts to perform the synthesis of Sn-BEA by dry gel conversion method failed when a dry gel containing no seed and no aluminium source was used. Assuming that, in hydrothermal crystallization route, the addition of seed crystals to a crystallization system typically results in increased nucleation and crystallization rates, it was thought to use oxyanions in the crystallization gel in place of seed. In 1996, R. Kumar et al. have reported [19] the enhancement in the rate of crystallization by addition of oxyanions in the form of acid or salt in the crystallization gel.

The information on prerequisites and need of development of facile route for the synthesis of Sn-BEA have triggered the interest to carry out the work on 'oxyanion induced hydrothermal synthesis of Sn-BEA in fluoride media using Al-free hydrogel comprising no seed (dealuminated or otherwise)' . In this chapter, the work related to oxyanion induced hydrothermal synthesis of microporous stannosilicate molecular sieve with BEA topology (Sn- BEA) using fluoride route using Al-free gel containing no seed is presented. It also describes the influence of molar ratios of TEA+/ SiO_2 and SiO_2/SnO_2 in initial gel composition on the crystallization period, % crystallinity and physico-chemical properties of Sn-BEA. Product characterization was carried out by Powder XRD, AAS, IR, DRUV-Vis and

SEM. The performance of Sn-BEA in BV oxidation reaction and N-methylation of aniline is also included in this chapter.

5.2. EXPERIMENTAL

5.2.1. Hydrothermal crystallization of Sn-BEA

The synthesis of Sn-BEA molecular sieve was carried out in a stainless steel high pressure autoclave of 250 ml. capacity at 140OC. The time dependent crystallization studies were conducted to obtain well crystalline and pure Sn-BEA phases. The extent of crystallization was monitored as a function of crystallization period where the time at which the autoclave attained the 140OC temperature was taken as zeroeth hour. The kinetic experiments were carried out by stopping the reaction at different time intervals. Before the withdrawal of the sample at room temperature, the synthesis mixture was stirred in order to homogenize the slurry. After withdrawal of the sample, the autoclave was sealed and subjected for further crystallization.

The raw materials used for the syntheses were tetraethyl orthosilicate (TEOS, 98%, Silbond), tetraethyl ammonium hydroxide (TEAOH, aq. 40% solution, V.P. Chemicals), hydrofluoric acid (HF, 48 wt %, Thomas Baker), Tin(IV) chloride ($SnCl_4$.5H2O, 98%, Loba Chem), sulfuric acid (H_2SO_4, 98%, Rankem), orthophosphoric acid (H_3PO_4, 95%, Qualigen), perchloric acid ($HClO_4$, 70%, Merck), sodium aluminate (43.8% Al_2O_3, 39.0% Na_2O, Loba Chem) , sodium hydroxide (NaOH, 98 % AR Loba Chem), silica sol (40% SiO_2, Loba Chem) and nitric acid (HNO_3, 60 %, Loba Chem) . In a typical synthesis procedure, 42.4 g of TEOS and 39.69 g of TEAOH were mixed together under vigorous stirring. The stirring was further continued at room temperature. The weight loss (~ 17 %) due to liberation of ethanol was observed. To this mixture, solution of 0.58 g of $SnCl_4.5H_2O$ in 10 m1 water and 4.5 g HF was added with constant stirring. Finally, 2.84 g of 70 % aqueous perchloric acid, used as promoter, was added to the above mixture with vigorous stirring, which was continued till homogeneous gel was formed. A molar composition of this resultant gel was estimated to be SiO_2 : 0.0083 SnO_2: 0.54 TEAOH: 0.54 HF : 0.1 $HClO_4$: 7.5 H_2O. The resultant starting gel was then transferred to autoclave and

subjected to hydrothermal treatment at 140^{o}C for crystallization time ranging from 6 to 30 days. After crystallization, the solid product was separated by vacuum filtration and dried at 120^{o}C for 4hr. The dried product was further calcined at 550^{o}C for 12 hr in air.

In order to investigate the influence of synthesis parameters such as type of oxyanion source, molar ratios of $(TEA)_2O/ SiO_2$, HF/SiO_2 and SiO_2/SnO_2 in gel on the type of phase formed and hence in turn, to optimize the molar gel composition for synthesis without aid of seed, a number of trials was conducted using homogenous gels having following molar compositions:

SiO_2: 0.0083 – 0.0166 SnO_2: 0.54 - 1.3 TEAOH: 0.54 - 1.3 HF: 7.5 H_2O: 0.0 - 0.1 H_2SO_4/ H_3PO_4 / $HClO_4$ (source of promoter).

The molar gel composition and result obtained from each trial is given in Table 5.1. All silica BEA sample (designated as sample E) was also prepared by following similar procedure except addition of tin source in the initial gel.

For comparison purpose, Sn-BEA was also synthesized from a gel containing seed (5 wt % w.r.t. SiO_2). The seed was prepared by dealuminating Al-BEA zeolite. The Al-BEA zeolite was synthesized by hydrothermal crystallization method. A solution of 0.78 g sodium aluminate and 0.25 g sodium hydroxide in 28 DM water was prepared and added to 19.6 g of aqueous solution of TEAOH under continuous stirring. To this solution, 15 g silica sol was slowly added under vigorous stirring. The resultant homogeneous gel has shown the molar gel composition as 6.0 $(TEA)_2O$: 2.4 Na_2O: 30.0 SiO_2:Al_2O_3: 840.0H_2O. This gel was then transferred to a stainless steel autoclave and heated at 140^{o}C for 3 days. The product was recovered by centrifugation, washed with distilled water and dried at 100^{o}C. The powder XRD data of this product match well with that of zeolite BEA and shown well crystalline nature without any impurity or amorphous phase contribution. This Al-BEA sample was dealuminated by treating 1 gm of beta zeolite with 60 g HNO_3 (60 wt %) at 80^{o}C for 24 hours. The solid was recovered by filtration, washed with water and dried with 100^{o}C. The crystallinity of this product was found to be comparable with that of crystallinity of parent sample and Si/Al was found around 1000.

5.2.2. Characterization

Powder X-ray diffraction (XRD) patterns of samples were recorded on X-ray diffractometer (Rigaku Miniflex, Japan) using Cu-Kα radiation. The diffraction data were collected in the 2θ range of 5o to 50o with a scanning rate of 1o min-1. The % crystallinity of the sample was calculated by comparing the integrated areas of the characteristic peaks appearing at 2θ = 7.8 o and 22.6 o of test sample to that of the most crystalline and pure beta phase obtained in the each series studied. The detail experimental procedure and equipment used for low temperature nitrogen adsorption, DRUV-Vis, FT-IR, SEM and chemical analyses are described in Chapter 2.

5.2.3. Catalytic reactions

Oxidation of cyclohexanone over selected Sn-BEA samples containing different Sn content was carried out batch wise in a glass vessel fitted with a condenser. 1 mmol of cyclohexanone (98%, Loba chem.) and 3 mmol of hydrogen peroxide (50 %, Fisher) were dissolved in dioxane(99% Aldrich). To this reaction mixture, 50 mg of Sn-BEA sample was added under stirring. Final mixture was heated at 80^{o}C for 7 h under stirring. The products were analyzed by gas chromatography (Varian, equipped with a capillary column, 20 m in length and flame ionization detector) and confirmed through authentic samples.

N-methylation of aniline was carried out for evaluation of Sn-BEA samples. Reactor set up, experimental details and analytical method are described in Chapter 3.

5.3. RESULTS AND DISCUSSION

5.3.1. Oxyanion induced hydrothermal crystallization

In case of isomorphously substituted titanosilicate with MFI structure (TS-1), the use of oxyanion in synthesis gel has been reported [19] to accelerate significantly the nucleation and crystallization processes on account of enhancement in the rate of formation of tetrameric silicate ions. Based on this, attempts were made to investigate the feasibility of oxyanion induced hydrothermal synthesis of Sn- BEA using fluoride route with gel containing no seed and no aluminium source. Moreover, optimization of synthesis parameters was also carried out. Kinetics of crystallization

was carried out to obtain well crystalline and pure Sn-BEA. The details of each synthesis trial disclosing the information related to the types of the phases from each gel , gel composition , promoter type and concentration, presence/absence of seed , time required to obtain pure and most crystalline BEA phase are summarized in Table 5.1.

Table 5.1. The influence of gel composition, oxyacid and seed on the required crystallization time to obtain crystalline Sn-BEA at 140^{o}C.

Expt. No.	Molar Gel Composition					Oxyacid	Seed	Time	Phase
	SiO2	SnO2	TEAOH	HF	H2O	(moles)	(wt %)	(days)	
1	1	0.0083	0.54	0.54	7.5	-	5	20	Beta
2	1	0.0083	0.54	0.54	7.5	-	-	30	A*
3	1	0.0083	0.54	0.54	7.5	0.1a	-	21	Beta
4	1	0.0083	0.54	0.54	7.5	0.1b	-	20	Beta
5	1	0.0083	0.54	0.54	7.5	0.1c	-	18	Beta
6	1	0.0083	0.70	0.54	7.5	0.1c		30	A*
7	1	0.0083	1.3	0.54	7.5	0.1c		30	A*
8	1	0.0083	0.70	0.7	7.5	0.1c	--	9	Beta
9	1	0.0083	1.3	1.3	7.5	0.1c		6	Beta
10	1	0.0100	1.3	1.3	7.5	0.1c		7	Beta
11	1	0.0125	1.3	1.3	7.5	0.1c		11	Beta
12	1	0.0166	1.3	1.3	7.5	0.1c		30	A*

*: Amorphous; a: H_2SO_4; b: H_3PO_4; c: $HClO_4$.

While following the reported procedure [6] for synthesis of Sn-BEA , the seed (dealuminated BEA zeolite) was used in the initial gel and then subjected for hydrothermal crystallization (Expt. No. 1 in Table 5.1). The overall crystallization period required to obtain well crystalline Sn-BEA was 20 days. The product was

recovered by filtration, dried and then calcined. This product was designated as Sample A. Under identical set of synthesis conditions, a gel without seed (Expt. No. 2 in Table 5.1) has yielded amorphous phase even if the crystallization period was prolonged to 30 days. It is clearly evident from these two syntheses trials that, addition of seed in the initial gel promotes the process of conversion of amorphous gel into crystalline BEA phase. However, even in presence of seed, it suffered from the longer crystallization period. In order to investigate In order to replace the seed by oxyanion, the addition of oxyanions, in particular, perchlorate, sulphate, phosphate was added in the initial reaction mixture. These oxyanions are used in the form of acid and the molar ratio of SiO2 to oxyacid in gel was kept 10. (Expt. Nos. 3, 4, 5 in Table 5.1). The time dependent crystallization studies were carried out. The crystallization kinetics curves are shown in Fig. 5.1. The least time to achieve pure well crystalline Sn-BEA was taken by the gel containing perchlorate ions. The effectiveness of promoters in decreasing the synthesis time follows the order HClO4 > H3PO4 > H2SO4 >>> none . Thus in present studies, the highest polarizing ability of perchlorate ions might be responsible for the facilitating the nucleation and crystallization processes to the maximum extent .

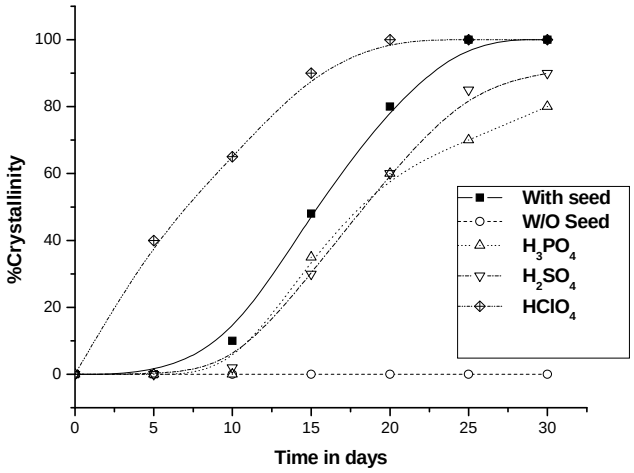

Fig. 5.1. Kinetics of crystallization of Sn-Beta synthesis in presence of seed and different oxyacids.

For further optimization studies, the gel composition of Expt. No.5 cited in Table 5.1 was selected. The influence of molar ratios of $(TEA)_2O/ SiO_2$, , HF/SiO_2 and SiO_2/SnO_2 in the gel on the type of phase formed and the period required to achieve Sn-BEA was studied systematically by varying one parameter at a time. To start with, the parameter, molar ratio of $(TEA)_2O/ SiO_2$ in the gel was considered. TEAOH is a simultaneous source of TEA^+ and OH^- which has an ability to enhance nucleation and crystallization [20]. Keeping molar ratio of SiO_2/SnO_2, HF/SiO_2, $HClO_4/SiO_2$ and H_2O/SiO_2 constant, the $(TEA)_2O/ SiO_2$ was systematically increased from 0.27 to 0.65 (Expts. 5,6,7 in Table 5.1). Except experiment Expt. No. 5, other two experiments, in particular, 6 & 7, were failed to yield any crystalline phase even if the crystallization period was prolonged to 30 days. Thus it was thought to increase HF concentration in such a way that molar TEAOH/HF ratio becomes unity. Therefore in next runs (Expt. Nos. 8, 9 in Table 5.1), the molar $(TEA)_2O/ SiO_2$ ratios were increased to 0.35 and 0.65 along with the increase in molar HF/SiO2 ratio such that molar TEAOH/HF ratio becomes unity. In other words, Expt. Nos. 8 and 9 were the modified gel compositions of 6 and 7 (Table 5.1) where moles of HF and TEAOH are identical. These, both the synthesis trials resulted in the formation of crystalline beta phases. Moreover, with increase in molar $(TEA)_2O/ SiO_2$ ratio, faster crystallization of Sn-beta was observed. The product obtained from Expt. No.9 in Table 5.1 was calcined and labeled as sample B. Very marginal decrease in the overall crystallization of beta phase was observed with further increase in molar $(TEA)_2O/ SiO_2$ ratio. Moreover, TEAOH is the most cost-bearing component in the reaction mixture; its minimum use is preferable. Thus the initial reaction mixture used in Expt. 9 is the optimum as Sn-BEA was synthesized in least crystallization period.

The application of Sn-BEA mostly depends on the concentration, coordination and dispersion of Sn in the framework [15, 21]. Therefore, it becomes essential to investigate the feasibility of synthesizing Sn-BEA as a function of amount of tin in the gel. In view of this, different gels with molar compositions SiO_2: 0.0083 – 0.0166 SnO_2: 1.3 TEAOH: 9.5 H_2O: 1.3 HF: 0.1 $HClO_4$, were prepared and subjected to hydrothermal crystallization (Expts. 10, 11 & 12). From crystallization kinetic data (not shown), it was observed that, increase in the SnO_2 content in the gel caused

increase in time required to form pure and well crystalline Sn-BEA. The gel with molar SnO_2/ SiO_2 = 0.0166 (Expt. 12) did not yield the BEA phase up to 30 hour of crystallization period. Therefore, the maximum tin insertion in the BEA framework achieved in the present studies was with a gel containing molar SnO_2/ SiO_2 ratio of 0.0125. The calcined products obtained from gels containing molar SnO_2/ SiO_2 ratios of 0.01 and 0.0125 were labeled as sample C and D respectively.

An attempt was also made to establish the kinetics of crystallization using 5 wt % seed along with perchlorate promoter oxyanions in gel used in Expt. 5 in Table 5.1. It is interesting to note that the formation of crystalline Sn-BEA phase occurred in 10 days which is much shorter period than that of required using seed and oxyanion alone. Thus, combination of seed and oxyanion enhances the process of crystallization of Sn-BEA dramatically by speeding up the nucleation and crystallization processes. However, use of seed is not preferable.

5.3.2. Characterization

To investigate the quality of the Sn-BEA, samples A, B, C, D and E (all silica BEA) were subjected to different characterizing techniques.

5.3.2.1. *Powder X-ray diffraction*

Fig. 5.2a depicts the powder XRD patterns of samples A, B, C, D and E. All samples have shown the characteristic peaks of BEA structure.

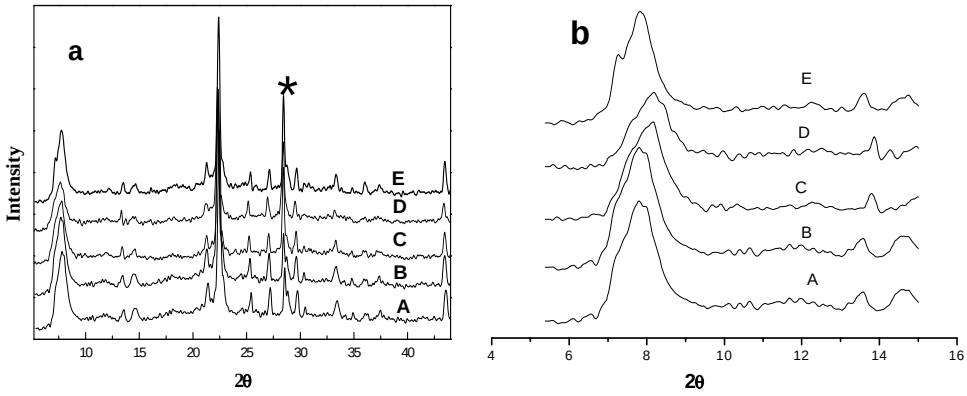

Fig. 5.2. a) Powder X-ray diffraction patterns of calcined Sn-BEA samples (* Silicon – internal standard) , b) XRD patterns of low angle peak.

The absence of amorphous matter or impurity phase indicated high purity and crystallinity of phases obtained. A broad reflection at lower 2θ range (6 – 10^o) is a characteristic of intergrowth of different polymorph viz. polymorph A and B. Sample E has exhibited a shoulder at around 2θ = 7.3^o which match well with that of BEA synthesized in fluoride medium [18, 21]. For better clarity, X-Ray diffraction patterns of all the samples in lower 2θ range were zoomed and shown as Fig. 5.2b. It is interesting to note that this shoulder becomes too weak/disappears as Sn gets incorporated in BEA framework. Moreover, with increase in Sn content, the peak has shifted to higher 2Θ value with reduced intensity. As the shape of this peak is sensitive to change with the change in relative proportion of polymoph A phase [2, 22-24], it could be concluded that, in present case, the contribution of polymoph A phase decreases with the increase in Sn content.

5.3.2.2. *Chemical compositions and textural properties*

The chemical composition in terms of SiO_2/SnO_2 molar ratio that was present in gel and the product obtained therefrom is provided in Table 5.2.

Table 5.2. The chemical compositions and textural properties of calcined samples.

Sample	Molar SiO2/SnO2 ratio		BET Surface area m2/gm	Micropore Surface area m2/gm	Pore volume ml/cc
	Gel	Product			
A	120	140	580	540	0.21
B	120	135	618	579	0.23
C	100	125	622	564	0.23
D	80	88	630	568	0.23
E	-	-	522	481	0.18

In all the Sn-BEA samples, the molar SiO_2/SnO_2 ratio was found to be higher than that of the respective gel. The product with the maximum tin content showed the

molar SiO_2/SnO_2 ratio of 88 in the present studies. The data in relation to the textural properties such as BET surface area, micropore area and pore volume are tabulated in Table 5.2. The sample B, prepared with modified gel composition, promoter, has exhibited higher BET surface area and pore volume than sample A which was prepared according to reported procedure. Samples B, C and D have exhibited increase in the BET surface area with the increase in Sn content without considerable change in their pore volumes. All Sn containing samples have shown higher surface area and pore volumes as compared to Sn-free beta sample. The extent of micropore surface area in total surface area amounts to 90-94 %.

5.3.2.3. *Infrared spectroscopy*

The framework IR spectra of all the samples are depicted in Fig. 5.3. All the spectra match well with that of reported ones [21]. Except sample E, all the samples showed a weak shoulder at ~960 cm-1 which has been assigned to Si-O-Sn vibration or Si-(OH) defect groups promoted by framework Sn from the possible substitution of Sn in the Si-O-Si units [25,26].

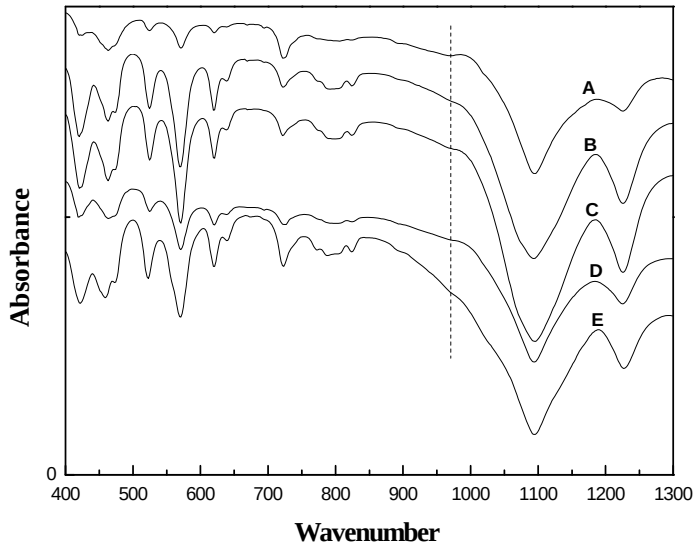

Fig. 5.3. FTIR spectra of samples A ,B,C,D and E

5.3.2.4. *Diffuse reflectance UV-Vis spectroscopy*

In order to deduce the nature of tin species formed in the Sn-BEA sample, DRUV–vis measurements were performed as it is a very sensitive probe for the presence of extra-framework heteroatom in molecular sieves. The DRUV–vis spectra of sample A to E are shown in Fig. 5.4. The spectra of the samples A to D display broad absorption band at 220 nm. The absorption band at 220 nm can be assigned due to charge transitions (CT) from O2- to Sn4+ in tetrahedral coordination [25-27]. Moreover, the intensity of this band was found to increase with increase of the Sn substitution in the Beta framework, while Sn-free silica BEA (E) shows no any absorption peak. All Sn-BEA samples showed no bands typical for polymeric Sn–O–Sn type species at 280 nm [26,27]. Although, spectra of all Sn-BEA samples reveal absorption at ~ 220 nm with lack of absorption at ~ 280 nm suggesting occupancy of tin atoms in site-isolated positions in the silica framework, it is manifested by the broader character. We believe that isolated Sn in a distorted tetrahedral environment and/or in penta- or octahedral coordination sphere may be associated with such broadening character of Sn-BEA spectra.

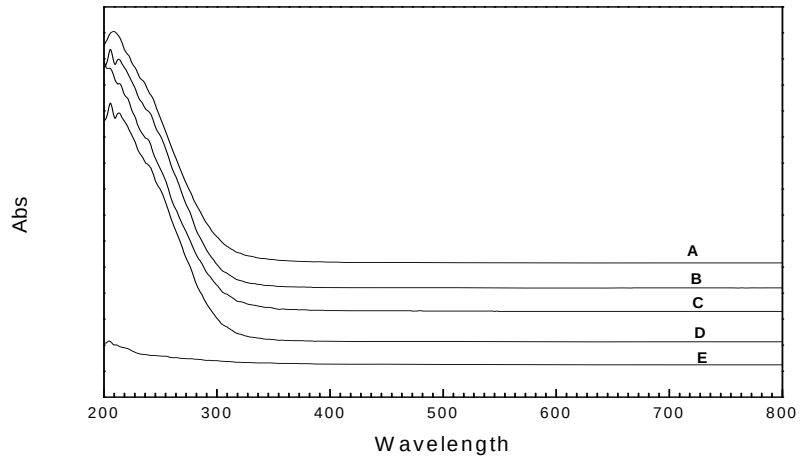

Fig. 5.4. DRUV-vis spectra of samples A,B,C,D and E.

5.3.2.5. *Scanning electron microscopy*

Fig. 5.5 shows influence of SiO2/SnO2 molar ratio in the initial gel mixture on the crystal morphology and size of well crystalline Sn-Beta. The Image of sample-A

exhibited aggregated spherical shaped particles having size of approximately 0.3 to 1 μm and sample-B show the truncated square morphology with size of approximately 1-3 μm. The seed and different period of crystallizations in the synthesis of sample A and B seems to be probable reason for the change in the morphology and size of particle.

The tendency towards changing the morphology and the size of particle with change of Sn in sample can be seen from SEM photographs of sample B-E. Sample-E, all silica BEA, exhibits mixed shape morphology with 10 □m size. Further, the size of particle is found to be increased from B to E as Sn decreases in the sample. The different rate of crystallization, due to change SiO2/SnO2 molar ratio in initial gel mixture, may be responsible for the change particle size.

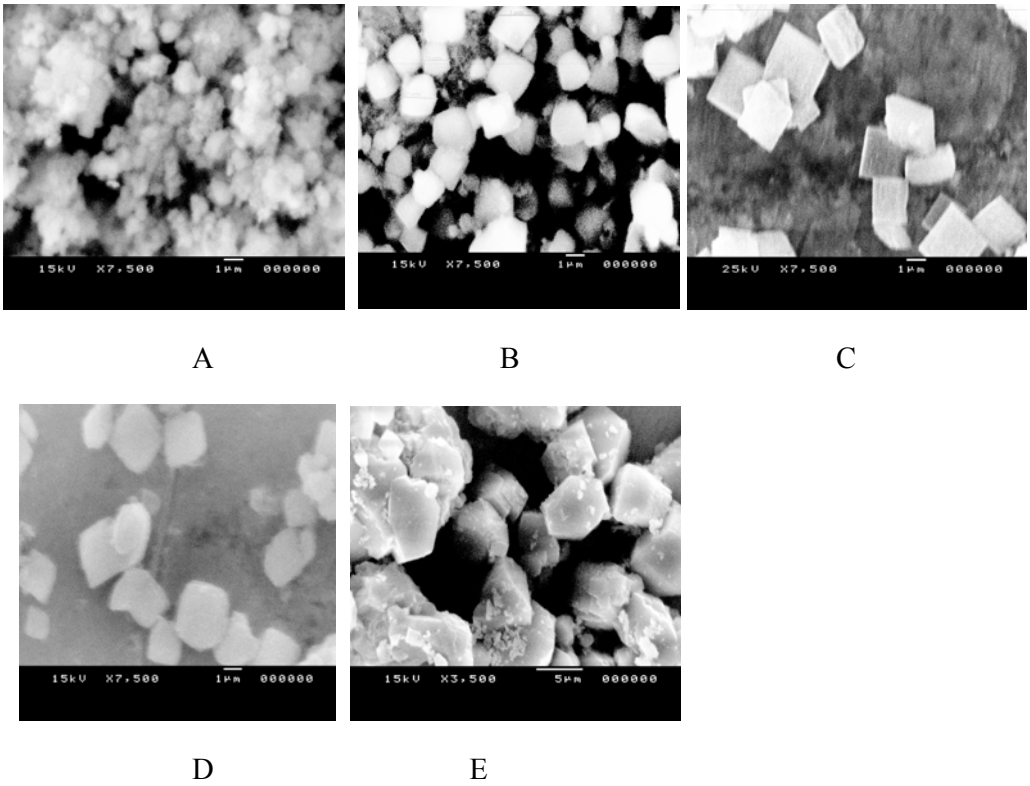

Fig. 5.5. Scanning Electron Micrographs of samples A,B,C,D and E..

5.3.3. Catalytic applications

(A) *Cyclohexnaone oxidation*

A. Corma et al [6] showed that tetrahedrally coordinated Sn in BEA framework acts as an efficient and stable catalyst for the Bayer-Villiger oxidation of saturated as well as unsaturated ketones by hydrogen peroxide, with more than 98 % selectivity of desired product. It is also reported [6,14,21] that SiO_2, pure silica zeolite BEA impregnated with a $SnCl_4$ solution and SnO_2 were not catalytically active for the above reaction. Thus, it emphasize that Sn requires tetrahedrally coordinated and to be situated within the zeolite framework for its catalytic application. Therefore, In view of collecting more information on the tin species and investigating the catalytic performance of Sn-BEA sample, the screening of A, B, C and D was carried out using cyclohexnaone oxidation reaction as a test reaction with H_2O_2 as oxidant. The activity data obtained under identical set of reaction conditions are summarized in the Table 5.3.

Table 5.3. Catalytic performance of Sn-Beta in the oxidation of cyclohexanone by H_2O_2[a].

Sr. No.	Catalyst	Conversion % (Mole)	TONb	Lacton selectivity
1	A	19.0	32.4	> 98
2	B	27.0	44.5	> 98
3	C	39.7	60.5	> 98
4	D	41.3	44.8	> 98

a Reaction Condition: Catalyst = 50 mg; Oxidant(H2O2) :Substrate(Cyclohexanone) = 3:1; Temperature : 70 °C; Time : 7 h.

b TON, Turnover number = moles of cyclohexane converted/moles Sn

The comparison of catalytic activity between sample A and B, comparatively higher cyclohexanone conversion (27%) and TON(44.5) has been exhibited by Sn-BEA prepared without seed than Sn-BEA prepared with seed (conversion 19% and

TON 32.4). Lower Sn content, morphology/ particle size and textural properties of sample A may be responsible declined catalytic performance.

Sample B to D have exhibited non-linear increase in cyclohexanone conversion (27 to 41.3%) as Sn increase in the sample. This indicates that, there is a presence of isolated Sn^{4+} ions of whose concentration increases with decrease in the molar SiO_2/SnO_2 ratio. This finding supports the earlier DRUV-vis results. However, the TON was found to increase in sample the B and C and it decreases in the sample D with the increase in tin content. Thus, the decrease of the TON in sample D suggests that, there exists a possibility of presence of two types of Sn species that are different in their activities.

(B) ***N-methylation of aniline***

Vapor phase methylation of aniline over Sn-BEA samples was carried out at 200^oC, atmospheric pressure, weight hourly space velocity of 3 h^{-1} and methanol to aniline molar ratio of 6. Table 5.4 illustrates the influence of SiO_2/SnO_2 molar ratio in Sn-BEA samples on aniline conversion and selectivity of products.

Table 5.4. Catalytic performance of Sn-BEA in the N-methylation of aniline

Sample	Performance			
	Aniline conversion %	% Sel. of N-Methyl Aniline	% Sel. of NN-Dimethyl Aniline	% Sel. of Other
A	23.9	63.5	32.2	4.3
B	24.8	63.7	32.7	3.6
C	37	62	36	2
D	41.1	42.7	50.2	7.1

Sample A shows marginally lower aniline conversion than B. Aniline conversion is acid driven reaction, acidity of Sn-BEA sample depend upon content of Sn in BEA, thus lower Sn content in the sample A may be responsible lower

conversion. However, NMA and NNMA selectivity in the sample A and B is found similar.

Based on the catalytic results shown by sample B, C and D, the conversion of aniline decreases with the increase of SiO_2/SnO_2 molar ratio. Maximum aniline conversion of 41.1 % was observed with SiO_2/SnO_2 molar ratio of 88 (Sample D). This may be due to higher number of active centers (more Sn), lower particle size and higher surface area as compared to other samples. The cumulative effect of these catalyst properties, increases aniline conversion and reduces marginally NMA formation, due to higher rate of NMA alkylation as compared to rate of aniline alkylation.

5.4. CONCLUSION

Sn- BEA molecular sieve has been synthesized in fluoride medium from unseeded gels containing source of oxyanion. Among different oxyacids, perchlorate oxyanions indicated the maximum reduction in the overall synthesis time. The molar ratios of TEAOH/SiO2, HF/SiO2 and SiO2/SnO2 in initial gel composition influences not only the nature of the phase but also crystallization period to get Sn-BEA. An increase in the TEAOH /SiO2 along with the HF/SiO2 to a magnitude of 1.3 and SiO2/SnO2 molar ratio viz. 120 in initial gel mixture resulted in the formation of Sn-BEA in 6 days. From XRD examinations, it was found that the increase in Sn content in Sn-BEA leads to the formation of polymorph B rich beta phase. The presence of these Sn4+ ions in tetrahedral coordination has been indicated by DRUV-vis and IR spectral studies. The Sn-BEA with the maximum tin content has showed the molar SiO2/SnO2 ratio of 88 in the present studies. The Sn-BEA sample prepared without seed has been exhibited higher cyclohexnaone conversion than sample prepared with seed. Increase in concentration of isolated Sn4+ ions led to increase in cyclohexnaone conversion. However, the decrease of the TON with higher sn content sample suggests that, there exists a possibility of presence of two types of Sn species that are different in their activities.

5.5. REFERENCES

[1] J. B. Higgins, R. B. La Pierre, J. L. Schlenker, A. C. Rohrman, J. D. Wood, G. T. Kerr, W. J. Rohrbaugh, Zeolites; 8 (1988) 446.

[2] J. M. Newsam, M. M. J. Treacy, W. T. Koestsier, C. B. de Gruyter, Proc. R. Soc. London Ser. A; 420 (1988) 375.

[3] M. A. Camblor, A. Corma, A. Martinez, J. Perez-Pariente, J. Chem. Soc. Chem. Commun.; (1992) 589.

[4] L. L. Murrell, R. A. Overbeek, US Patent 6,004,527 (1999)

[5] T. Takewaki, S. H. Hwang, H. Yamashita, M. E. Davis, Micropor. Mesopor. Mat.; 32 (1999) 265.

[6] A. Corma, L. T. Nemeth, M. Renz, S. Valencia, Nature ; 412 (2001) 423.

[7] T. Sen, M. Chatterjee, S. J. Sivsanker, Chem. Soc. Chem. Commun. (1995) 207.

[8] J. C. van der Waal, H. van Bekkum, J. Mol. Catal. A-Chem.; 124 (1997) 137.

[9] M. A. Camblor, A. Corma, J. Perez-Pariente, Zeolites; 13 (1993) 82.

[10] J. C. Jansen, E. J. Creyghton, S. L. Njo, H. van Koningsveld, H. van Bekkum, Catal. Today; 38 (1997) 205.

[11] M. A. Camblor, M. Costantini, A. Corma, L. Gilbert, P. Esteve, A. Martinez and S. Valencia, Chem. Commun.; (1996) 1339.

[12] N. K. Mal, A. V. Ramaswamy, Chem. Commun. ; (1997) 425.

[13] S. Valencia, A. Corma, US Patent 5968473A (1999).

[14] S. P. Panchgalle, U. R. Kalkote, P. S. Niphadkar, P. N. Joshi, S. P. Chavan, G. M. Chaphekar, Green Chem.; 6 (2004) 308.

[15] A. Corma, M. E. Domine, L. Nemeth, S. Valencia, J. Am. Chem. Soc.; 124 (2002) 3194.

[16] A. Corma, M. E. Domine, S. Valencia, J. Catal.; 215 (2003) 294.

[17] M. A. Camblor, A. Corma, S. Valencia, Chem. Commun.; (1996) 2367.

[18] M. A. Camblor, A. Corma, S. Valencia, Chem. Commun.; (1996) 2365.

[19] R. Kumar, A. Bhaumik, R. K. Adedi, S.Ganapathy, Nature; 381 (1996) 298.

[20] M. A. Camblor, A. Mifsud, J. Peerez-Periente, Zeolites; 11(1991) 792.

[21] M. Renz, T. Blasco, A. Corma, V. Fornes, R. Jensen and L. Nemeth, Chem. Eur. J.; 8 (2002) 4708.

[22] T. Blasco, M. A. Camblor, A. Corma, P. Esteve, J. M. Guil, A. Martı´nez, J. A. Perdigo´n-Melo´n, and S. Valencia, J. Phys. Chem. B; 102 (1998) 75.

[23] M. D. Kadgaonkar, M. W. Kasture, D. S. Bhange, P. N. Joshi, V. Ramaswamy, N. M. Gupta, R. Kumar, Micropor. Mesopor. Mat.; 105, 1-2 (2007), 82.

[24] M. D. Kadgaonkar, M. W. Kasture, D. S. Bhange, P. N. Joshi, V. Ramaswamy, N. M. Gupta, R. Kumar, Gupta, N.M., Kumar, R. Micropor. Mesopor. Mat.; 101, (2007) 108.

[25] K. Chaudhari, T. K. Das, P. R. Rammohan, K. Lazar, S. Sivshankar, A. J. Chandwadkar, J. Catal.; 183(1999) 281.

[26] M. Casagrande, L. Storaro, M. Lenarda, J. Gersich, L. Stievano, F. E. Wagner, T. Montanari, J. Mater. Chem.;14 (2004) 1010.

[27] N. K. Mal, A. V. Ramaswamy J. Mol. Cat. A-Chem.; 105 (1996) 149.

CHAPTER 6

SYNTHESIS, CHARACTERIZATION AND CATALYTIC APPLICATION OF MESOPOROUS Sn-MCM-41 and MICRO-/ MESOPOROUS COMPOSITE Sn-MFI/MCM-41

6.1. INTRODUCTION

By virtue of uniform their micropore size, large internal surface area and flexible framework for insertion of desired active sites, zeolites and zeolite-like materials have been widely used as adsorbents, catalysts and molecular sieves [1]. With the discovery of the M41S family of mesoporous molecular sieves [2-4], a new way for expanding the pore size range from micro to meso brought about the beginning of a new age in the silica based mesoporous molecular sieves. The factors such as spacing regularity in material, pore size distribution, surface area and thermal/hydrothermal stability are of significant importance, which govern the performance of these materials in most of their applications.

In view of developing eco-friendly and efficient solid catalysts, tin containing micro- and meso- porous silicates [5-30] have received considerable attention in heterogeneous catalysis on account of their Lewis acidity and unique structural features. Although, both the Sn-containing microporous and mesoporous molecular sieves have shown their excellence in catalytic performances, they have their own limitations. Microporous Sn-containing materials have the disadvantage of inability to perform, when bulkier molecules are involved and Sn- mesoporous materials suffer from weak acidity and poor hydrothermal stability. The benefits and disadvantages of Sn-containing microporous and mesoporous molecular sieves have triggered our interest to synthesize Sn-containing material, which possesses combined advantages of both microporous and mesoporous materials. Recent progress in similar area primarily involved the syntheses and advantages of Al-, Ti-, V- containing mesoporous silicates with zeolitic character (combined micro-mesoporous material or micro/mesoporous composites) addressing improved diffusion rates for transport in catalytic process [31], better hydrothermal stability [32], controlled leaching rates for a constant and gradual release of active component [33-34].

Different strategies were employed to prepare micro-mesoporous composite materials. Mesoporous zeolites can be synthesized by post-synthesis methods such as dealumination of full-grown zeolites using steam or acid leach [35-36], as well as by controlled desilication by an alkaline treatment [37-39]. Both techniques destruct part

of the zeolite, which can be a problem towards reproducibility. Another method involves preparation of mesoporous molecular sieve followed by recrystallization of amorphous walls into crystalline zeolitic walls via introduction of organic template prior to hydrothermal treatment [40-41]. In yet another approach, carbon based particles are added as a secondary template into the reaction mixture. Upon completion of the synthesis, they are removed by calcinations, leading to the formation of mesoporous zeolite single crystals [41-43]. Recently, Jinka et al. have reported [44] microwave-synthesized mesoporous Sn-MFI catalyst.

Motivated by the need and high degree of flexibility of Sn insertion in unidimentional mesoporous MCM-41 and tridimentional microporous MFI, the work in relation to the synthesis, characterization, optimization of synthesis parameter and catalytic application of micro/mesoporous stannosilicate composite consisting of MCM-41 and MFI as meso- and micro- structural components (Sn-MFI/MCM-41) was undertaken.

This chapter describes the synthesis of Sn-MFI/MCM-41 composite material via two-step crystallization process, influence of various process parameters on the type of the phase formation and characterization of Sn-MFI/MCM-41 composite by Powder XRD, FTIR, SEM, TEM, low temperature nitrogen sorption measurement and DRUV-vis.

6.2. EXPERIMENTAL

6.2.1. Synthesis of Sn-MFI/MCM-41 composite

In present studies, Sn-containing microporous (Sn-MFI), mesoporous (Sn-MCM-41) molecular sieves and micro/mesoporous composite (Sn-MFI/MCM-41) were the three phases formed during two-step crystallization process. Aiming at synthesis of Sn-MFI/MCM-41 composite, in first step, different homogeneous gels with molar ratios SiO_2/SnO_2=50-200, $TPAOH/SiO_2$= 0.35-0.55, and H_2O/SiO_2 =35 were prepared by mixing appropriate quantities of tetraethylorthosilicate (TEOS, 98 %, Aldrich), tetrapropylammonium hydroxide (TPAOH, 20% aqueous solution, V. P. Chemical, Pune, India) , $SnCl_4.5H_2O$ (Loba chemicals) and H_2O. The clear gel was then transferred to a stainless steel autoclave and heated/aged statically at 100^oC for

desired length of period. After cooling to room temperature, in second step, the aged gel was added to the appropriate quantity of aq. cetyltrimethylammonium bromide (CTMABr, 98%, Dishman, Banglore, India) solution to yield a final gel whose molar composition match well with SiO_2: 0.033 - 0.005 SnO_2: 0.34 - 0.55 TPAOH: 0.12 - 0.48 CTMABr : 118 H_2O. This homogeneous gel was then transferred to an autoclave and re-crystallized at temperature ranging from 100 to 160^{0}C and monitored the phase formation/transformation as a function of time. After termination of crystallization process, the solid product was recovered, which is dried and then calcined to remove the templates of TPAOH and CTMABr.

In a typical example of preparation of Sn-MFI/MCM-41, in first step, a solution prepared by dissolving 0.36 g $SnCl_4.5H_2O$ in 10 ml H_2O was added to 21.26 g of TEOS with constant stirring. The stirring was continued for 15 min. This mixture was then added to 45.83 g of aq. TPAOH solution slowly with constant stirring. After stirring the resultant mixture for 2 h, 16.4 g of water was added with constant stirring to yield a gel with molar gel composition SiO_2: 0.01SnO_2: 0.45 TPAOH: 35 H_2O which was pre-optimized during our earlier work [16]. This gel was then aged at 100^{o}C for 4 hr. After cooling to room temperature, in second step, the aged gel was added to a solution prepared by dissolving 8.92 g CTMABr in 149.5 g of water with constant stirring. After complete addition, stirring was continued for 3 h. This final gel with molar composition SiO_2: 0.01SnO_2: 0.45TPAOH: 0.24 CTMABr: 118 H_2O was then transferred to an autoclave and re-crystallized at 130^{o}C for 12 h. After quenching, the solid product was recovered by filtration, washed with water, dried at 80^{o}C for 12 h and calcined at 550^{o}C for 6 h in air flow.

Well-ordered Sn-MCM-41 and crystalline Sn-MFI were obtained from the same gel, however the re-crystallization times were 8 and 20 h respectively instead of 12 h.

6.2.2. Characterization Sn-MFI/MCM-41 composite

Powder X-ray diffraction patterns were recorded on a Rigaku Miniflex diffractometer using nickel filtered Cu-Kα radiations. The XRD data were collected in the 2θ range between 1.5 and 30^o with 0.02^o step size and scan rate of 2^o, min^{-1}. A

conventional volumetric nitrogen adsorption apparatus (Micromeritics ASAP 2010 system) was used for evaluating the textural properties of the test samples. The calcined sample was degassed at 300^{o}C for 10 h at 0.00133 Pa, prior to the measurements. The sample was then cooled to –196^{o}C using liquid nitrogen and the sorption of nitrogen was carried out at different equilibrium pressures. The specific surface area of the sample was calculated using BET method. Mesopore size distribution and pore volume was calculated using Barrett-Joyner-Halenda (BJH) model and t-plot analysis were used to determine the micropore surface area and pore volume.

Thermal analyses (TG-DTA) of the as-synthesized products were performed on Perkin-Elmer Diamond TGDTA thermal analyzer. The measurements were carried out under air flow with heating rate of 10^{o}C/ min. FTIR spectra of samples were recorded using Shimadzu model-8300 equipped with DTGS detector in the frequency range 400–1300 cm $^{-1}$. Scanning Electron Microscope (SEM) images were obtained using microscope (LEICA Stereo Scan 440) after coating the sample with Au-Pd evaporated film. The arrangement of micro- and mesopores was investigated with a high-resolution transmission electron microscopy (Tecnai F30). Diffuse reflectance UV–vis spectra were recorded in the range 200–600 nm with a Perkin-Elmer Lambda 6 spectrometer equipped with a diffuse reflectance attachment using $BaSO_4$ as the reference.

6.2.3. Catalytic study

The hydroxyalkylation of *p*-cresol with formaldehyde was carried out in a magnetically stirred glass reactor (Capacity 50 mL) fitted with a reflux condenser and an arrangement for temperature control. In a typical experiment, *p*-cresol (4.5 g), formaldehyde (0.25 g), toluene (10 g) and catalyst (0.5 g) were added to the reactor, and then heated to 80^{o}C for 2 h. The product distribution was determined using a HP6890 series GC System (Hewlett Packard) coupled with FID detector and HP-1 capillary column (30 m length X 0.32 mm i.d.). The products were identified by ^{1}H NMR, ^{13}C NMR and by GC-MS.

6.3. RESULTS AND DISCUSSION

6.3.1. Synthesis of Sn-MFI/MCM-41 composite

In initial probing experiments, the syntheses trials were conducted to examine the applicability of two-step crystallization route for synthesis of Sn-MFI/MCM-41. Based on our earlier work, in first step, the pre-optimized gel was aged at 100^{o}C for 4 hr to obtain MFI building units. In second step, the progressive development of phase/s was examined by varying re-crystallization time ranging from 1 to 30 h at 130 ^{o}C. The overall procedure followed was identical with that of typical example described in sec. 6.2.1.

Time dependent studies revealed that, as re-crystallization time progresses, not only intensity of characteristic peaks of MCM-41 phase increases but also peak shifts towards lower 2θ values. Shifting of the peak to lower 2θ values suggest growth of the unit cell with time. In order to verify such improvement in the degree of ordering, the unit cell parameter 'a_o' was calculated using the relation $2d_{100}/\sqrt{3}$. The progressive increase in unit cell parameter was found to occur with the increase in synthesis time, reached to maximum and then decreased slightly on further heating. The sample recovered after 8 hrs (designated as S-08) of re-crystallization time has shown well ordered mesoporous MCM-41 phase [8] with maximum intensity of d_{100} diffraction peak and a_o value. Moreover, non-appearance of any peak at higher 2θ angle has indicated absence of microporous, in particular, MFI phase [16]. Extending the re-crystallization time to 12 hrs (sample designated as S-12), both the intensity and a_o values were found to decrease with appearance of MFI phase with considerable intensity. Based on distinctive XRD pattern of S-12, it can be concluded that well ordered mesoporous MCM-41 stannosilicate was successfully assembled from microporous MFI seeds. In other words, two-step crystallization route seems to be applicable for the synthesis of Sn-MFI/MCM-41 composite material. Further extension of re-crystallization period resulted in the increase in the intensity of MFI phase with decrease in MCM-41 content. The sample recovered after 20 hrs of re-crystallization period (designated as S-20) has shown maximum crystallinity of MFI phase with no single characteristic peak of MCM-41 phase. No any phase

change/transformation was observed with further increase in re-crystallization period upto 48 hrs. Fig. 6.1 presents X-ray diffractions pattern of S-08, S-12 and S-20 samples in their as-prepared forms.

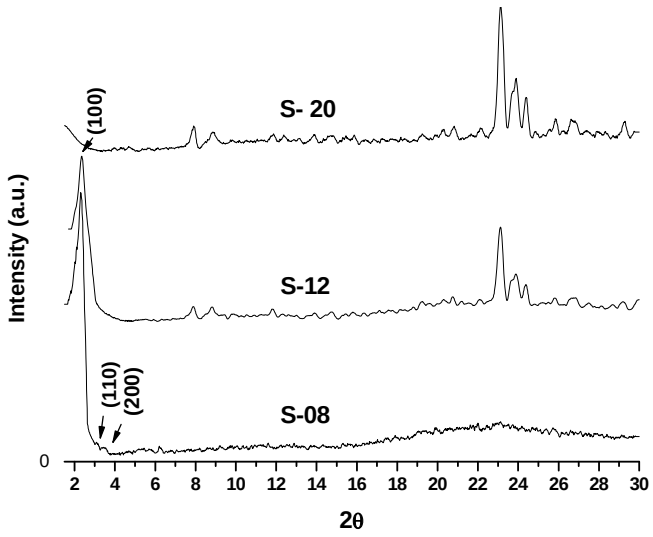

Fig.6.1. Powder X-ray diffraction patterns of S-08, S-12 and S-20 samples in as-prepared forms.

6.3.2. Characterization

To confirm formation Sn-MFI/MCM-41 composite, calcined S-08, S-12 and S-20 samples were characterized different technique.

6.3.2.1. *Powder X-ray diffraction*

Powder X-ray diffraction patterns of calcined S-08, S-12 and S-20 samples are represented in Fig. 6.2. Upon calcination, both the mesoporous materials resulted in the formation of surfactant-free MCM-41 structured materials. In XRD, these calcined materials have shown shifting of 2θ to higher values. Contraction of the lattice occurs during the surfactant removal process on account of condensation of the terminal -OH groups on the wall. An extent of such lattice contraction was estimated by calculating the difference in unit cell parameters, before and after calcination (denoted as 'Δa_0') and tabulated in Table 6.1. It is evident from Table 6.1 that, the

population of terminal –OH units in the channel wall follows the trend as: S-08 > S-12. Given that the more contraction of unit cell after calcination is caused by fewer fractions of $T(OT)_4$ where T = Si and/or Sn structural units in wall. It is understandable that the wall of S-12 contain higher $T(OT)_4$ species as compared to S-08.

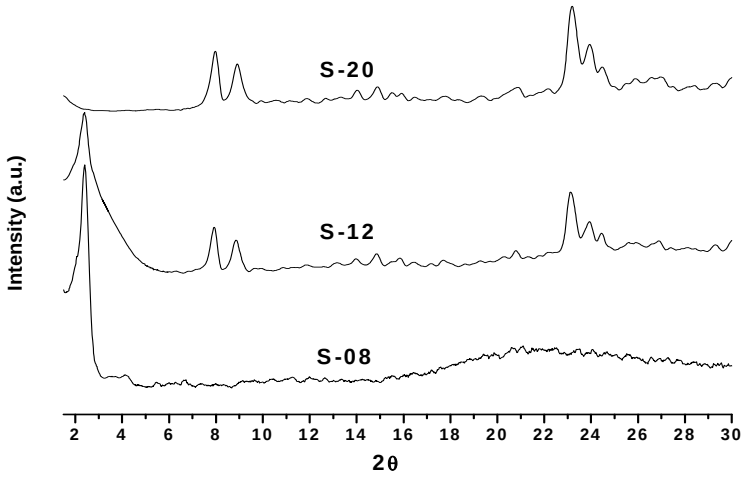

Fig.6.2. Powder X-ray diffraction patterns of S-08, S-12 and S-20 samples in calcined forms.

Table 6.1. Structural and textural properties of sample S-08, S-12 and S-20.

Sample	**Sn Wt %**	**d_{100}, nm**		**a_o, nm**		**Δa_o nm**	**a_o cont. (%)**	**Wall thickness nm**	**BET Surface area[b] m^2/g**	**Pore dia. nm**	**Pore volume [b] cm^3/g**
		As-syn.	**Cal.**	**As-Syn.**	**Cal.**						
S-08	1.89	3.94	3.80	4.55	4.39	0.16	2.95	2.19	1162(53)	2.2	0.98(0.03)
S-12	1.82	3.76	3.66	4.34	4.23	0.11	2.53	2.03	783(117)	2.2	0.55(0.1)
S-20	1.70	-	-	-	-	-	-	-	93(694)	-	0.08(0.23)

Unit cell parameter $a_o = 2d_{100}/\sqrt{3}$, Wall thickness = a_o- average mesopore size

[b] The values in parentheses are micropore surface area or pore volume.

As-syn. = As synthesized, Cal.= Calcined and Cont.=contraction.

6.3.2.2. *Nitrogen sorption studies*

Calcined forms of all these three samples were further characterized for their textural properties. Low temperature (–196^{o}C) nitrogen adsorption-desorption isotherms for calcined S-08, S-12 and S-20 samples are depicted in **Fig.6. 3a**.

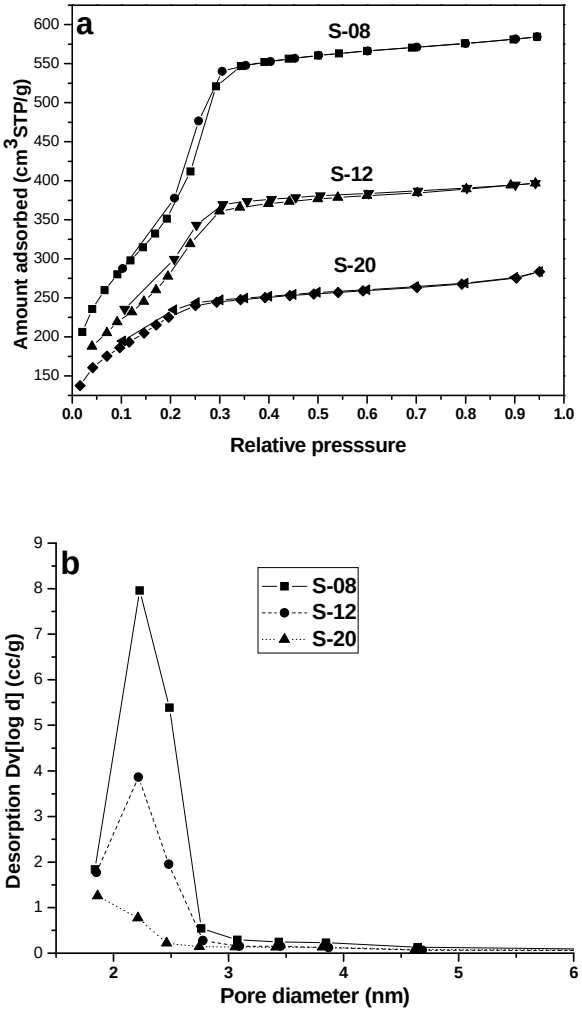

Fig.6.3. Nitrogen sorption isotherm (a) and pore size distribution (b) of calcined S-08, S-12 and S-20.

Sample S-08 has shown reversible type IV isotherm with a well-defined inflection at relative pressures from 0.2 to 0.4. This inflection corresponds to

capillary condensation of nitrogen inside the primary mesopores, which is a typical presentation of mesoporous materials. The isotherm of S-20 has shown some deviation from typical MFI isotherm [32]. It has exhibited slow uptake at low relative pressure. The total BET surface area was found to be higher than micropore surface area obtained by t-plot analysis. The values for surface areas and pore volumes are tabulated in Table 6.1. Thus, it is likely that such behavior might be associated with the presence of XRD invisible meso-structured phase in S-20. The sample S-12 exhibited the isotherm combining the characteristics of type I and type IV indicating a close resemblance to both the micro- and meso- porous materials. It has shown high uptake at low relative pressures with an inflection at relative pressures 0.2–0.4 with gentle slop. The simultaneous existence of both the characters was also supported by its XRD-profile. The gradual transformation of Sn-MFI/MCM-41 composite material to microporous Sn-MFI leads to decrease in BET surface area (Table 6.1).

In view of further verification, the pore size distribution patterns were obtained by employing BJH model and are illustrated in Fig. 6.3b. It can be clearly seen that, the narrow distribution of mesopore centered at 2.2 nm was demonstrated by the samples S-08 and S-12 but not by S-20.

The corresponding properties of mesoporous materials deduced from the XRD and nitrogen sorption measurements are summarized in Table 6.1. The changes in the structural and textural properties are consistent with gradual transformation of mesoporous material to micro/mesoporous composite to microporous material with re-crystallization time. The actual amount of Sn incorporated into the calcined product (expressed as Sn wt%) is also included in Table 6.1.

6.3.2.3. *Infrared spectroscopy*

The structural features of composite material were further characterized by infrared spectroscopy. Fig. 6.4 provides the FTIR spectra of S-08, S-12 and S-20. All the samples exhibit band around 440-450 cm^{-1} and at 800 cm^{-1}, which are attributed to Si-O-T bonds where T = Si or Sn [45]. Interestingly, a prominent band at 555 cm^{-1} has been found in both Sn-MFI and Sn-MFI/MCM-41 composite material which is indicative of the five and six membered ring existence in the MFI zeolite structure

[46]. The presence of this band in S-12 may be treated as an evidence for existence of MFI building units in mesoporous wall [47].

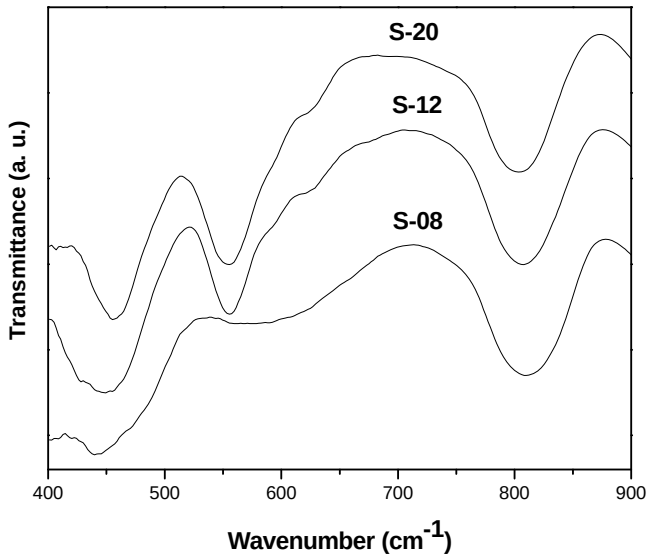

Fig.6. 4. FTIR Spectra of the calcined S-08, S-12 and S-20.

6.3.2.4. *Thermal analysis*

The thermogravimetric analysis of samples containing occluded structure directing agents is expected to provide the inputs to elucidate further the difference in porous structures between S-08, S-12 and S-20. Fig. 6.5 shows TG and DTA curves of as synthesized samples S-08, S-12 and S-20 which has shown the total weight loss of the magnitude 51.3, 55.4 and 42.3 wt %, respectively over the entire temperature range. Based on the % weight loss in the temperature ranging from 30 to 200 ^{o}C, samples have shown the decreasing trend as: S-12 (19.7 %) > S-08(16.8%) > S-20 (12.1%).The weight loss up to 100^{o}C is assigned to desorption of water and 100-200^{o}C is associated with free structure directing agent which is known to decompose or evaporate below 200^{o}C [48]. However, weight loss due to the organic additives/structure directing agents in channel was noticed in two temperatures ranges viz. 200 to 350 and 350 to 500^{o}C. Weight loss in temperature range 200 to 350

^{o}C is assigned to the thermal decomposition of surfactant in mesoporous structure [45] and the trend observed in this range is S-08 (29.7 %) > S-12 (27.7 %) > S-20 (21.8 %). Thermal decomposition of the TPA^{+} incorporated in microporous phase occurs in the temperature range 350 to 500^{o}C [45]. The weight loss trend observed in this range is S-08 (4.8 %) < S-12 (8.0 %) < S-20 (8.4 %). The decrease in amount of surfactant with simultaneous increase in amount of TPA^{+} retained in samples S-08, S-12 and S-20 suggest the gradual shift from meso- to micro- structured phase with the increase in re-crystallization time. Similar results were also observed while synthesizing ZSM-5/MCM-48 composite materials when aging time of the precursor zeolite species was increased [45].

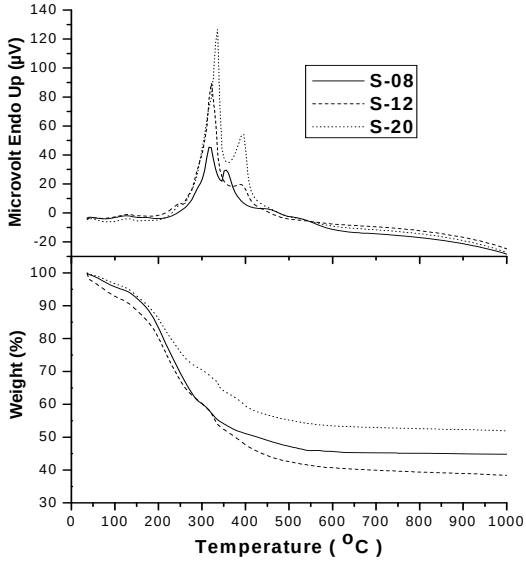

Fig. 6.5. Thermogravemetric analysis curves of as-prepared S-08, S-12 and S-20.

6.3.2.5. **Scanning electron microscopy**

The size and shape of particles in the samples S-08, S-12 and S-20 were investigated using scanning electron microscopy and images are shown **in Fig. 6.6.** Samples S-08 and S-12 exhibited nearly spherical shaped particles having size of 0.1-0.2 μm. Sample S-20 also showed spherical shaped particles but with size ranging from 0.2 to 0.5 μm. No morphological changes were observed with the change in

phase. Therefore, SEM provided no basis for the meaningful conclusion as far as the structural aspects of the phases under present studies are concerned.

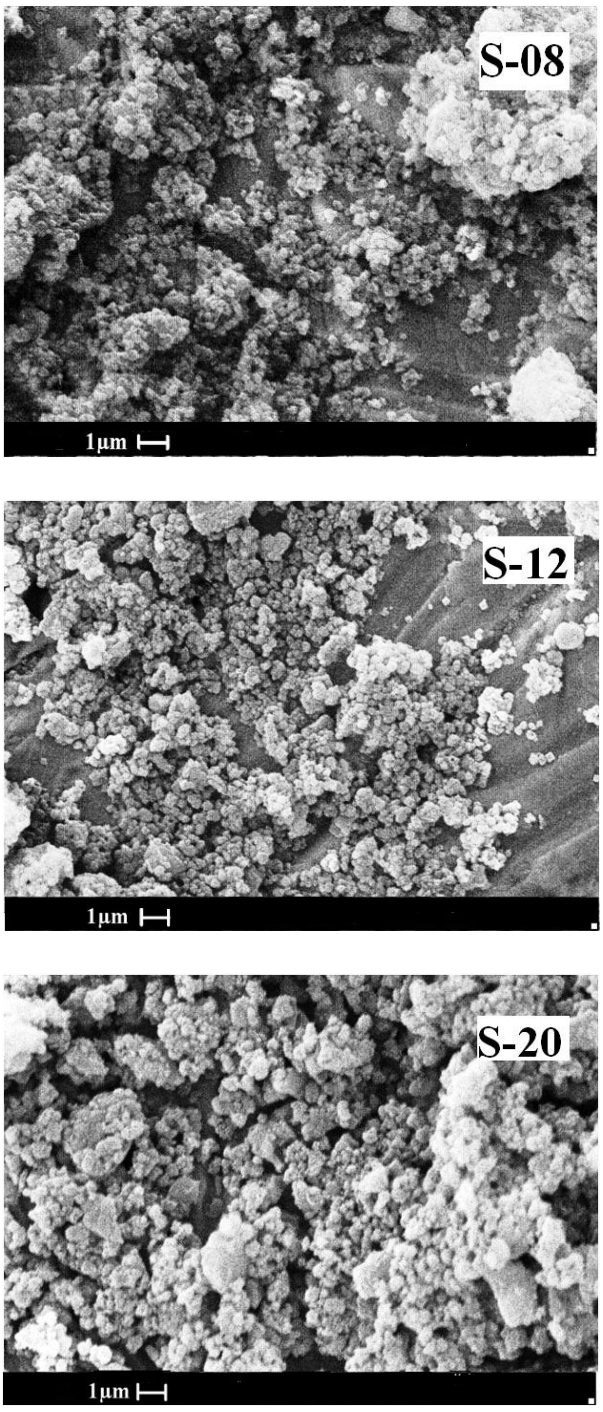

Fig. 6.6. SEM image of sample S-08, S-012 and S-20.

6.3.2.6. ***Transmission electron microscopy***

Transmission electron microscopy (TEM) was used for further probing into the structural pore ordering and morphology of samples S-08 and S-12. The TEM images of these samples are illustrated in Fig. 6.7. Sample S-08 has exhibited well ordered structure possessing mesopores with hexagonal arrangement. The composite material (sample S-12) also exhibited hexagonally arranged mesopores but structurally it is less ordered as compared to S-08. This observation is well supported by XRD analyses. Moreover, absence of different/isolated morphology suggests that, no MFI phase exists separately. Thus, Sn-MFI/MCM-41 composite possesses a disordered mesoporous phase and a crystalline microporous phase simultaneously indicating a composite nature rather than the physical mixture. A gradual increase in the crystallinity of MFI phase in the wall of MCM-41 seems to occur with progress in re-crystallization process.

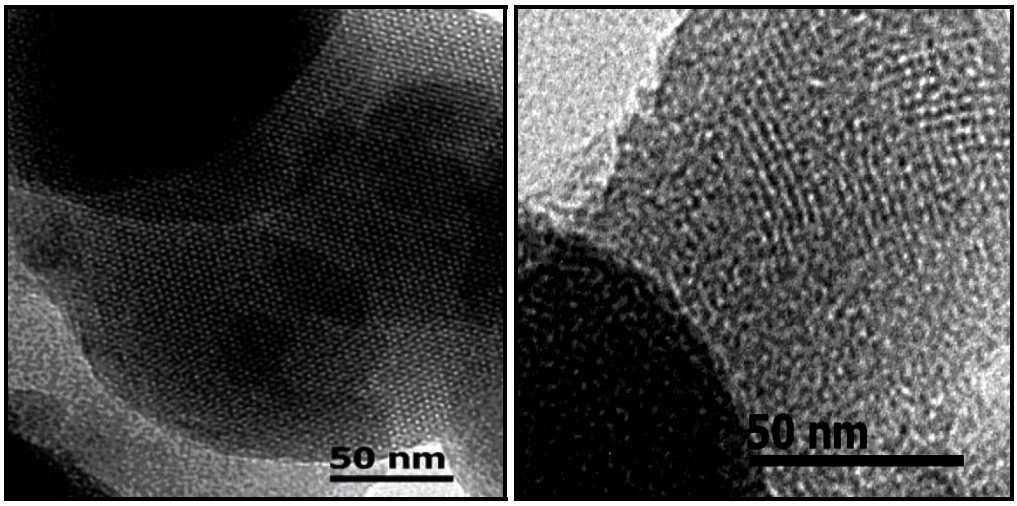

S-08 **S-12**

Fig. 6.7. TEM images of calcined S-08, and S-12.

6.3.2.7. ***Diffuse reflectance UV–vis Spectroscopy (DRUV-Vis)***

The detection of type and coordination state of Sn species was carried out using diffuse reflectance UV–vis spectroscopy. Fig. 6.8 shows the UV–vis diffuse reflectance spectra of calcined samples S-08, S-12, and S-20. Every sample exhibited

an absorption at ~ 220 nm which can be assigned to charge transitions (CT) from O^{2-} to Sn^{4+} in tetrahedral coordination [10, 21, 49]. All samples showed no band at 280 nm which is attributed to polymeric Sn–O–Sn type species [10, 21, 49]. Thus, it can be concluded that the incorporation of tetrahedral Sn species has been successfully occurred in the silica framework and the status of inserted Sn remained unaffected during transformation of Sn-MCM-41 to Sn-MFI.

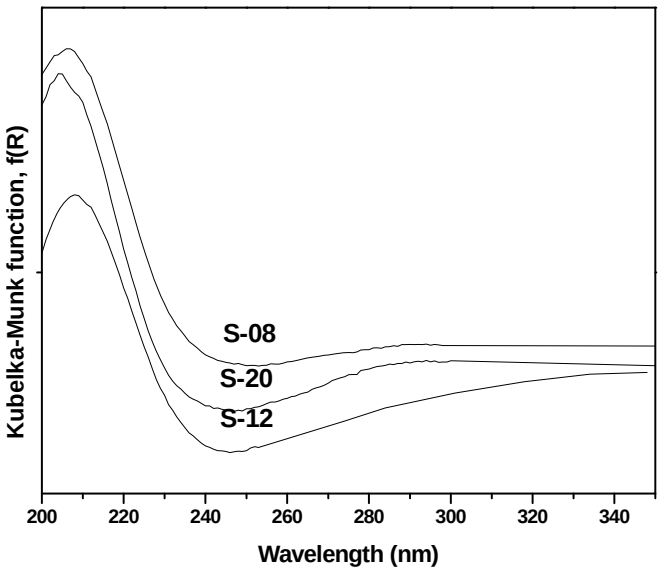

Fig. 6.8. DRUV–vis spectra of calcined S-08, S-12 and S-20 .

6.3.3 Catalytic study: Hydroxyalkylation of p-cressol

The screening of Sn-MFI/MCM-41 sample was carried out for their catalytic performance in an industrially important reaction viz. hydroxyalkylation of *p*-cresol to DAM. [2, 2-'methylenebis (4-methylphenol)]. Besides, an interest in further characterization, another purpose was to explore the possibility of identifying a promising cost-effective heterogeneous catalyst for environmentally benign and economic industrial process. The catalytic activity results of S-08, S-12 and S-20 for hydroxyalkylation of *p*-cresol were presented in **Table 6.2**. Among the three, S-20 has shown least (20%) product yield with 97% and 3% selectivity to DAM and carbinol

respectively. Interestingly, no trimer formation was observed with S-20 unlike in the case of S-12 and S-08. The lower product yield and negligible selectivity to trimer with S-20 could be due to its smaller pore size/volume, which restricts the diffusion of reactants and products inside a pore and thereby retarding their interaction with active Sn sites present in the catalyst. This limitation of microporous S-20 seems to overcome by using materials like S-08 and S-12 having larger pore sizes/volumes. S-08 has shown 70 % product yield with 88 % selectivity to DAM and 12 % selectivity to trimer. Lowering of the DAM selectivity might be caused by it's inter-conversion leading to predominant formation of trimer. S-12 has shown 59 % product yield with 89 %, 9 % and 2% selectivity to DAM, trimer and carbinol respectively. Interestingly, the formation of carbinol was observed with S-12 catalyst similar to that observed in case of S-20. Moreover, S-12, the pore dimensions of which are analogous to that of S-08 showed the formation of DAM and trimer as that of S-08 though with lower product yield. Thus, S-12 has exhibited a catalytic performance which is expected from a Sn-containing material possessing combined characteristics of both microporous and mesoporous materials. In other words, based on the catalytic activity results, it can be concluded that the synthesis of Sn-MFI/MCM-41 composite material has been successfully achieved via two-step crystallization process. The work related to maximizing the DAM selectivity and product yield is in progress.

Table 6.2. Catalytic performance of S-08, S-12, and S-20 in hydroxyalkylation of *p*-cresol reaction[a].

No.	Catalysts	Product yield (%)	Selectivity (%)		
			DAM	Trimer	Carbinol
1	S-08	70	88	12	0
2	S-12	59	89	9	2
3	S-20	20	97	0	3

[a] reaction conditions: reaction mixture composition - *p*-cresol (4.5 g), formaldehyde (0.25 g), toluene (10 g) and catalyst (0.5 g), reaction temperature- 80^{o}C, time – 2 h.

6.3.4. Optimization of synthesis parameters

Though, Sn-MFI/MCM-41 composite has been synthesized successfully through a two step crystallization process, it will be inadequate if optimal synthesis conditions have not been established. In present work, it was observed that, both the end members viz. Sn-MFI and Sn-MCM-41 can be obtained from the same precursor MFI solution if an appropriate re-crystallization time was allowed. Thus, it is necessary to establish the relationship between the process parameters such as aging time, re-crystallization temperature, time, molar gel compositions (molar ratios of $TPAOH/SiO_2$, $CTMABr/SiO_2$ and SiO_2/SnO_2) and the pathway for the preparation of Sn-MFI/MCM-41 composite material. One parameter was changed at one time keeping other parameters including addition sequence constant.

6.3.4.1. *Aging time*

In two step crystallization process, the first step involved the aging of the gel for certain time to yield Sn-MFI precursors whereas in second step, re-crystallization of the gel prepared by addition of aged gel to surfactant solution. In present study, we have subjected the gel having molar composition of SiO_2: $0.1SnO_2$: 0.45TPAOH:45 H_2O to different aging times viz. 2 h, 4h and 6h at 100^oC. In second step, the resulting preformed precursor was added to surfactant solution to give a gel with molar gel composition SiO_2: 0.24CTMABr:$0.1SnO_2$: 0.45TPAOH: 118 H_2O and then time dependent studies were conducted while re-crystallizing the final gel at 130^oC.

When the gel was aged for 2 h in first step, in second step, initially the products has shown the only characteristic peak of Sn-MCM-41 phase ($2\theta = 2.3^o$) the intensity of which increases, reaches to maximum and then disappears on further heating. The mesophase was found completely absent at 10^{th} h. However, on extending the time further, only MFI phase was found to appear. Thus, there was no simultaneous formation of meso- and micro- porous phases when gel was aged for 2h. When gel was aged for 4 h, the time dependent studies in re-crystallization step revealed that, the transformation from Sn-MCM-41 to Sn-MFI/MCM-41 composite to Sn-MFI occurs with time. Extending the aging time for 6 h, from beginning, only MFI phase was formed in the re-crystallization step. **Fig. 6.9** show the powder XRD

patterns showing progressive development of phases at 130°C after aging at 100°C for (a) 2 h , (b) 4 h and (c) 6h.

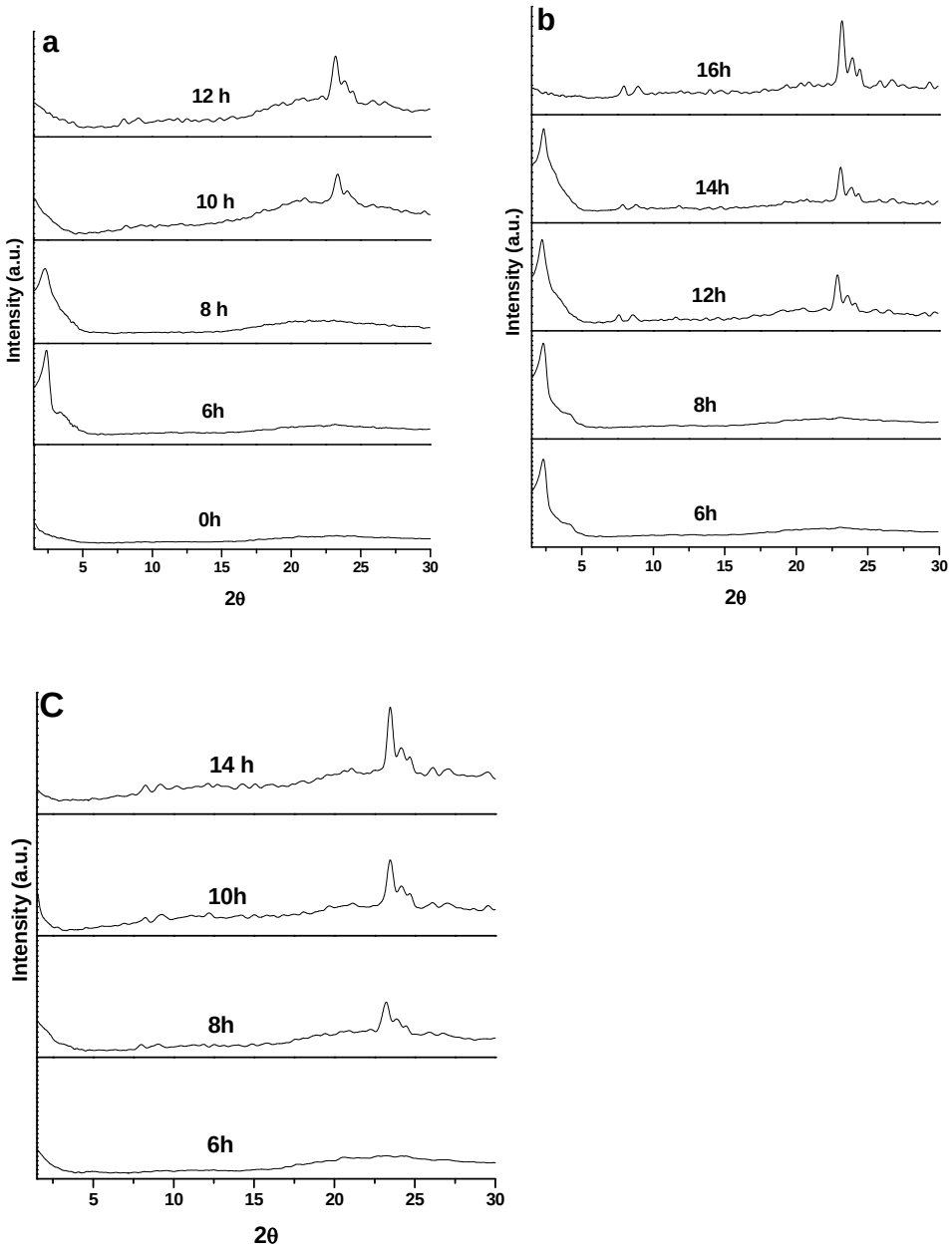

Fig. 6.9. Powder XRD patterns showing progressive development of phases at 130°C after aging at 100°C for (a) 2 h , (b) 4 h and (c) 6h.

Thus, the formation of Sn-MFI/MCM-41 composite was favored when the precursor MFI species aged for 4 h at 100 ^{o}C. Probably, aging period of 4 h seems to optimum for the formation of optimum level of nuclei, building units and remaining adequate stannosilicate gel for the formation of Sn-MFI/MCM-41 composite. The lower/higher magnitude of the Sn-MFI precursors formed by decreasing/increasing the aging time could be responsible for not crystallizing Sn-MFI phase along with mesophase.

6. 3.4.2. *Re-crystallization temperature*

The influence of re-crystallization temperature on progressive development of phases was investigated in the temperature ranging from 100 to 160^{o}C. The overall procedure followed was same as described earlier keeping aging time fixed (4 hr at 100^{o}C) in the first step. Except 130^{o}, no temperature was found suitable to yield Sn-MFI/MCM-41 composite even upto 35 h of re-crystallization time. At 100^{o}C , only Sn-MCM-41 was formed and no indication of either transformation to Sn-MFI or formation of Sn-MFI/MCM-41 composite was observed even if the re-crystallization time was extended upto 35 h. The direct crystallization of Sn-MFI without formation of mesophase was observed at 160^{o}C. Beside, optimum level of nuclei, the concentration of the components (Si and Sn species) in the liquid phase appears as controlling factor for the formation of the phase. Change in temperature may cause shift in the concentration of liquid phase. Thus, formation of Sn-MFI/MCM-41 composite seems to be sensitive to the re-crystallization temperature. **Fig.6.10** shows powder XRD patterns showing progressive development of phases at (a) 100^{o}C (b) 130^{o}C and (c) 160^{o}C ageing at 100^{o}C for 4 h.

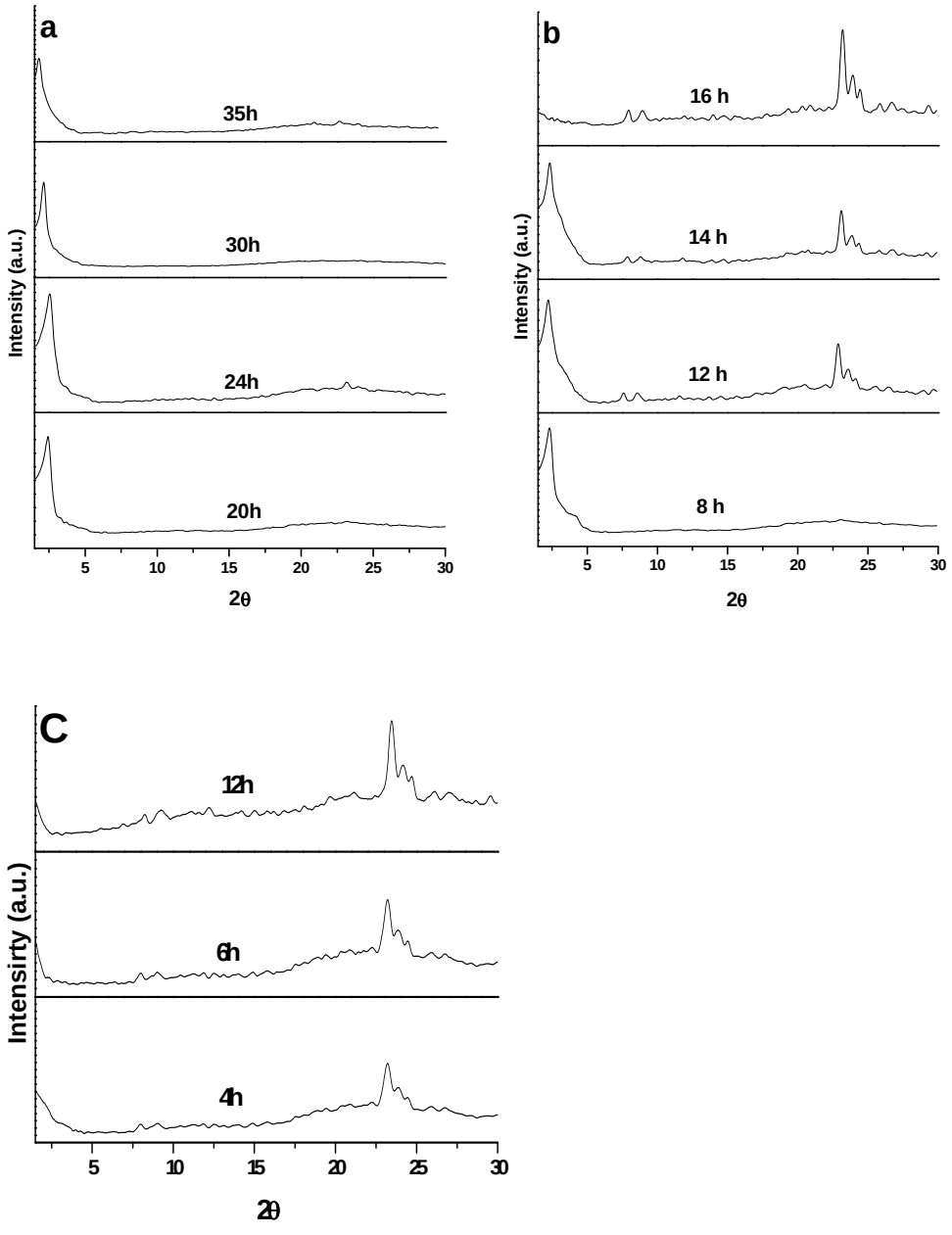

Fig.6. 10. Powder XRD patterns showing progressive development of phases at (a) 100°C (b) 130°C and (c) 160°C ageing at 100°C for 4 h.

6.3.4.3. *Molar TPAOH/SiO_2 ratio in gel*

The role of TPAOH in the micro/meso composite phase formation is to form nuclei of MFI phase in aging step and then enhance the MFI crystal growth in the mesopore wall in re-crystallization step. The influence of concentration of TPAOH in the starting gel on phase formation was investigated by varying molar TPAOH/SiO_2 ratio in the starting gel in the range of 0.35–0.55 keeping other parameters constant. The molar ratios of SiO_2/SnO_2, CTMABr/SiO_2, H_2O/SiO_2 in the gel were 100, 0.24 and 118 respectively. After aging at 100^oC for 4 hr, the progressive development of phases was monitored at 130^oC as a function of time. **Fig. 6.11** shows Powder XRD patterns showing progressive development of phases at 130^oC after ageing gel with TPAOH/SiO_2 molar ratio (a) 0.35 (b) 0.45 and (c) 0.55 at 100^oC for 4 h.

Time dependent studies using a gel with molar ratio TPAOH/SiO_2 of 0.35 revealed that, initially, only mesophase was formed which then became amorphous at 16th h. Prolonged re-crystallization time even upto 20 h, no indication of MFI phase was observed. The gel with TPAOH/SiO_2 = 0.45, the formation and transformation of Sn-MCM-41 into Sn-MFI/MCM-41 composite and then into Sn-MFI was found to occur with time. In two-step process wherein a gel with molar TPAOH/SiO_2 ratio of 0.55 was used, only Sn-MFI phase was formed of which crystallinity was found to increase with time upto 18 h without indication of any other phase/s. Considering these results and the role of TPAOH in the synthesis of Sn-MFI/MCM-41 composite, it can be concluded that Sn-MFI/MCM-41 composite forms only when the molar TPAOH/SiO_2 ratio in the gel was 0.45 (optimum in present case) which forms optimum level of nuclei.

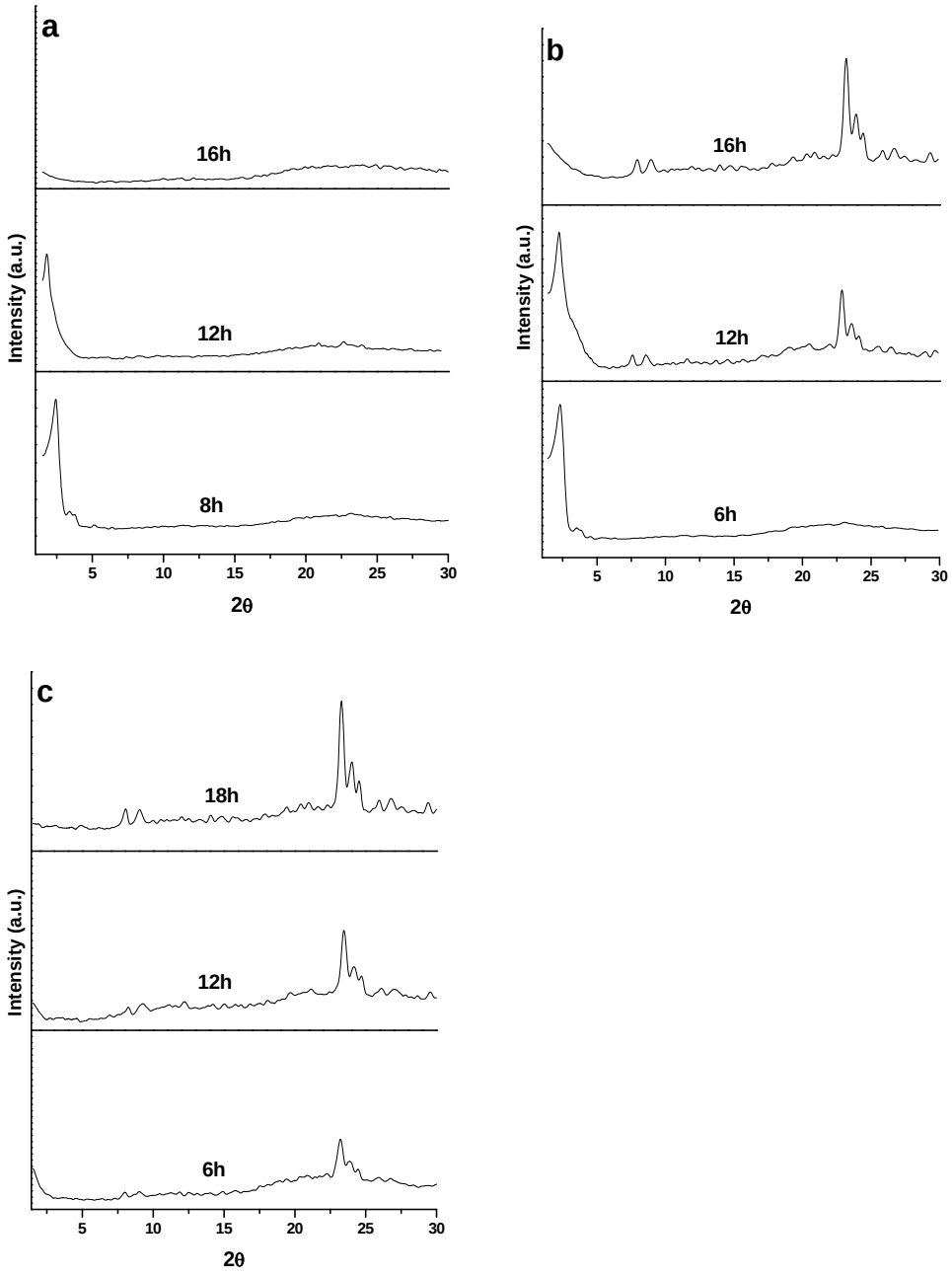

Fig.6.11. Powder XRD patterns showing progressive development of phases at 130^{o}C after ageing gel with TPAOH/SiO_2 molar ratio (a) 0.35 (b) 0.45 and (c) 0.55 at 100^{o}C for 4 h.

6.3.4.4. *Molar CTMABr/SiO_2 ratio in gel*

Yet another variable, viz. molar CTMABr/SiO_2 ratio in gel was considered in optimization studies as concentration of CTMABr influences the formation of MCM-41 [8] materials. The dependence of the phase quality on the concentration of surfactant was investigated by varying the CTMABr/SiO_2 molar ratio in the range from 0.12 to 0.48 keeping molar SiO_2/SnO, TPAOH/SiO_2 and H_2O/SiO_2 ratio 100, 0.45 and 118 respectively fixed. The powder XRD patterns of products obtained from these gels by subjecting it to aging period of 4h at 100^{o}C and then re-crystallized at 130^{o}C for 12 h were illustrated in Fig. 6.12.

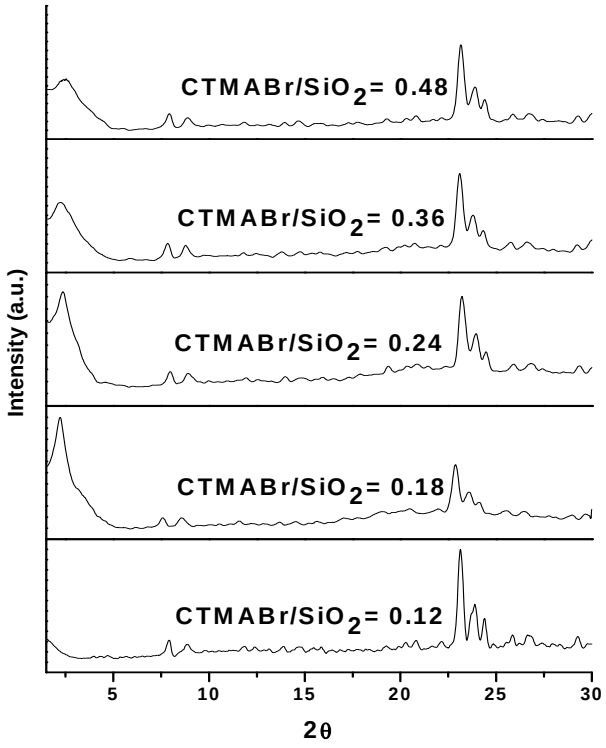

Fig. 6.12. Powder XRD patterns of the phases obtained at 12 th h of re-crystallization time at different molar CTMABr/SiO_2 ratios in the gel (as indicated on the profile)

At molar CTMABr/SiO_2 ratio of 0.12, only characteristic peaks of MFI were observed. Thus, the concentration of CTMABr used, may not be sufficient to form any mesophase. As expected, when, the synthesis was performed using higher

CTMABr/SiO_2 molar ratio ranging from 0.18 to 0.48, the products were Sn-MFI/MCM-41 composites. Compared to product obtained using CTMABr/SiO_2 molar ratio of 0.24, the lower concentration of CTMABr yielded a composite with lower proportion of MFI phase; higher concentration leads to lower the proportion of mesophase at the cost of MFI phase. Thus under identical set of synthesis conditions, molar ratio of CTMABr/SiO_2 not only decide the type of phase formed but also proportion of each phase in the composite material.

6.3.4.5. *Molar SiO_2/SnO_2 ratio in gel*

Since the catalytic application of Sn-MFI/MCM-41 composites is likely to depend on the concentration and coordination of Sn that is incorporated in the wall of mesoporous phase, it becomes essential to investigate the feasibility of synthesizing composite phase as a function of amount of tin in the gel. In view of this, experiments were conducted to investigate the influence of molar ratio of SiO_2/SnO_2 in gel on the progressive development of composite material wherein the molar SiO_2/SnO_2 ratio in the gel was varied from 50 to 200 keeping molar ratios of TPAOH/SiO_2=0.45, H_2O/SiO_2=118, CTMA/SiO2 = 0.24 fixed. The products were collected at pre-decided interval of time from each batch after aging at 100^oC for 4 hr followed by re-crystallization at 130^oC . **Fig. 6.13** depicts powder XRD patterns showing progressive development of phases at 130^oC after ageing gel with SiO_2/ SnO_2 molar ratio (a) 50 (b) 100, (c) 150 and (d)200 at 100^oC for 4 h. Shorter time was found to require for the formation of Sn-MFI/MCM-41 composites when gel with higher SiO_2/SnO_2 molar ratio was used. This behavior can be attributed to formation of lower population of MFI nuclei in first step and low rate of crystallization of Sn-MFI phase in second step when there is higher SiO_2/SnO_2 molar ratio in the gel.

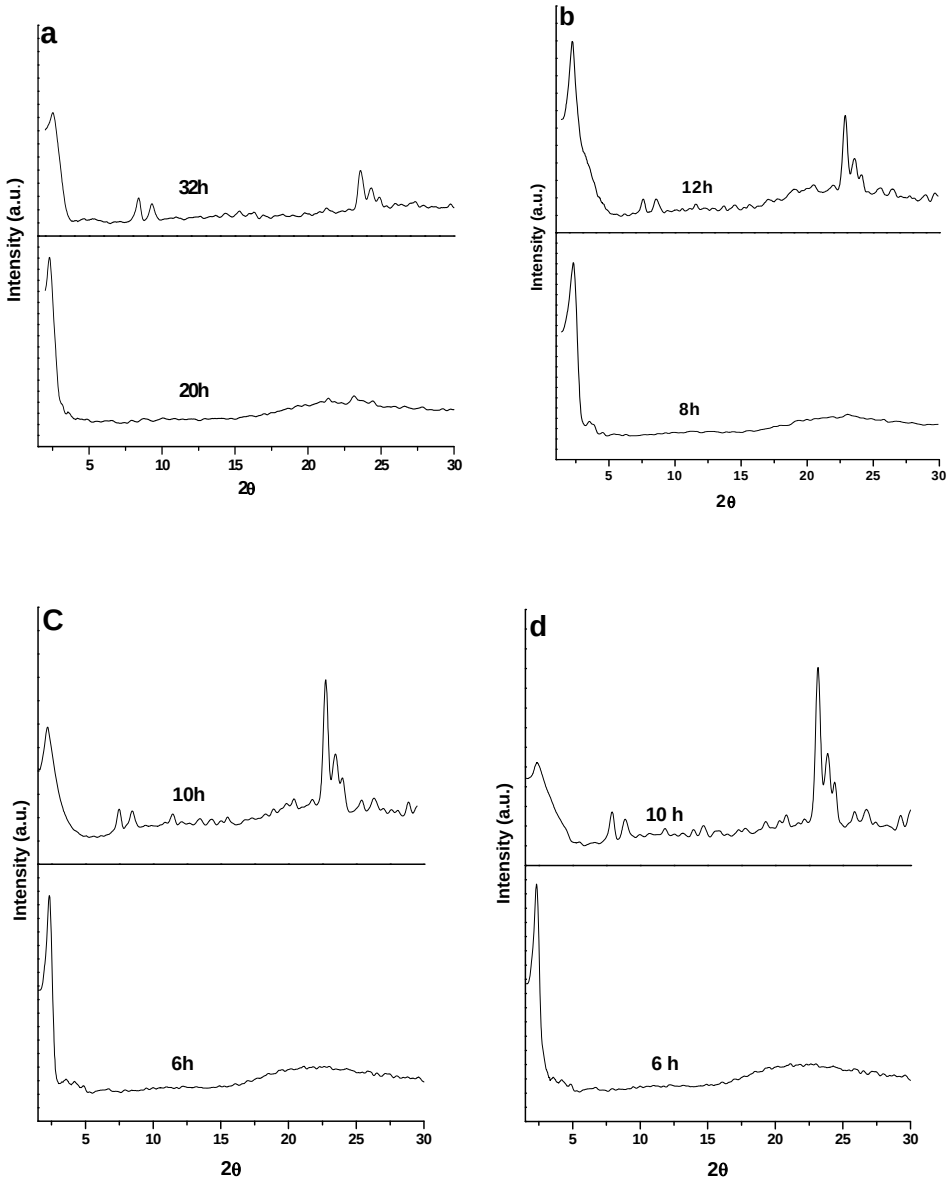

Fig.6.13. Powder XRD patterns showing progressive development of phases at 130^{o}C after ageing gel with SiO_2/ SnO_2 molar ratio (a) 50 (b) 100, (c) 150 and (d)200 at 100^{o}C for 4 h.

6.4. CONCLUSION

Micro-/meso-porous stannosilicate composite (Sn-MFI/MCM-41) material has been successfully synthesized via two-step crystallization method. The end members viz. Sn-MCM-41 and Sn-MFI can be synthesized by varying the length of period allowed for the crystallization of the precursor species. The type of phase formed was found to depend on various process parameters such as aging time, re-crystallization temperature, time and molar ratios of, TPAOH/SiO_2, CTMABr/SiO_2 and SiO_2/SnO_2 in the gel. Powder XRD, FT-IR, SEM, TEM, nitrogen sorption measurement, DRUV-Vis and hydroxyalkylation of *p*-cresol reaction were used as the characterization tools.

Aging of a gel having molar composition SiO_2: 0.005 - 0.02 SnO_2: 0.45 TPAOH: 35 H_2O at 100^oC for 4 h in first step and re-crystallization of final gel with molar composition SiO_2: 0.005- 0.02 SnO_2: 0.45 TPAOH: 0.18 - 0.48 CTMABr :118 H_2O at 130^oC for 10-32 h was found to be optimum synthesis conditions for synthesizing Sn-MFI/MCM-41 composite materials. UV-vis spectrum exhibited absorption at ~ 220 nm and absence of band at 280 nm suggesting the successful incorporation of tetrahedral Sn species in the silica framework. Sn-MFI/MCM-41 composite material was found to catalyze hydroxyalkylation of *p*-cresol reaction. The formation of carbinol was observed with Sn-MFI/MCM-41 composite similar to that observed in case of Sn-MFI. Moreover, Sn-MFI/MCM-41, the pore dimensions of which are analogous to that of Sn-MCM-41 showed the formation of DAM and trimer as that of Sn-MCM-41 though with lower product yield. Thus, Sn-MFI/MCM-41 has exhibited a catalytic performance which is expected from a Sn-containing material possessing combined characteristics of both microporous and mesoporous materials.

6.5. REFERENCES

[1] M.E. Davis, Nature; 417 (2002) 813.

[2] J.S. Beck, C.T.W. Chu, I.D. Johnson, C.T. Kresge, M.E. Leonowicz, W.J. Roth, J.W. Vartuli, WO Pat. 91/11390 (1991).

[3] C.T. Kresge, M.E. Leonowicz, W.J. Roth, J.C. Vartuli and J.S. Beck , Nature; 359 (1992) 710.

[4] J.S. Beck, J.C. Vartuli, W.J. Roth, M.E. Leonowicz, C.T. Kresge, K.D. Schmitt, C.T-W. Chu, D.H. Olson, E.W. Sheppard, S.B. McCullen, J.B. Higgins and J.L. Schlenker, J. Am. Chem. Soc. 114 (1992) 10834.

[5] S. P. Panchgalle, U. R. Kalkote, P. S. Niphadkar, P. N. Joshi, S. P. Chavan, G. M. Chaphekar, Green Chem. 6 (2004) 308.

[6] A. Corma, L. Nemeth, M. Renz and S. Valencia, Nature; 412 (2001) 423.

[7] N.K. Mal, A. Bhaumik, R. Kumar, A.V.Ramaswamy, Catal. Lett.; 33 (1995) 387.

[8] T.R. Gaydhankar, P.N. Joshi, P. Kalita, R. Kumar, J. Mol. Catal. A: Chem.; 265 (2007) 306.

[9] N.K Mal, V. Ramaswamy, P.R. Rajamohanan, A.V. Ramaswamy, Micropor. Mater. 12 (1997) 331-340.

[10] N.K. Mal, A.V. Ramaswamy, J. Mol. Catal. A : Chem.; 105 (1996) 1491.

[11] N.K. Mal, A.V. Ramaswamy, Appl. Catal. A-Gen.; 143 (1996) 75.

[12] S. Samanta, N.K. Mal, A. Manna, A. Bhaumik, Appl. Catal. A-Gen. 273 (2004) 157.

[13] M. Boronat, A. Corma, M. Renz , J. Phys. Chem. B; 110 (2006) 21168.

[14] A. Corma, M. E. Domine, S. Valencia, J. Catal. 215 (2003) 294.

[15] N.K. Mal, V. Ramaswamy, S. Ganapathy and A. V. Ramaswamy, J. Chem. Soc., Chem. Commun. (1994) 1933.

[16] P.S. Niphadkar, M.S. Kotwal, S.S. Deshpande, V.V. Bokade, P.N. Joshi, Mater. Chem. Phys.; 114 (2009) 344.

[17] A. Corma, M.E. Domine, L. Nemeth, S. Valencia, J. Am. Chem. Soc.; 124 (2002) 3194.

[18] A. Corma, M. Renz, Chem. Commun.; (2004) 550.

[19] N. K. Mal, V. Ramaswamy, S. Ganapathy, A.V. Ramaswamy Appl. Catal. A-Gen.; 125 (1995) 233.

[20] P.S. Niphadkar, P. N. Joshi, H.R. Gaurav, S.S. Deshpande, V.V.Bokade, Catal. Lett.; 133 (2009) 175.

[21] K. Chaudhari, T.K. Das, P.R. Rajmohanan, K. Lazar, S. Sivasanker and A.J. Chandwadkar J. Catal. **183** (1999) 281.

[22] P. P. Samuel, S. Shylesh and A.P. Singh, J. Mol. Catal. A: Chem.; 266 (2007) 11.

[23] U.S Taralkar, P Kalita, R. Kumar, P.N. Joshi, Appl. Catal. A-Gen.; 358 (2009) 88.

[24] A. Corma, M.T. Navarro, L. Nemeth, M. Renz, Chem. Commun.; (2001) 2190.

[25] V. Ramaswamy, P. Shah, K. Lazar and A. V. Ramaswamy, Catal. Surveys from Asia; 12 (2008) 283.

[26] T.M. Abdel-Fattah, T.J. Pinnavaia, Chem. Commun.; (1996) 665.

[27] N. Candu, S. Coman, V.I. Parvulescu ,J. E. Haskouri , P. Amoros, D. Beltran, Top Catal.; 52 (2009) 571.

[28] K. Bachari , O. Cherifi Applied Catalysis A: Gen.; 319 (2007) 259.

[29] A. Corma , M.Renz ,M. Susarte, Top. Catal.; 52 (2009) 1182.

[30] M. Renz, T. Blasco, A. Corma, V. Fornés, R. Jensen, L. Nemeth, Chem. Eur. J.; 8 (2002) 4708.

[31] J. Lee, Y. Park, P. Kim, J. Yi, J Mater. Chem.; 14 (2004) 1050.

[32] A. Karlsson, M. StÖcker, R. Schmidt, Micropor. Mesopor. Mat.; 27 (1999) 181.

[33] M. Kruk, M. Jarnoniec, S. H. Joo, R. Ryoo, J. Phy. Chem. B; 107 (2002) 2205.

[34] P. Van der Voort, P.I. Ravikovitch, K. P. De Jong, M. Benjelloun, E. Van Bavel, A. H. Janssen, A. v. Neimark, B. M. weckhuysen, E. F. Vansant, J. Phy. Chem. B; 106 (2002) 5873.

[35] S. van Donk, A.H. Janssen, J.H. Bitter, K.P. de Jong, Catal. Rev. Sci. Eng. ; 45 (2003) 297-319.

[36] A. Corma, V. Fornes, S.B. Pergher, T.L. Maessen, J.G. Buglass, Nature; 396 (1998) 353.

[37] J.C. Groen, W. Zhu, S. Brouwer, S.J. Huynink, F. Kapteijn, J.A. Moulijn, J. Pérez- Ramirez, J. Am. Chem. Soc.; 129 (2007) 355.

[38] J.C. Groen, L.A.A. Peffer, J.A. Moulijn, J. Pérez-Ramirez, Micropor. Mesopor. Mat.; 69 (2004) 29.

[39] M. Ogura, Catal Surv. Asia; 12 (2008)12.

[40] A.A. Campos, L. Dimitrov, C.R. Da Silva, M. Wallau, E.A. Urquieta-Gonzalez, Micropor. Mesopor. Mat.; 95 (2006) 92.

[41] C.J.H. Jacobsen, C. Madsen, J. Houzvicka, I. Schmidt, A. Carlsson, J. Am. Chem. Soc.; 122 (2000) 7116.

[42] A.H. Janssen, I. Schmidt, C.J.H. Jacobsen, A.J. Koster, K.P. de Jong, Micropor. Mesopor. Mat.; 65 (2003) 59.

[43] I. Schmidt, A. Boisen, E. Gustavsson, K. Stahl, S. Pehrson, S. Dahl, A. Carlsson, C.J.H. Jacobsen, Chem. Mater.; 13 (2001) 4416.

[44] K.M. Jinka, S.C. Lee, S. E. Park, R.V. Jasra, Stud. Surf. Sci. Catal.; 174 B (2008) 1187.,

[45] Y. Xia, R. Mokaya, J. Mater. Chem.; 14 (2004) 863.

[46] Y. Liu, W. Zhang, T. J. Pinnavaia, Angew. Chem. Int. Ed.; 40 (2001) 1255.

[47] L. Liu, G. Xiong, X. Wang, J. Cai, Z. Zhao, Micropor. Mesopor. Mat.; 123 (2009) 221.

[48] C. Y. Hsu, A. S. T. Chiang, R. Selvin, R. W. Thompson , J Phys Chem B; 109 (2005) 18804.

[49] X. Wang, H. Xu, X. Fu, P. Liu, F. Lefebvre, J.M. Basset, J. Mol. Catal. A: Chem.; (2005) 185.

CHAPTER 7

SUMMARY AND CONCLUSIONS

Sn-containing molecular sieves, in particular, microporous and mesoporous stannosilicates are interesting materials as they are potential candidates for their various applications such as adsorbent, ionic conductor and as catalysts in several hydrocarbon conversion processes. Even though, there are several reports on Sn-containing molecular sieve, most of them are focused on its catalytic application and no systematic studies with regards to optimization of synthesis parameters in selected topology. Therefore, the objective of thesis was focused on the synthesis, characterization and catalytic application of tin-containing microporous and mesoporous molecular sieves. The data obtained by employing simple and novel methods of preparation, characterization, establishing the cause and effect relationship between synthesis parameters and product quality, catalytic performance represented a convenient vehicle for the preparation of tailor-made material for a particular application. This chapter present a brief summary of the work described in previous chapters and general conclusions arrived from the work.

Tin-silicalite-1 (Sn-MFI) has been successfully synthesized by dry gel conversion (DGC) method. The influence of various synthesis parameters such as crystallization time, temperature, water content at the bottom of autoclave, molar ratios of $(TPA)_2O/SiO_2$ and SiO_2/SnO_2 in dry gel on the crystallization kinetics and physico-chemical properties of Sn-MFI materials has been investigated. Time dependent studies revealed that, the progressive crystallization of Sn-MFI depend not only on the synthesis time but also on the other various synthesis parameters. Increase in the crystallization temperature, water content at bottom of autoclave, $(TPA)_2O/SiO_2$ and SiO_2/SnO_2 molar ratios in dry gel resulted in the lowering of overall crystallization period. A good correspondence between the chemical composition of the surface and

the bulk indicated the uniform distribution of Sn^{4+} ions. The presence of these ions in tetrahedral coordination has been indicated by DRUV-vis spectral studies. Although, not better but comparable activity has been shown by Sn-MFI prepared by dry gel conversion method with Sn-MFI prepared by conventional hydrothermal crystallization method in the hydroxylation of phenol reaction.

Thermal expansion properties of the representative Sn-MFI sample and its comparison with that of Sn-free Si-MFI sample were investigated by an *in-situ* high temperature X-ray diffraction studies. Both the phases have not shown any drop in crystallinity or phase transformations up to 700^{o}C. Sn-MFI showed a strong negative thermal expansion similar to Si-MFI in anisotropic manner in the temperature range of 100 – 700^{o}C. The trend observed in contraction along the axes was as: a > c > b. The substitution of Sn^{4+} in MFI framework resulted in the increase in the lattice thermal expansion coefficient (from -43.437 x 10^{-6} K^{-1} to -38.611 x 10^{-6} $K^{-1)}$ in the temperature range 200 – 700^{o}C.

The nature, strength and density of surface acid sites in Sn-MFI molecular sieves with different Sn-content were characterized by N 1s high resolution photoelectron peak of chemisorbed pyridine in combination with pyridine-IR and TPAD. Two peaks emerged at 399.5±0.2 and 401.5±0.2eV by deconvoluting composite N 1s peak were assigned to chemisorbed pyridine on weak and relatively strong Lewis acid sites respectively. The relative percentage of strong Lewis acid sites was found to increase with the decrease of framework Sn content. A close agreement was observed between the ratios of weak Lewis acid sites to strong Lewis acid sites obtained from XPS and TPAD.

Vapor phase methylation of aniline over Sn-MFI was systematically studied and optimizations of process parameters were carried out. Sn-MFI (SiO_2/SnO_2 = 50) was found to be optimum catalyst with 55% aniline conversion and 60% N-methylaniline selectivity. At lower space velocity (higher contact time) of $1h^{-1}$, aniline conversion was found to be increased to 71% with reduction in N-methylaniline (NMA) selectivity to 39% and increased in N,N-Dimethylaniline (NNDMA) selectivity to 58%. The reaction follows first order kinetics with respect to aniline having activation energy of 7.3 kcal/mol.

The existence of synergy between Lewis and Bronsted acid sites in Al-Sn-MFI was investigated in acid catalyzed aniline N-methylation reaction with a view to maximize the aniline conversion as well as N-methyl aniline (NMA) selectivity. Different degree of isomorphous substitution of Al^{3+} in the stannosilicate framework with MFI topology resulted into alteration in the ratios of Bronsted and Lewis acid sites. These catalysts were synthesized by hydrothermal crystallization of gels having molar compositions SiO_2: x SnO_2: y Al_2O_3: 0.23 $(TPA)_2O$: 35H_2O, where x ranges from 0 to 200 and y from 0 to 400. Although, Sn: Al ratio was varied (ca. 1:0, 1:0.33, 1:1, 1:3, 0:1), the overall molar Si/ (Al+Sn) ratio was kept constant as 50. Powder X-ray diffraction, DRUV-vis spectroscopy, Temperature Programmed Ammonia Desorption (TPAD) and FTIR spectroscopy were the techniques used for catalyst characterization. It was evident from the TPAD results that, the framework tin species create the weak acid sites whereas insertion of Al lead to the creation of both the weaker as well as relatively stronger acid sites. Pyridine IR spectra of samples having the simultaneous presence of Al^{3+} and Sn^{4+} in the MFI framework revealed a trend in

the Bronsted/Lewis acidity ratio as M75 (0.67) < M50 (0.91) < M25 (1.27). These samples showed higher aniline conversion than the samples containing either Al or Sn alone. Interestingly, an increase in stronger acid sites with an increase in framework Al^{3+} leads to decrease in aniline conversion. Thus, synergy between Bronsted and Lewis acid sites in Al-Sn-MFI catalysts was demonstrated to exist in aniline N-methylation reaction. Upon process parameter optimization, Al-Sn-MFI with Si/Al = 50.2 , Si/Sn= 93.8, Si/(Al+Sn) = 43.2 showed the maximum aniline conversion (67 %) and NMA selectivity (81 %) at reaction temperature = 220^{o}C, WHSV = 3h^{-1}, molar ratio (aniline to methanol) = 1:8 and TOS = 4 h.

Microporous stannosilicate molecular sieve with BEA topology (Sn- BEA) has been crystallized hydrothermally in fluoride medium from seeded gels containing source of oxyanion. Different gels with molar compositions: SiO_2: 0.0083 – 0.0166 SnO2: 0.54 - 1.3 TEAOH: 0.54 - 1.3 HF: 7.5 H_2O: 0.0 - 0.1 oxyacid (promoter) with were prepared and subjected for hydrothermal treatment at 140^{0}C. The overall synthesis time required to form Sn-BEA from gels with/without use of seed/promoter was found to follow the trend as: none > promoter > seed. Irrespective of usage of seed in the gel, perchlorate oxyanions indicated the maximum reduction in the overall synthesis time. The influence of molar ratios of TEAOH/SiO_2, HF/SiO_2 and SiO_2/SnO_2 in initial gel composition on the nature of the phase and crystallization period has also been investigated. An increase in the TEAOH /SiO_2 along with the HF/SiO_2 to a magnitude of 1.3 and SiO_2/SnO_2 molar ratio viz. 120 in initial gel mixture resulted in the formation of Sn-BEA in 7 days. Based on the DRUV-vis and

FT-IR spectral studies, Sn-BEA has shown the presence of Sn^{4+} ions in tetrahedral coordination.

Sn-MFI/MCM-41 composite material was successfully synthesized by monitoring the re-crystallization time in a simple two-step crystallization process. The length of period allowed for the recrystallization of the precursor species was found to be a controlling factor to achieve either the end members viz. Sn-MCM-41 and Sn-MFI or Sn-MFI/MCM-41 composite material. Powder XRD, FT-IR, SEM, TEM, nitrogen sorption measurement, DRUV-vis and hydroxyalkylation of *p*-cresol reaction were used as the characterization tools. Attempts were also made to establish the relationship between type of phase formed and the process parameters such as aging time, re-crystallization temperature, time and molar ratios of $TPAOH/SiO_2$, $CTMABr/SiO_2$ and SiO_2/SnO_2 in the gel.

List of publications:

A. Papers published/communicated:

1. Influence of Al^{3+} insertion in the stannosilicate MFI framework on the catalytic performance in vapour phase aniline N-methylation.
   Niphadkar P.S., Joshi P. N., Bokade V. V
   Applied Catalysis A: General, 401, 2011, 182-188.
2. Thermal expansion properties of stannosilicate molecular sieve with MFI type structure
   Niphadkar P.S., Bhange D.S., Selvaraj K., Joshi *P.N.*
   Materials Letters (Under Review, Manuscript # MLBLUE-D-11-00218).
3. Characterization of surface acid site in Tin-Silicalite-1 (Sn-MFI) molecular sieve**.**
   Niphadkar P.S., Patil K.R., Joshi P.N**.**
   Microporous and Mesoporous Materials, 141, 2011, 236-240.
4. Micro-/meso-porous stannosilicate composites (Sn-MFI/MCM-41) via two-step crystallization process: Process parameter-phase relationship.
   Niphadkar P.S., Garade A.C., Jha R.K., Rode C.V., Joshi P.N.
   Microporous and Mesoporous Materials, 136, 2010, 115-125**.**
5. Hydroxyalkylation of p-Cresol to 2,2 '-Methylenebis(4-methylphenol) Using Sn/Si-MCM-41 Catalysts
   Garade A.C.**Niphadkar P.S**., Joshi P.N., Rode C.V.
   Chemistry Letters, 39, 2010, 126-127.
6. Synthesis of N-methylaniline by Aniline Alkylation with Methanol over Sn-MFI Molecular Sieve.
   Niphadkar P.S., Joshi P.N., Gurav H.R., Deshpande S.S., Bokade V.V.
   Catalysis Letters, 133, 2009, 175-184.
7. Tin-silicalite-1: Synthesis by dry gel conversion, characterization and catalytic performance in phenol hydroxylation reaction.
   Niphadkar P.S., Kotwal M.S., Deshpande S.S., Bokade V.V., Joshi P.N.
   Materials Chemistry and Physics, 114, 2009, 344-349.

8. Sn-beta molecular sieve catalysed Baeyer-Villiger oxidation in ionic liquid at room temperature.

   Panchgalle S.P., Kalkote U.R., **Niphadkar P.S.,** Joshi P.N., Chavan S.P., Chaphekar G.M.

   Green Chemistry, 6, 2004, 308-309.

9. Oxyanion-induced hydrothermal crystallization of Sn-BEA molecular sieve in fluoride medium
   from unseeded gels.
   Niphadkar P.S., Joshi P.N.

   Microporous and Mesoporous Materials, (to be communicated)

B. Posters presented in Conferences:

1. Conversion of dry-gel to stannosilicate molecular sieve with MFI topology in presence of steam.
P.S.Niphadkar, V.V.Paike, V.V.Bokade and **P.N.Joshi**
Presented and published in Book of Abstracts on 'From zeolites to porous MOF materials'
[Eds. Y.Liu and W.Yan, 15th International Zeolite Conference held at Beijing, China during August 12-17, 2007 , pp. 325-326].

C. List of patents

1. Stannosilicate molecular sieve with zeolite Beta structure (Sn-BEA)

   Application in process (NCL Ref. No. INV-2010-17 dated on 21/5/2010)